Efficient Pareto Frontier Algorithms for Computing Structured Signal Representations

vorgelegt von
M.Sc.
Metin Vural

von der Fakultät IV - Elektrotechnik und Informatik
der Technischen Universität Berlin
zur Erlangung des akademischen Grades

Doktor der Ingenieurwissenschaften
-Dr.-Ing.-

genehmigte Dissertation

Promotionsausschuss:

Vorsitzender: Prof. Dr. Jörg Raisch
Gutachter: Prof. Dr. Sławomir Stańczak
Gutachter: Prof. Dr. Aydin Sezgin
Gutachter: Assoc. Prof. Dr. Aleksandr Aravkin
Tag der wissenschaftlichen Aussprache: 14. Dezember 2021

Berlin 2022

Abstract

ℓ_p-norm minimization plays a significant role in a variety of disciplines. It is not only important for the signal recovery in compressed sensing but also beneficial for finding meaningful signal representations as for the sparse and anti-sparse coding related applications. Therefore, minimizing ℓ_p-norms in an efficient manner sparked interest in a variety of works.

This thesis is concerned with the noise-constrained ℓ_p-norm minimization for $1 \leq p \leq \infty$. Although there are various optimization problem formulations that may be used to minimize an ℓ_p-norm, constraining the noise can offer a more meaningful optimization problem definition since when there is a known noise tolerance in an application, one can simply canalise it into the optimization problem and formulate exactly what to solve. Thus, it is often easier to set the noise tolerance from the optimization perspective. Despite this, there is a lack of computationally efficient algorithms in the literature for the noise-constrained ℓ_p-norm minimization problem because its feasible area can be complicated. Different optimization problem formulations can provide equivalent solutions and some of them might be easier to solve than the others. Therefore, it might be tempting to solve a computationally efficient problem in order to have the solution to another one. In this thesis, we solved constrained ℓ_p-norm regularization to reach the solution of the noise-constrained ℓ_p-norm problem. We introduce optimality tracing based ℓ_p-norm minimization approaches with simple root finding iterations for $1 \leq p \leq \infty$. The optimality trade-off between both objectives, the ℓ_p-norm and a loss function that measures the data misfit, is formulated as a nonlinear equation root finding problem. We present and employ several simple, derivative-free and cost-efficient nonlinear equation root finding methods to trace this optimality over a Pareto frontier. Some of these root finding methods do not require differentiable loss functions and are applicable for both convex and nonconvex data misfits and extend such problems to a broader class of applications. We also introduce a warm-start strategy of taking linear least-squares solution with the one that has minimum ℓ_2-norm which is named *method of frames* (MOF) as an input to require fewer iterations. This warm-start may provide flexible and meaningful starting point initialization for many applications where MOF already exists and can be improved with a better understanding of finite-dimensional geometry, e.g. n-widths. The impact of the overcomplete matrix on the

convergence rate of some of the presented approaches is demonstrated for matrices fulfilling the Uniform Uncertainty Principle and Uncertainty Principle. These properties were formerly introduced to analyze the performance of random matrices for ℓ_1 and ℓ_∞-norm related applications respectively.

In the last part of the thesis, i.e. in Chapter 7, ℓ_p-norm minimization related applications are probed with using several loss functions such as least-squares, Huber and a nonconvex penalty Student's t. ℓ_1-norm is minimized with a typical compressed sensing example. Also, a generic test benchmark is utilized for the comparison of the nonlinear equation root finders for ℓ_1-norm minimization. A new communication scheme is introduced by minimizing ℓ_∞-norm. Outlier detection problem is studied with the minimized ℓ_∞-norm, and a prior is offered for the minimized ℓ_∞-norm with its performance on *peak-to-average power ratio* (PAPR). Noise-constrained nuclear norm is minimized as well for the Euclidean distance matrix completion problem with the application of wireless sensor network localization.

Zusammenfassung

Die Minimierung von ℓ_p-Normen spielt in einer Vielzahl von Disziplinen eine bedeutende Rolle. Sie ist nicht nur wichtig für die Signalwiederherstellung bei der komprimierten Abtastung, sondern auch nützlich, um sinnvolle Signaldarstellungen zu finden, wie für Anwendungen mit geringer und anti-sparse Codierung. Daher hat die effiziente Minimierung von ℓ_p-Normen das Interesse an einer Vielzahl von Arbeiten geweckt.

Diese Dissertation beschäftigt sich mit der rauschbeschränkten ℓ_p-Normminimierung für $1 \leq p \leq \infty$. Obwohl es verschiedene Formulierungen von Optimierungsproblemen gibt, die verwendet werden können, um eine ℓ_p-Norm zu minimieren, kann die Beschränkung des Rauschens eine sinnvollere Definition des Optimierungsproblems bieten. Bei bekannter Rauschtoleranz in einer Anwendung kann man diese in das Optimierungsproblem kanalisieren/integrieren/einbauen und genau formulieren, was/welches Problem zu lösen ist. Daher ist es aus Optimierungssicht oft einfacher, die Rauschtoleranz einzustellen. Trotzdem fehlt es in der Literatur an recheneffizienten Algorithmen für das rauschbeschränkte ℓ_p-Norm-Minimierungsproblem, da sein zulässiger Bereich kompliziert sein kann. Verschiedene Formulierungen von Optimierungsproblemen können äquivalente Lösungen liefern und einige von ihnen sind möglicherweise einfacher zu lösen als andere. Daher kann es verlockend sein, ein recheneffizientes Problem zu lösen, um die Lösung für ein anderes zu erhalten. In dieser Arbeit wurde die eingeschränkte ℓ_p-Norm-Regularisierung gelöst, um die Lösung des rauschbeschränkten ℓ_p-Norm-Problems zu erreichen. Die auf der Optimalitätsverfolgung basierenden ℓ_p-Norm-Minimierungsansätze mit einfachen Wurzelfindungsiterationen für $1 \leq p \leq \infty$ werden hierzu vorgestellt. Der Optimalitäts-Trade-off zwischen beiden Zielen, der ℓ_p-Norm und einer Verlustfunktion, die die Datenfehlanpassung misst, wird als nichtlineares Gleichungswurzelfindungsproblem formuliert. Mehrere einfache, ableitungsfreie und kosteneffiziente Methoden zum Auffinden von nichtlinearen Gleichungswurzeln werden präsentiert und verwendet, um diese Optimalität über eine Pareto-Grenze zu verfolgen. Einige dieser Wurzelfindungsverfahren erfordern keine differenzierbaren Verlustfunktionen und sind sowohl für konvexe als auch für nichtkonvexe Datenfehlanpassungen anwendbar und erweitern solche Probleme auf eine breitere Klasse von Anwendungen. Wir führen auch eine Warmstart-Strategie ein, die eine lineare Lösung der kleinsten Quadrate mit derjenigen mit minimaler ℓ_2-Norm,

die *method of frames* (MOF) heißt, als Eingabe verwendet, um weniger Iterationen zu erfordern. Dieser Warmstart kann für viele Anwendungen, bei denen MOF bereits existiert, eine flexible und sinnvolle Startpunktinitialisierung bieten und durch ein besseres Verständnis der endlichdimensionalen Geometrie verbessert werden, z.B. n-widths. Der Einfluss der übervollständigen Matrix auf die Konvergenzrate einiger der vorgestellten Ansätze wird für Matrizen gezeigt, die das Uniform Uncertainty Principle und das Uncertainty Principle erfüllen. Diese Eigenschaften wurden früher eingeführt, um die Leistung von Zufallsmatrizen für ℓ_1- bzw. ℓ_∞-normbezogene Anwendungen zu analysieren.

Im letzten Teil der Arbeit, d. h. in Kapitel 7, werden ℓ_p-Norm-Minimierungs-bezogene Anwendungen mit verschiedenen Verlustfunktionen wie Least-Squares, Huber und einer nichtkonvexen Penalty untersucht Student's t. ℓ_1-norm wird mit einem typischen Compressed-Sensing-Beispiel minimiert. Außerdem wird ein generischer Testbenchmark für den Vergleich der nichtlinearen Gleichungswurzelfinder für die ℓ_1-Norm-Minimierung verwendet. Durch Minimierung der ℓ_∞-Norm wird ein neues Kommunikationsschema eingeführt. Das Problem der Ausreißererkennung wird mit der minimierten ℓ_∞-Norm untersucht und ein Prior wird für die minimierte ℓ_∞-Norm mit ihrer Leistung auf *peak-to-average power ratio* (PAPR) angeboten. Die rauschbeschränkte Nuklearnorm wird auch für das Euklidische Distanzmatrix-Ergänzungsproblem mit der Anwendung der drahtlosen Sensornetzwerklokalisierung minimiert.

To my loved ones...

Acknowledgements

This work benefited from the support, help and encouragement of many people.

First of all, I would like to express my deepest gratitude to my supervisor Prof. Sławomir Stańczak for giving me the opportunity to work with his group at the Technical University of Berlin and always being very supportive. I am sincerely grateful to Dr. Peter Jung for taking his time to many discussions and giving me constant feedback throughout my time at the Technical University of Berlin. I also would like to thank Prof. Aleksandr Aravkin from the University of Washington for the insightful discussions, and I sincerely appreciate his collaboration. My gratitude extends to my co-authors Dr. Nicola Kleppmann and M.Sc. Chun Yuan for our collaborations, Prof. Aydin Sezgin, for devoting his time to be a referee of this thesis and serving in my thesis committee.

I would like to thank all of my colleagues at the Heinrich-Hertz-Institut Fraunhofer and the Technical University of Berlin for creating a stimulating research and work environment.

Lastly, there are no words to adequately express my thankfulness to my lovely family, my fiancée Aysel, for their unconditional and unwavering support as well as to my beloved uncle Mehmet, whom I lost in September 2020 to Covid19, for always being a true role model for me and inspiring me to strive for the best.

Table of Contents

List of Figures

List of Tables

Acronyms

ANN *approximate nearest neighbour*.

BBU *baseband unit*.

C-RANs *cloud radio access networks*.

CDMA *code division multiple access*.

CS *compressive sensing*.

DoS *denial-of-service*.

EDM *Euclidean distance matrix*.

EDMC *Euclidean distance matrix completion*.

EM *expectation maximization*.

i.i.d. *independent identically distributed*.

MDS *multidimensional scaling*.

MIPS *maximum inner product search*.

MLE *maximum likelihood estimation*.

MOF *method of frames*.

MSE *minimum squared error*.

OFDM *orthogonal frequency division multiplexing*.

OPR *one-point retention*.

PAPR *peak-to-average power ratio*.

RIP *restricted isometry property*.

RMSD *root mean square deviation*.

RRHs *remote radio heads*.

RSS *received signal strengths*.

Acronyms

SDP *semidefinite programming*.

UEs *user equipments*.

UP *uncertainty principle*.

UUP *uniform uncertainty principle*.

WSN *wireless sensor network*.

ZF *zero-forcing*.

Chapter 1

Introduction

1.1 Motivation

ℓ_p-norm minimization is an important subject in a wide range of fields and applications involving ℓ_p-norm minimization can be broadly divided into two categories.

The first category of ℓ_p-norm minimization problems pertains to the nonlinear decoding, associates the applications of signal recovery and applied in *compressive sensing* (CS) which is a procedure of reconstructing signals from a very few samples and an emerging topic in signal processing, statistics, wireless communication, physics and more after the prominent works of [Can+06; CRT06; CT06a],[Don06]. CS can recover a signal from some incoherent measurements with a sampling rate significantly lower than the Nyquist rate by using the fact that a signal is sparse in some transform domain [Yar15]. For problems like compression [SCE01], image processing [PM92], denoising [DD95], sparse signals and the concept of sparsity have been widely utilized in signal processing. Mathematically, when a signal $\mathbf{x}$ has at most k nonzero elements, it is said to be k-sparse, in other expression $\|\mathbf{x}\|_0 \leq k$. For a given linear map of a signal $\mathbf{x}$ and under the assumption that the original signal $\mathbf{x}$ is sparse or compressible, it is instinctive to minimize $\|\mathbf{x}\|_0$ to recover sparse $\mathbf{x}$ from this linear mapping under the constraint of some consistency [FR13]. However, ℓ_p-norms are nonconvex for $p \in [0, 1)$, and hence minimizing $\|\mathbf{x}\|_0$ is difficult, computationally infeasible and NP-hard [Mut05; Nat95]. Convex problems are computationally tractable and can be solved efficiently with various optimization tools. $\|\mathbf{x}\|_1$ is convex and also promotes sparsity, therefore minimizing $\|\mathbf{x}\|_1$ instead of $\|\mathbf{x}\|_0$ makes the sparse recovery problem tractable and solvable with several fast solvers.

The second category of ℓ_p-norm minimization problems involves the applications that seek meaningful signal representations. They are referred to as pursuit of overcomplete signal representations since the signal representations are found by using an overcomplete matrix. Overcomplete signal representations provide many important advantages like robustness to additive and quantization noise, resilience to erasures and losses on the (communication) channel and design freedom for many problems in signal processing, communications and information theory for the applications in various areas such as coding theory [HP02], analog-to-digital converters [BH01; BPY06], *compressive sensing* (CS) [CT06b], *code division multiple access* (CDMA) [VA99], *orthogonal frequency division multiplexing* (OFDM) systems [CA07], denoising [Dra+03], segmentation and classification [Uns95], multiantenna code design [Sho+01], robust transmission [GKV99; GKK01], etc. Overcomplete signal representations can be obtained in several ways and one important class of the overcomplete representations is a representation with minimal ℓ_p-norm which can be obtained by solving an optimization problem with the ℓ_p-norm regularizer and a penalty function to calculate the data misfit. We call ℓ_p-norm representations for the overcomplete representations that are obtained via minimizing an ℓ_p-norm.

ℓ_p-norm minimization is a significant topic in a variety of fields, therefore efficient solvers are required. In this thesis, we introduce ℓ_p-norm minimization methods for convex ℓ_p-norms, i.e. ℓ_p-norms for $1 \leq p \leq \infty$, with simple root finding iterations. We are particularly interested in the noise-constrained ℓ_p-norm minimization. Although there are numerous optimization problem formulations that can be used to minimize an ℓ_p-norm, constraining the noise can provide a more meaningful optimization problem definition because when there is a known noise tolerance in an application, it can simply be inserted into the optimization problem and clearly formulate what to solve. Despite this, there are certain problems in addressing noise-constrained ℓ_p-norm minimization and plentiful computationally more efficient methods have been proposed for several forms of ℓ_p-norm minimization problem than the noise-constrained one. Since several optimization formulations can provide equivalent solutions, we solved a relatively simpler problem and used its solution to reach the solution of noise-constrained ℓ_p-norm minimization problem by tracing the optimality between the objectives ℓ_p-norm and a loss function which measures the data misfit. This optimality tracing is formulated as a nonlinear equation root finding problem and several methods are introduced and employed to solve it. The given root finders in this thesis can handle both non-differentiable and nonconvex loss functions, which extends the ℓ_p-norm minimization problems to a broader class of applications.

Unitary ℓ_p-norm balls for some different p values are depicted in Figure 1.1.

1.2 ℓ_p-norm Minimization

Let us assume that $\mathbf{D} \in \mathbb{R}^{M \times N}$ is an overcomplete matrix (can also commonly named as frame matrix) with the redundancy ratio $\omega = \frac{N}{M}$ where $M < N$, consider the ℓ_p-norm as a regularizer and ρ as a gauge[1][2] penalty to ensure data consistency, in

[1] A function ρ is called a *gauge* if it is nonnegative, positively homogeneous, convex and $\rho(0) = 0$.

[2] In this thesis, we considered ρ as to be a gauge for our analysis.

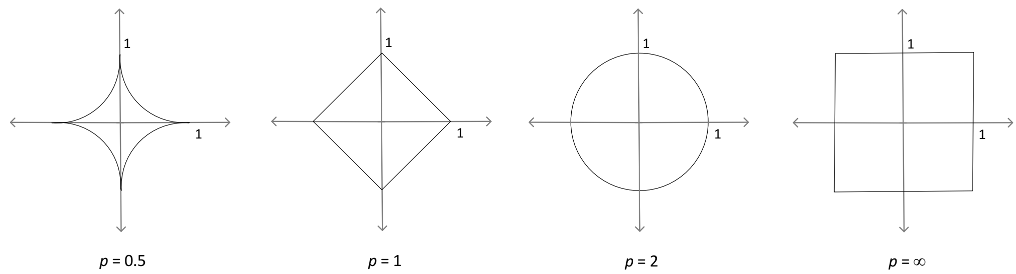

Figure 1.1: Unitary ℓ_p-norm balls for some different p.

order to obtain an ℓ_p-norm representation of a signal $\mathbf{y} \in \mathbb{R}^M$, or in other words recover an original $\mathbf{x} \in \mathbb{R}^N$ from a given measurement $\mathbf{y} \in \mathbb{R}^M$, first commonly utilized formulation is called noise-aware (or noise-constrained) ℓ_p-norm minimization problem and can be depicted as

$$(\mathrm{P}_\sigma^p) \qquad \underset{\mathbf{x}\in\mathbb{R}^N}{\text{minimize}} \quad \|\mathbf{x}\|_p \ \text{ s.t. } \ \rho(\mathbf{y}-\mathbf{D}\mathbf{x}) \leq \sigma,$$

where σ indicates the noise tolerance level. Second one is an unconstrained optimization problem, can be considered as a *Lagrangian* reformulation of (P_σ^p), and interpreted such

$$(\mathrm{P}_\lambda^p) \qquad \underset{\mathbf{x}\in\mathbb{R}^N}{\text{minimize}} \quad \lambda \|\mathbf{x}\|_p + \rho(\mathbf{y}-\mathbf{D}\mathbf{x}),$$

where $0 < \lambda$ is related to the *Lagrange multiplier* of the constraint in (P_σ) and controls the trade-off between the data misfit and the ℓ_p-norm. Third approach is the ℓ_p-norm constrained problem, which is

$$(\mathrm{P}_\tau^p) \qquad \underset{\mathbf{x}\in\mathbb{R}^N}{\text{minimize}} \quad \rho(\mathbf{y}-\mathbf{D}\mathbf{x}) \ \text{ s.t. } \ \|\mathbf{x}\|_p \leq \tau.$$

Among these optimization problems, (P_σ^p) is one of the most desired formulation to solve because of its real-life implication, e.g. when there is a known noise tolerance in an application, one can simply canalise it into the optimization problem and formulate exactly what to solve. Thus, it is often easier to set σ rather than λ and τ. Despite this, there are numerous computationally efficient algorithms introduced to solve (P_λ^p) and (P_τ^p) for several penalty functions which makes them more appealing and preferable to deal with rather than (P_σ^p).

Taking into account that (P_σ^p), (P_λ^p) and (P_τ^p) can provide equivalent solutions [FR13], the idea of solving (P_τ^p) to obtain the solution of (P_σ^p) is presented in [BF09; BF11] and applied for the ℓ_1-norm minimization. Their idea is based on tracing the optimal trade-off between the minimum ℓ_p-norm and a differentiable convex Pareto frontier which is the data misfit function. This optimality tracing is formulized as a non-linear equation root finding problem for a given σ such as

$$\text{find} \quad \tau \quad \text{such that} \quad \rho(\mathbf{r}_\tau) = \sigma, \tag{1.1}$$

where $\mathbf{r}_\tau = \mathbf{y} - \mathbf{D}\mathbf{x}_\tau$ is the residual for $\mathbf{x}_\tau$ which is the optimal solution of the (P_τ^p). Finding the τ that satisfies the noise tolerance condition in (1.1) is important, because then instead of solving (P_σ^p), solving (P_τ^p) that satisfies the condition in (1.1) can be an option since they will share the equivalent solution on the Pareto optimality.

The same concept of solving (P_σ^p) by tracing the Pareto optimal solutions has also been applied in [GLW12]. In order to solve (P_τ^1), an *accelerated proximal gradient method* is utilized in [GLW12], while a *spectral gradient-projection method* was employed in [BF09; BF11]. These works use convex losses and employ Newton's root finding method to solve (1.1). Newton's method requires differentiable loss functions, thus an inexact secant method has also been developed to address the differentiability issue in [Ara+19]. Ensuingly, it has been shown that the relationship between (P_σ^p) and (P_τ^p) does not require convexity [ABF13].

Newton's, secant and their vaiants can not guarantee to solve (1.1) if ρ is a nonconvex loss since the tangent or secant lines may cross the feasible region and can arrive to a negative τ. Hence, new root finding methods which are applicable for both convex and nonconvex losses can extend the problems (P_σ^p), (P_λ^p) and (P_τ^p) to the wider class of applications. Furthermore, Newton's method requires differentiable function in τ and derivative calculation of a loss function can be a costly operation in most of the cases. Beside differentiable loss function necessity and not offering convergence guarantee for a nonconvex ρ, Newton's method does not allow flexible starting points as well. For example, $\tau = 0$ is taken as an initial starting point of the Newton's method in [BF09; GLW12; BF11; Van09]. If ρ is convex, $\rho(\mathbf{r}_\tau)$ is convex decreasing in τ [Van09] and $\tau = 0$ can be considered as a good starting point for convergence speed since the absolute value of the derivative of a convex decreasing function also decreases with the function itself (envelope), however $\tau = 0$ relates to the maximum of the Pareto frontier and occurs at the maximum noise tolerance since the data misfit decreases in τ [Van09], i.e. it is the farthest point from the solution of small σ values. Higher values of τ causes lower step sizes for Newton's method iterations or even a divergence. Thus, Newton's method can not offer much flexibility about a warm-start strategy, however designing algorithms with a warm-start strategy that can lead to costly efficient iterations could be important.

1.3 Outline and Contributions of the Thesis

In this thesis, we introduce nonlinear equation root finding approaches to solve the problem (P_σ^p) for $1 \leq p \leq \infty$. Some of these root finding methods do not require differentiable loss functions and are applicable for both convex and nonconvex data misfits and extends ℓ_p-norm minimization problems to a broader class of applications. We also introduce an n-widths based warm-start strategy that provides meaningful and flexible starting point in many fields and accelerates (P_σ^p) solving. For matrices satisfying the *uniform uncertainty principle* (UUP) and *uncertainty principle* (UP), the impact of the overcomplete matrix on the convergence rate of some of the provided methods is presented. UUP and UP were formerly developed to investigate the performance of random matrices in ℓ_1 and ℓ_∞-norm related applications. This thesis is outlined as follows.

Chapter 2 introduces the frames and establishes the foundation for overcomplete representations. We remind that ℓ_p-norm minimization problems are formulated with using overcomplete matrices. Therefore, frame theory is required to comprehend overcomplete representations and ℓ_p-norm minimization. MOF and some ℓ_p-norms as overcomplete representations are also described in this chapter.

Chapter 3 explains the relation between finite-dimensional geometry in approximation theory and ℓ_p-norm representations using the concept n-widths. Unit ball in a normed space should satisfy some inequalities that can be expressed by n-widths. We use them to introduce ℓ_p-norm representation levels, which play an important role for our warm-start strategy.

Chapter 4 presents the matrix properties UUP and UP, which are developed to investigate the performance of random matrices in ℓ_1 and ℓ_∞-norm related applications. UUP and UP are important properties for understanding the performance of the measurement matrix for related recovery or representation methods. UUP and UP for some random matrices are given as well.

In **Chapter 5**, we present Pareto approach for (P_σ^p) minimization. The idea here is to trace the optimality trade-off between an ℓ_p-norm and a loss function, which makes possible to (P_σ^p) by solving relatively considered to be simpler problem of (P_τ^p). This optimality tracing is formulated as nonlinear equaiton root finding problem. We introduce and propose several nonlinear equation root finders to make solving (P_σ^p) easier with simple iterations. We divided root finders into categories according to whether they bracket the root or not. Every root finders have different benefits, e.g. bracketing-type root finders ensure convergence while open-type ones usually converge fast. Some of these root finding methods do not require differentiable loss functions and are applicable for both convex and nonconvex data misfits and extends (P_σ^p) to a wider range of applications. Moving outside of the convex class opens the door to many useful nonconvex models in (P_σ^p) formulations and is an appealing feature since loss functions in real-world applications are more likely to be nonconvex [GBC16]. For example, [SBV10] and [BG11] consider mixture models whose negative log-likelihood are nonconvex, with applications to high-dimensional inhomogeneous data where the number of covariates could be larger than sample size. Nonconvex losses are more difficult to cope with, but they can outperform their convex counterparts [MBM18; VAS21]. For instance, [ABP12; ABP13; Ara+12] use nonconvex Student's t likelihoods to develop outlier-robust approaches. In this chapter, we also introduce a warm-start strategy based on n-widths to require less iterations for solving (P_σ^p). Applicability of nonconvex losses are also inspected.

Chapter 6 presents the steps of solving (P_σ^p) which requires (P_τ^p) solvers and nonlinear equation root finders. We employ both projected gradient and projection-free Frank-Wolfe methods to solve (P_τ^p).

In **Chapter 7**, ℓ_p-norm related applications are investigated with some loss functions including a nonconvex one. (P_σ^p) is solved with some of the introduced approaches in this dissertation. ℓ_1-norm is minimized with a typical compressed sensing example. With minimizing ℓ_∞-norm a new communication architecture is introduced, outlier detection problem is studied and a prior is proposed for the minimized ℓ_∞-norm based on its performance on PAPR. With the applications of noisy Euclidean distance realization and wireless sensor network localization, the noise-constrained nuclear norm is also minimized with the introduced Pareto approach for the Euclidean distance matrix completion problem. Parts of the material in Chapter 7 were previously published in [1], [2], [3], [4], [7], [8].

In **Chapter 8**, we summarize our findings and contributions.

Further results that are not part of this dissertation

During my doctoral study, we obtained some results that are not part of this dissertation.

- In [5], we develop a novel semi-definite programming method to improve the localization estimation accuracy in noisy non-line-of-sight environments especially when there is not enough understanding of the environment. In addition to the localization approach, an innovative obstacle prediction method in such surroundings is proposed. Simulation results are significantly better than for existing similar approaches in the literature.

- In [9], some physical layer design approaches for quantize and forward strategies are investigated to improve and support machine type communication in existing and near future small-cell networks. Quantization effects on sum rate, equalization and soft demodulation are investigated with the introduced approaches.

Copyright Information

Parts of this thesis have already been published as journal articles and in conference and workshop proceedings as listed in the "List of Publication" on page 117. These parts, which are, up to minor modifications, identical with the corresponding scientific publication are copyrighted by the IEEE.

1.4 Notations

About notation, bold lowercase letters are used for vectors and bold uppercase letters stand for matrices. supp($\mathbf{x}$) stands for the support of a vector $\mathbf{x}$, which is the set of the indices corresponding to the non-zero elements in the vector $\mathbf{x}$. p^* represents the dual norm index of p, i.e. $1/p + 1/p^* = 1$ and the ℓ_p-norm of a vector $\mathbf{x} \in \mathbb{R}^N$ is given as follows:

$$||\mathbf{x}||_p = \begin{cases} \left(\sum_{i=1}^{N} |x_i|^p \right)^{\frac{1}{p}} & \text{if } \ 1 < p < \infty, \\ \max_{i \in \{1,\ldots,N\}} \{|x_i|\} & \text{if } \ p = \infty. \end{cases} \tag{1.2}$$

The Frobenius norm defined as $||\mathbf{X}||_F = \sqrt{\mathrm{tr}(\mathbf{X}\mathbf{X}^T)}$. ρ° represents the polar of a gauge function ρ and defined as

$$\rho^\circ(\mathbf{a}) := \sup_{\mathbf{b}} \{\mathbf{b}^T\mathbf{a} | \ \rho(\mathbf{b}) \leq 1\}. \tag{1.3}$$

Reminding that if ρ is an ℓ_p-norm then ρ° is the dual norm [ROC70], and the convex conjugate of a function $f(\mathbf{a})$ is defined as

$$f^*(\mathbf{b}) := \sup_{\mathbf{a}} \{\mathbf{b}^T\mathbf{a} - f(\mathbf{a})\}. \tag{1.4}$$

sign is the signum function is defined as follows:

$$\mathrm{sign}(x) = \begin{cases} -1 & \text{if } \ x < 0, \\ 0 & \text{if } \ x = 0, \\ 1 & \text{if } \ x > 0. \end{cases} \tag{1.5}$$

$\mathcal{B}_p^N \triangleq \{\mathbf{c} \in \mathbb{R}^N \ : \ \|\mathbf{c}\|_p \leq 1\}$ is the unit ball in ℓ_p.

Apart from the above introduced notation, we also use the following symbols:

Further notations

$\mathbb{R}$	the set of real numbers
$\mathbb{C}$	the set of complex numbers
$\mathsf{P}\{.\}$	probability
$\mathbb{E}[.]$	expectation operator
$\mathrm{proj}_{\mathcal{B}}$	projection on set $\mathcal{B}$
prox	proximal operator
$:=$	equal by definition
$\subseteq$	subset
$\cap$	intersection
$\circ$	Hadamard product
exp	exponential function
sech	hyperbolic secant
tanh	hyperbolic tangent
$\log(.)$	the base 2 logarithm $\log_2(.)$
$\mathbf{1}$	vector of all ones
$\mathrm{tr}\,(.)$	the trace operator
$\lceil . \rceil$	ceiling function that maps a real number to closest greater or equal integer
$\langle ., . \rangle$	inner product
$\forall$	for all
$\lvert . \rvert$	cardinality of a set or absolute value of a scalar
∇	gradient
$\mathrm{Diag}(\mathbf{X})$	diagonal entries of matrix $\mathbf{X}$
$\mathcal{O}(.)$	order of the function
min	minimum
max	maximum
arg min	argument of the minimum
$\mathbf{I}$	the identity matrix
$(.)^T$	transpose of a vector or matrix
$(.)^{-1}$	inverse of a matrix
$(.)^*$	adjoint of a matrix
$(.)^\dagger$	Moore–Penrose inverse

Chapter 2

Frame Theory and Overcomplete Representations

Frames were introduced for the first time by Duffin and Schaeffer [DS52] and have gained increasing interest in many applications, specifically the aspect of redundant linear signal expansion namely overcomplete representations, through these works [Dau88; Dau90; Dau92; DGM09; HW89; Sid98]. In an overcomplete representation the number of basis vectors is greater than the dimensionality of the input. Also, the overcomplete representation of an input is not a unique combination of basis vectors and there are infinitely many representation possibilities. Having representation solutions regarding the number of basis vectors can be classified such:

- If the number of basis vectors is greater than the dimensionality of the input data, we have infinitely many solutions. This is the overcomplete representation case.
- If the number of basis vectors is equal to the dimensionality of the input data, we have a unique solution.
- If the number of basis vectors is smaller than the dimensionality of the input data, we may have no solutions. This condition occurs in the non-redundant representation case.

Main disadvantage of non-redundant signal expansions is that any loss, corruption or erasure of expansion coefficients can cause crucial reconstruction errors. On the contrary, it is well-known that the frame based overcomplete signal representations offer robustness to additive and quantization noise, resilience to erausures and losses on the channel and design freedom for many problems in communications, signal processing and information theory. The idea of using them is to benefit from the redundancy of the frame both in the case of random losses of transmitted signal by alleviating the reconstruction error and existing noises like quantization and/or channel. Distributing the information (most preferably equally) among the transmitted signal and creating dependency between transmitted signal elements is an important topic here since dependency between these signal elements is a necessity to reconstruct the source vector. Because of these appealing properties, overcomplete representations have been studied in several different fields. A pleasant literature review about overcomplete representations and applications can be found in [BES06; KC08] and references therein.

2.1 Frame-Based Approaches as Decomposition into Overcomplete Systems

Let us introduce a simple motivating signal expansion example.

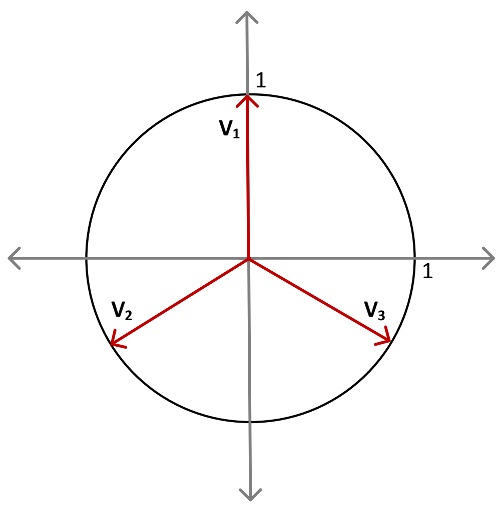

Figure 2.1: The Mercedes-Benz frame.

Example 2.1. *(Mercedes-Benz Frame [KC08]). Consider following vectors*

$$\mathbf{v}_1 = \begin{bmatrix} 0 \\ 1 \end{bmatrix}, \quad \mathbf{v}_2 = \begin{bmatrix} -\sqrt{3}/2 \\ -1/2 \end{bmatrix}, \quad \mathbf{v}_3 = \begin{bmatrix} \sqrt{3}/2 \\ -1/2 \end{bmatrix}, \tag{2.1}$$

in $\mathbb{R}^2$*. Vectors* $\mathbf{v}_1$*,* $\mathbf{v}_2$ *and* $\mathbf{v}_3$ *forms the Mercedes-Benz frame which is depicted in Figure 2.1. A signal* $\mathbf{y}$ *can be represented as the following linear combination of the basis vectors* $\mathbf{v}_1$*,* $\mathbf{v}_2$ *and* $\mathbf{v}_3$ *such:*

$$\mathbf{y} = \langle \mathbf{y}, \mathbf{v}_1 \rangle \mathbf{v}_1 + \langle \mathbf{y}, \mathbf{v}_2 \rangle \mathbf{v}_2 + \langle \mathbf{y}, \mathbf{v}_3 \rangle \mathbf{v}_3. \tag{2.2}$$

Let us define the expansion coefficients as

$$\mathbf{x} = \begin{bmatrix} x_1 \\ x_2 \\ x_3 \end{bmatrix} := \begin{bmatrix} \langle \mathbf{y}, \mathbf{v}_1 \rangle \\ \langle \mathbf{y}, \mathbf{v}_2 \rangle \\ \langle \mathbf{y}, \mathbf{v}_3 \rangle \end{bmatrix} = \begin{bmatrix} \mathbf{v}_1^T \\ \mathbf{v}_2^T \\ \mathbf{v}_3^T \end{bmatrix} \mathbf{y}, \tag{2.3}$$

and define the matrix

$$\mathbf{T} := \begin{bmatrix} \mathbf{v}_1^T \\ \mathbf{v}_2^T \\ \mathbf{v}_3^T \end{bmatrix} = \begin{bmatrix} 0 & 1 \\ -\sqrt{3}/2 & -1/2 \\ \sqrt{3}/2 & -1/2 \end{bmatrix}. \tag{2.4}$$

Then it will be

$$\mathbf{x} = \mathbf{T}\mathbf{y}. \tag{2.5}$$

The matrix $\mathbf{T}$ *is called analysis operator which multiplies the signal* $\mathbf{y}$ *to generate the representation vector and the signal* $\mathbf{y}$ *can be reconstructed from the representation vector* $\mathbf{x}$ *such*

$$\mathbf{y} = \mathbf{T}^T\mathbf{x}. \tag{2.6}$$

The adjoint $\mathbf{T}^*$ *of the analysis operator* $\mathbf{T}$ *is called the synthesis operator.*

Definition 2.1. A matrix $\mathbf{T}^T \in \mathbb{R}^{M \times N}$ with $M \leq N$ is a frame matrix where it columns are set of vectors and satisfies following frame condition: if there exists $0 < A \leq B < \infty$ such that

$$A||\mathbf{t}||_2^2 \leq ||\mathbf{T}\mathbf{t}||_2^2 \leq B||\mathbf{t}||_2^2, \tag{2.7}$$

holds for any vector $\mathbf{t} \in \mathbb{R}^M$. A and B are called as lower and upper frame bounds $(A \in \mathbb{R}, B \in \mathbb{R})$ respectively.
A frame is called

- *tight frame* if $A = B$,
- *normalized tight frame (or Parseval) frame* if $A = B = 1$,
- *uniform frame* if all of its rows have the equal norm and $A = B$,
- *uniform tight frame* if all of its rows have the same norm equal to 1 and $A = B$. For a uniform frame, frame bound gives the redundancy ratio.

A shorthand formulation of (2.7) is

$$A\mathbf{I}_M \leq \mathbf{T}^T\mathbf{T} \leq B\mathbf{I}_M, \tag{2.8}$$

where $\mathbf{I}_M$ is the $M \times M$ identity matrix, and $A\mathbf{I}_M = B\mathbf{I}_M = \mathbf{T}^T\mathbf{T}$ if and only if $\mathbf{T}^T$ is a tight frame operator.

2.2 Method of Frames

Overcomplete representation of a signal can be obtained in several ways as indicated in [CDS01]. Some methods are *matching pursuit* [MZ93], *basis pursuit* [CDS01; CD94] and *best orthogonal basis* [CW92]. Besides these methods, one of the well-known decomposition into an overcomplete system method is called *method of frames* (MOF), proposed in [Dau88]. MOF yields the linear least-squares solution with the minimum ℓ_2-norm.

Let us denote the MOF with $\mathbf{x}_{MF}$, then

$$\mathbf{x}_{MF} = \arg\min_{\mathbf{x}\in\mathbb{R}^N} \{\|\mathbf{x}\|_2 \quad \text{s.t.} \quad \mathbf{y} = \mathbf{D}\mathbf{x}\}. \tag{2.9}$$

$\mathbf{x}_{MF}$ can be obtained with the Moore–Penrose inverse linear mapping such that $\mathbf{x}_{MF} = \mathbf{D}^\dagger \mathbf{y}$.

A similar notion, frame expansion, is the case when the signal to be represented is expanded by a frame matrix [GKV99; GKK01]. It has very close relation with the MOF related with the frame bounds. A frame expansion of $\mathbf{y}$ denoted as $\mathbf{x}_F = \mathbf{D}^T\mathbf{y}$ (and $\mathbf{x}_F = A\mathbf{x}_{MF} = B\mathbf{x}_{MF}$ for tight frames since $A\mathbf{I}_M = B\mathbf{I}_M = \mathbf{D}\mathbf{D}^T$). For the clearness of this work, analysis will be based on MOF in this thesis, however since frame expansions have an important place in many fields, its relation with MOF is pointed out as well.

Frame-based approaches as decomposition into overcomplete systems are not unique and different applications may require different goals. Thus, several disciplines have been looking for finding useful redundant representations using frames instead of frame (or MOF) representations. Most obvious example for that is the ℓ_1-norm representation where most of the representation coefficients are equal to 0. Another, relatively very less investigated, example is the ℓ_∞-norm representation where most of the representation coefficients are equal.

2.3 Some ℓ_p-norms as Approximate Overcomplete Representations

ℓ_p-norms are used for finding approximate overcomplete representations for several purposes in many applications and can be obtained by solving optimization problems such $(\mathrm{P}^p_\sigma), (\mathrm{P}^p_\tau)$ and (P^p_λ). Because these optimization problems can take noise into account, ℓ_p-norms are used to find approximate overcomplete representations. If $\sigma = 0$, then the representations become exact.

2.3.1 ℓ_1-norm Representations

ℓ_1-norm representations, also called sparse representations, are powerful tools for many purposes like compressing, representing, efficiently acquiring and reconstructing of signals, etc. Moreover, they have been widely used in recent years [Wri+10; DE03; Ela10; EFM10; Fuc04; ZEP10; GN03; Yan+11; Mo+13; Nik+15]. The main purpose of the sparse representations is to represent signals with as few meaningful coefficients as possible. A comprehensive literature review about sparse representations and applications can be found in [Zha+15] and references therein.

2.3.2 ℓ_2-norm Representations

Finding ℓ_2-norm representations, which can also be named *least-squares* representations, is very common in many disciplines particularly in signal processing and communication applications. For instance, ℓ_2-norm representations are used for least-squares precoding, i.e. linear zero-forcing precoding, as well as [SL13]. It is very commonly used in communication because of computational efficiency, in contrast to other linear precoding strategies [WES08].

The main motivation of minimizing ℓ_2-norm is to find a representation with the minimum energy. Particularly, when there is no noise, the solution of (P^2_σ) will have a closed form and unique solution which makes solving the optimization problem unnecessary. This solution was formerly introduced as MOF.

2.3.3 ℓ_∞-norm Representations

Although ℓ_1 and ℓ_2-norm representations are well studied, ℓ_∞-norm representations (can also be named as Kashin's, democratic, spread, anti-sparse representations in different studies) did not get the attention it deserved. It is a very useful instrument in many applications such as peak-to-average power ratio (PAPR) reduction, vector quantization, approximate neighbour search and control engineering [Stu+14], [SYB12]. The most appealing feature of the ℓ_∞-norm minimization problem is to provide democratic representation by enforcing the signal to be spread evenly [JFF11; Fuc11]. Lyubarskii presented that some frames that satisfy some properties yield computable ℓ_∞-norm representations that empower the representation with the smallest possible dynamic range [LV10]. Studer proposed algorithms to obtain as they called democratic representations and utilized them for peak to average power ratio reduction in multi-carrier transmissions on orthogonal frequency division multiplexing systems [Stu+14; SYB12; SL13]. [JFF11] and [VJS17a] both presented new methods to obtain these ℓ_∞-norm minimized representations and used them to perform better approximate nearest neighbour search. [ECD17] and [VJS17b] approached this topic in a probabilistic perspective and proposed priors. Minimized ℓ_∞-norms are also utilized for robust beamforming in [Jia+18] and for *minimum-effort control problem* in [Neu62; Cad71].

[FJ09] studied the relationship between the PAPR and achievable data rates via ℓ_∞-norm representations while [EH20] proposed a methodology to accelerate solving the ℓ_∞-norm minimization problem.

An example of ℓ_p-norm representations are depicted in Figure 2.3. A signal $\mathbf{y} \in \mathbb{R}^{75}$, plotted in Figure 2.2, is created and an example of its ℓ_1, ℓ_2 and ℓ_∞-norm representations, $\mathbf{x} \in \mathbb{R}^{200}$, is generated with a normally distributed Parseval frame $\mathrm{D} \in \mathbb{R}^{75\times 200}$ via solving (P^p_σ) with $\sigma = 0$.

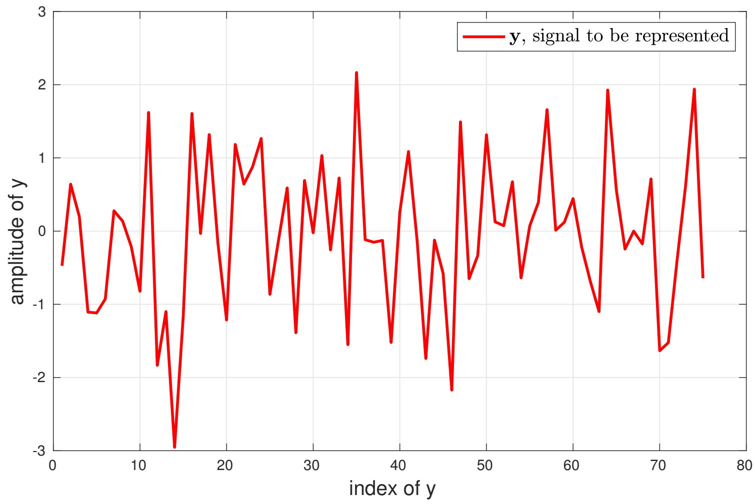

Figure 2.2: A signal $\mathbf{y}$ to be represented.

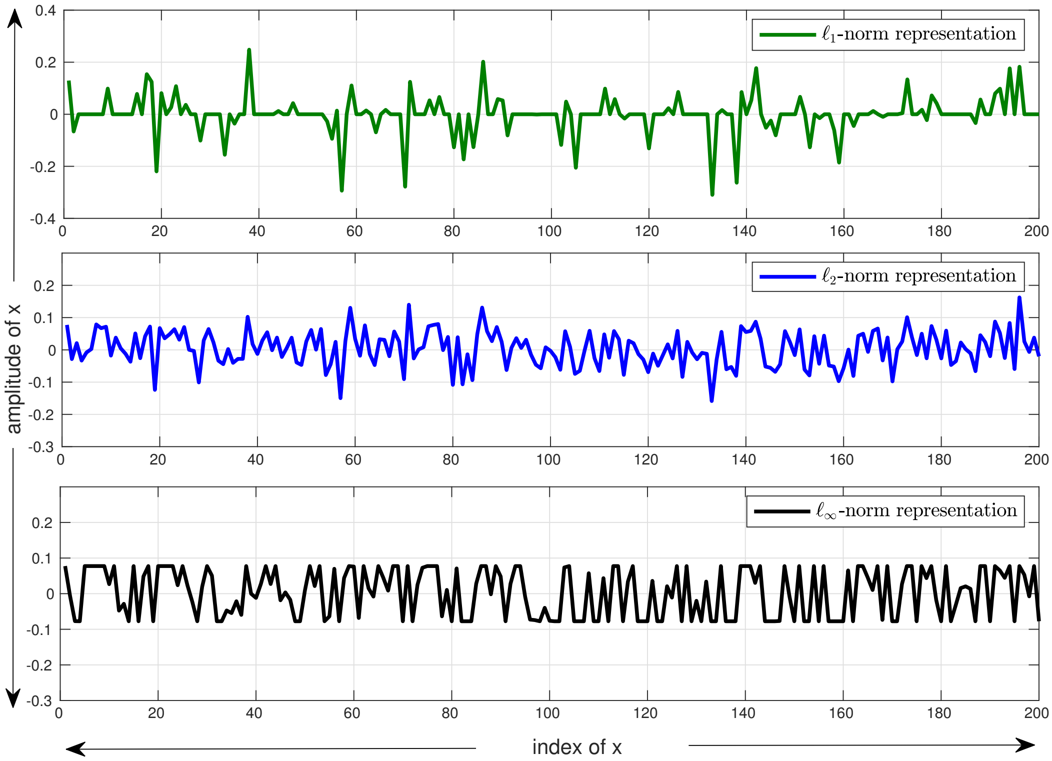

Figure 2.3: From top to bottom, examples of ℓ_1, ℓ_2 and ℓ_∞-norm representations.

Chapter 3

n-widths and ℓ_p-norm Representations

Finite-dimensional geometry in approximation theory helps us to understand the relation between the ℓ_p-norm representation and the concept n-widths.

3.1 Gelfand n-widths

In this work, we utilize the Gelfand n-widths for our analysis. Comprehensive analysis about n-widths can be found in [Pin85].

Definition 3.1. Let us denote ℓ_q^N to represent ℓ_q-norm of a vector in $\mathbb{R}^N$ and $\mathcal{B}_p^N \triangleq \{\mathbf{c} \in \mathbb{R}^N \ : \ \|\mathbf{c}\|_p \leq 1\}$ is the unit ball in ℓ_q^N. For a normed linear space ℓ_q^N and a closed, convex, centrally symmetric subset like $\mathcal{B}_p^N$, the Gelfand n-width is defined as

$$d^n(\mathcal{B}_p^N)_{\ell_q^N} := \inf_{\mathcal{L}^n} \sup_{\mathbf{x} \in \mathcal{B}_p^N \cap \mathcal{L}^n} \|\mathbf{x}\|_q \,, \tag{3.1}$$

where $\mathcal{L}^n$ is a subspaces that varies over all subspaces of ℓ_q^N of codimension n.

Corollary 3.1. *Gelfand widths satisfy the inequality* $d^n(\mathcal{B}_p^N)_{\ell_q^N} \leq d^n(\mathcal{B}_{q^*}^N)_{\ell_p^N}$.

Proof.

$$\begin{aligned}
d^n(\mathcal{B}_p^N)_{\ell_q^N} = \inf_{\mathcal{L}^n} \sup_{\mathbf{a}\in\mathcal{B}_p^N\cap\mathcal{L}^n} \|\mathbf{a}\|_q \leq \sup_{\mathbf{a}\in\mathcal{B}_p^N\cap\mathcal{L}^n} \|\mathbf{a}\|_q \\
= \sup_{\mathbf{a}\in\mathcal{B}_p^N\cap\mathcal{L}^n} \sup_{\mathbf{b}\in\mathcal{B}_{q^*}^N} \langle \mathbf{a}, \mathbf{b}\rangle \\
= \sup_{\mathbf{a}\in\mathcal{B}_p^N\cap\mathcal{L}^n} \sup_{\mathbf{b}\in\mathcal{B}_{q^*}^N\cap\mathcal{L}^n} \langle \mathbf{a}, \mathbf{b}\rangle \\
= \sup_{\mathbf{b}\in\mathcal{B}_{q^*}^N\cap\mathcal{L}^n} \sup_{\mathbf{a}\in\mathcal{B}_p^N\cap\mathcal{L}^n} \langle \mathbf{a}, \mathbf{b}\rangle \\
\leq \sup_{\mathbf{b}\in\mathcal{B}_{q^*}^N\cap\mathcal{L}^n} \|\mathbf{b}\|_{p^*} \sup_{\mathbf{a}\in\mathcal{B}_p^N\cap\mathcal{L}^n} \|\mathbf{a}\|_p \\
\leq \sup_{\mathbf{b}\in\mathcal{B}_{q^*}^N\cap\mathcal{L}^n} \|\mathbf{b}\|_{p^*} \sup_{\mathbf{a}\in\mathcal{B}_p^N} \|\mathbf{a}\|_p = d^n(\mathcal{B}_{q^*}^N)_{\ell_p^N}
\end{aligned} \tag{3.2}$$

□

3.2 n-widths and ℓ_p-norm Representations

In order to obtain an ℓ_p-norm representation of a signal $\mathbf{y} \in \mathbb{R}^M$, $\mathbf{D}$ is introduced as a measurement matrix, can also be considered as an encoder, that maps $\mathbb{R}^N$ into $\mathbb{R}^M$, where $N > M$ such

$$\mathbf{y} = \mathbf{D}\mathbf{x}. \tag{3.3}$$

We are aware that $\mathbf{y}$ holds information about $\mathbf{x}$.

Allow us define a decoder, Δ, that performs reverse mapping from $\mathbb{R}^M$ to $\mathbb{R}^N$,

$$\bar{\mathbf{x}} = \Delta(\mathbf{y}) = \Delta(\mathbf{D}\mathbf{x}). \tag{3.4}$$

Essence of the ℓ_p-norm representations is to comprehend the relation between the encoding and decoding, in particularly to answer what are the satisfactory $\mathbf{D}$ and Δ.

Let us measure the error on $\mathbf{x}$ between the encoder and the decoder with ℓ_X-norm as following

$$E(\mathbf{x}, \mathbf{D}, \Delta)_X := \|\mathbf{x} - \Delta(\mathbf{D}\mathbf{x})\|_X . \tag{3.5}$$

Now consider any closed and bounded set in $\mathbb{R}^N$ like $\mathcal{B}_p^N$, then a worst-case error between the mapping and the reverse mapping Δ on $\mathcal{B}_p^N$ is

$$E(\mathcal{B}_p^N, \mathbf{D}, \Delta)_X := \sup_{\mathbf{x}\in\mathcal{B}_p^N} E(\mathbf{x}, \mathbf{D}, \Delta)_X \tag{3.6}$$

since the largest error on the set $\mathcal{B}_p^N$ determines the error. Let $\mathcal{A}_{M,N}$ denotes all possible encoder/decoder pairs $(\mathbf{D}, \Delta)$. Then the worst reconstruction error for the best pair of $(\mathbf{D}, \Delta)$ is

$$E_{M,N}(\mathcal{B}_p^N)_X := \inf_{(\mathbf{D},\Delta)\in\mathcal{A}_{M,N}} E(\mathcal{B}_p^N, \mathbf{D}, \Delta)_X, \tag{3.7}$$

Between n-widths and the optimal ℓ_p-norm representations, there is a clear and straightforward link.

Proposition 3.1. *Assume $X = (\mathbb{R}^N, \|.\|_X)$ is a normed space and $K \subset \mathbb{R}^N$ is a closed compact set such that $K = -K$ and $K + K \subset C_0 K$ for some constant C_0. Then*

$$d^n(K)_X \leq E_{M,N}(K)_X \leq C_0 d^n(K)_X, \qquad 1 \leq M \leq N. \tag{3.8}$$

For the proof of Proposition 3.1 please check [Proposition 3.8 [FR11]].

Theorem 3.1. *[Glu84, Theorem 1] For $1 \leq n \leq N < \infty$ and $1 \leq p, q \leq \infty$, let us define*

$$\Phi(N,n,p,q) = \begin{cases} (N-n+1)^{\frac{1}{q}-\frac{1}{p}} & \text{if } 1 \leq q \leq p \leq \infty \\ \left(\min\{1, N^{1-\frac{1}{p}} n^{-\frac{1}{2}}\}\right)^{\frac{\frac{1}{p}-\frac{1}{q}}{\frac{1}{p}-\frac{1}{2}}} & \text{if } 1 < p < q \leq 2 \\ \max\{N^{\frac{1}{q}-\frac{1}{p}}, \sqrt{1-\frac{n}{N}}^{\frac{\frac{1}{p}-\frac{1}{q}}{\frac{1}{2}-\frac{1}{q}}}\} & \text{if } 2 \leq p < q \leq \infty \\ \max\{N^{\frac{1}{q}-\frac{1}{p}}, \min\{1, N^{1-\frac{1}{p}} n^{-\frac{1}{2}}\}\sqrt{1-\frac{n}{N}}\} & \text{if } 1 < p \leq 2 < q \leq \infty \end{cases} \tag{3.9}$$

Then

$$d^n(\mathcal{B}_p^N)_{\ell_q^N} \leq C_{p,q}\Phi(N,n,p,q), \tag{3.10}$$

where $C_{p,q}$ is a constant that ensures $d^n(\mathcal{B}_p^N)_{\ell_q^N} \leq 1$, and only depends on p and q.

Furthermore, according to [GG84], there exists a constant $C_{1,2} > 0$ independent of N and n for which

$$d^n(\mathcal{B}_1^N)_{\ell_2^N} \leq C_{1,2} \left(\frac{\log(1+\frac{N}{n})}{n} \right)^{1/2}. \tag{3.11}$$

Remark 3.1. By using eq. (3.11) and Corollary 3.1, it is also possible to note $d^n(\mathcal{B}_2^N)_{\ell_\infty^N} \leq d^n(\mathcal{B}_1^N)_{\ell_2^N}$.

Asymptotic behavior of the Gelfand n-width of the unit ball in a normed space, i.e. $d^n(\mathcal{B}_p^N)_{\ell_q^N}$, is investigated in several works[1] [Vyb08]. Bounds on the $d^n(\mathcal{B}_p^N)_{\ell_q^N}$ implies the existence of a projection of the ℓ_p-ball onto a subspace with a lower dimension and provides favorable properties for ℓ_p-norm representations, e.g. lower bounds of $d^n(\mathcal{B}_1^N)_{\ell_2^N}$ allow us to analyze the minimal number of required samples for an approximate sparse recovery using any recovery method via any measurement matrix

[1]Some studies investigated *Kolmogorov widths* which is related with the *Gelfand widths* by the duality formula.

D. In the same way upper bounds for $d^n(\mathcal{B}_p^N)_{\ell_q^N}$ provide insight about the order of the projection of the ℓ_p-ball onto a subspace as it is investigated for $d^n(\mathcal{B}_2^N)_{\ell_\infty^N}$ in [LV10]. Upper bounds for the $d^n(\mathcal{B}_p^N)_{\ell_q^N}$ are given in Theorem 3.1 for different p and q.

In this work, obtaining ℓ_p-norm representations took our interest and that can be considered as finding an M-dimensional subset $\mathcal{B}_2^N$ of ℓ_p^N, thus bound of $d^{N-M}(\mathcal{B}_2^N)_{\ell_q^N}$ can provide some important knowledge about the *representation level* of ℓ_p-norms which is introduced in Corollary 3.2.

Corollary 3.2. *Representation level of ℓ_p-norms based on n-widths: For any $M \leq N$, for all $\mathbf{y}$ there exists an $\mathbf{x}$ and $\mathbf{D}$ with $\mathbf{y} = \mathbf{D}\mathbf{x}$, satisfies $\|\mathbf{x}\|_p \leq K_p \|\mathbf{y}\|_2$ with the level of $K_p = d^{N-M}(\mathcal{B}_2^N)_{\ell_q^N}$.*

Remark 3.2. With the help of Corollary 3.2

$$\begin{aligned} K_\infty &= C_{2,\infty} \left(\sqrt{\frac{1}{N-M} \log\left(1 + \frac{N}{N-M}\right)} \right) \\ &= \frac{C_{2,\infty}}{\sqrt{N}} \left(\sqrt{\frac{\omega}{\omega-1} \log\left(1 + \frac{\omega}{\omega-1}\right)} \right) \end{aligned} \tag{3.12}$$

and

$$K_1 = C_{2,1} \left(\sqrt{M+1} \right) \tag{3.13}$$

can be derived.

The term $C_{2,\infty} \left(\sqrt{\frac{\omega}{\omega-1} \log\left(1 + \frac{\omega}{\omega-1}\right)} \right)$ is called Kashin level and depends only on the redundany ratio $\omega = N/M$. Reminding that K_∞ is based on the classical result of [Kas77] and the optimal dependency is given in [GG84].

Chapter 4

Matrix Conditioning

One of the main concerns about ℓ_p-norm representations is to comprehend the performance of the measurement matrix and in order to inspect the quality of the measurement matrix for associated recovery or representation algorithms, there are some properties that are introduced for some specific cases of (P_σ^p), especially for (P_σ^1), such as *k-neighborly polytopes* [DT05], *restricted isometry property* (RIP) [Don06], [CRT06], some modified versions of RIP [Ber+08] and some others can be found in [IR08]. RIP, also called *uniform uncertainty principle* (UUP), places an isometry condition on the measurement matrix $\mathbf{D}$ and it is the most referenced property in regards to evaluating the measurement matrix quality. Similar notion is introduced in [LV10] to show the existence of a Kashin level, called *uncertainty principle* (UP).

4.1 Matrix Properties

The UUP and the UP are analogous, however the UUP has stronger assumptions than the UP [LV10]. Both of them condition the measurement matrix $\mathbf{D} \in \mathbb{R}^{M \times N}$ with bounds $\alpha_t, \beta_t \in \mathbb{R}^+$, for given s such

$$\alpha_t \|\mathbf{x}\|_t \leq \|\mathbf{D}\mathbf{x}\|_t \leq \beta_t \|\mathbf{x}\|_t \,, \quad \text{for all} \;\; |\mathrm{supp}(\mathbf{x})| \leq s. \tag{4.1}$$

4.1.1 Uniform Uncertainty Principle

Definition 4.1. *Uniform Uncertainty Principle* [CT05]: A matrix $\mathbf{D} \in \mathbb{R}^{M \times N}$ satisfies the UUP, with order of s and constant $\epsilon \in (0, 1)$, if eq. (4.1) holds where $t = 2$, $\alpha_2 = (1 - \epsilon)$, $\beta_2 = (1 + \epsilon)$.

4.1.2 Uncertainty Principle

Definition 4.2. *Uncertainty Principle* [LV10]: A frame $\mathbf{D} \in \mathbb{R}^{M \times N}$ satisfies the UP with constants $\delta \in (0, 1)$ and η, if eq. (4.1) holds where $t = 2$, $\alpha_2 = 0$, i.e. there is no condition on α_2, $\beta_2 = \eta$ and $s = \delta N$.

Relation between UP and UUP for matrices with orthonormal rows is given in [LV10] with the following Corollary 4.1.

Corollary 4.1. *The UUP with parameters s and ϵ follows the UP with $\eta = \frac{1+\epsilon}{1-\epsilon}\sqrt{\frac{M}{N}}, \delta$ for the uniform tight frames.*

For the proof of Corollary 4.1, please check [LV10].

4.2 Random Matrices and Matrix Properties

In this section, UP and UUP with some random matrices are presented. UUP for random sub-Gaussian matrices is given in Section 4.2.1 while UP for random orthogonal matrices, random partial Fourier matrices and random sub-Gaussian matrices which are given in [LV10] summarized in Section 4.2.2.

Definition 4.3. A random variable X is called to be sub-Gaussian with parameter ς if

$$\mathsf{P}\{|X| > t\} \leq \exp(1 - t^2/\varsigma^2), \quad \forall t > 0. \tag{4.2}$$

Matrices with orthonormal rows plays an important role for the UP and sub-Gaussian matrices, i.e. random matrices with *independent identically distributed* (i.i.d.) sub-Gaussian entries, mostly do not have orthonormal rows. In order to handle this situation, almost orthogonality of sub-Gaussian matrices expressed in [LV10; Lit+05].

Lemma 4.1. *(Almost Orthogonality of sub-Gaussian Matrices) Assume $\mathbf{D}$ is a $M \times N$ matrix with i.i.d. zero mean sub-Gaussian random variable entries with parameter ς and with variance 1. One can find some positive constants ($e(\varsigma)$, $E(\varsigma)$) depending only on ς such that $N > \frac{E(\varsigma)}{\xi^2}\log\left(\frac{2}{\xi}\right)M$ for some $\xi \in (0,1)$ that (which) induces*

$$\mathsf{P}\left\{\left\|\mathbf{I}_{M\times M} - \frac{1}{N}\mathbf{D}\mathbf{D}^T\right\|_2 > \xi\right\} \geq 1 - 2\exp(-e(\varsigma)N\xi^2), \quad \forall t > 0. \tag{4.3}$$

Corollary 4.2. *Assume $\mathbf{D} \in \mathbb{R}^{M\times N}$ is a matrix such as mentioned in Lemma 4.1. Then $\frac{1}{\sqrt{N}}\mathbf{D}$ is a ξ-Parseval frame with the frame bounds $A = 1-\xi, B = 1+\xi$ for some small $\xi > 0$ (for proof check [LV10]).*

4.2.1 UUP with Random Matrices

Theorem 4.1. *UUP for sub-Gaussian Matrices: Consider a matrix $\mathbf{D} \in \mathbb{R}^{M\times N}$ with i.i.d. zero mean sub-Gaussian random variable entries with parameter ς. $\frac{1}{\sqrt{M}}\mathbf{D}$ satisfies the Uniform Uncertainty Principle with probability at least $1-\epsilon$ provided that $M > C_\varsigma \epsilon^{-2} s \log(N/s)$ where C_ς is a constant depending on ς [FR13].*

4.2.2 UP with Random Matrices

Theorem 4.2. *(UP for Random Orthogonal Matrices) Assume there is a constant* $0 < c_1 = \omega - 1$*. A random orthogonal matrix* $\mathbf{D} \in \mathbb{R}^{M\times N}$ *satisfies the UP with the parameters*

$$\eta = 1 - \frac{c_1}{4}, \tag{4.4}$$

$$\delta = \frac{c_2 c_1^2}{\log\left(\frac{1}{c_1}\right)}, \tag{4.5}$$

with probability at least $1 - 2\exp(-c_2 c_1^2 M)$ *where* $0 < c_2$ *is an absolute constant.*

Theorem 4.3. *(UP for Random Partial Fourier Matrices) Assume* Ψ *is an orthogonal* $N \times N$ *matrix and its entries are upper bounded with* $c_3\sqrt{N}$ *with some constant* c_3*. Let* $\mathbf{D}$ *is a* $M \times N$ *submatrix of* Ψ *and* $N = (1 + c_4)M$ *for some* $c_4 \in (0, 1]$*, then for any* $p \in (0, 1)$ *there exists a constant* $0 < c_5$ *depends on the* p *and* c_3 *such that the matrix* $\mathbf{D}$ *satisfies the UP with the parameters*

$$\eta = 1 - \frac{c_4}{4}, \tag{4.6}$$

$$\delta = \frac{c_5 c_4^2}{\log^4(N)}, \tag{4.7}$$

with probability at least $1 - p$*.*

Theorem 4.4. *(UP for sub-Gaussian Matrices) Consider a matrix* $\mathbf{D} \in \mathbb{R}^{M\times N}$ *with i.i.d. zero mean sub-Gaussian random variable entries with parameter* ς*.* $\frac{1}{\sqrt{N}}\mathbf{D}$ *satisfies the UP for* $\omega \geq 2$ *with parameters*

$$\eta = c_6 \varsigma \sqrt{\frac{\log(\omega)}{\omega}}, \tag{4.8}$$

$$s = \frac{c_7}{\omega}, \tag{4.9}$$

with probability at least $1 - (\omega)^{-M}$ *where* c_6 *and* c_7 *are the positive absolute constants.*

Corollary 4.3. *Let us consider the following events:* S_1 *as a matrix* $\mathbf{D}$ *as in Theorem 4.4 that satisfies the UP and* S_2 *as the event of the same matrix being* ξ*-Parseval frame, i.e.* $S_2 := \left\{\left\|\mathbf{I}_{M\times M} - \frac{1}{N}\mathbf{D}\mathbf{D}^T\right\|_2 > \xi\right\}$*. Probability of* S_1 *and* S_2 *happening at the same time can be bounded such*

$$1 - \exp(\min\{-1, -C_{\varsigma,\xi}\}\log(\omega)M) \leq \mathsf{P}\{S_1 \cap S_2\} \tag{4.10}$$

where $C_{\varsigma,\xi}$ *is a constant depends on* ς *and* ξ*.*

Proof. By using the union bound

$$\begin{aligned}
\mathsf{P}\{S_1\} + \mathsf{P}\{S_2\} - 1 &\leq \mathsf{P}\{S_1 \cap S_2\} \\
1 - \exp(-e(\varsigma)N\xi^2 + \log 2) - \exp(-M\log(\omega)) &\leq \mathsf{P}\{S_1 \cap S_2\} \\
1 - \exp(\min\{-e(\varsigma)\log(\omega)M\xi^2, -M\log(\omega)\}) &\leq \mathsf{P}\{S_1 \cap S_2\} \\
1 - \exp(\min\{-1, -C_{\varsigma,\xi}\}\log(\omega)M) &\leq \mathsf{P}\{S_1 \cap S_2\}
\end{aligned} \tag{4.11}$$

since $N/M \geq 2$ is a requisite for S_1, $\omega > \log(\omega)$ is taken into account for the derivation of (4.11). $\square$

As a result of Corollary 4.2 and Theorem 4.4, frames whose entries are i.i.d. sub-Gaussian random variables satisfy the UP with high probability for the frame bounds $A = 1 - \xi, B = 1 + \xi$ for small $\xi > 0$, therefore can be used to compute the ℓ_∞-norm representation. Probability of satisfying the UP and being a ξ-Parseval frame at the same is bounded in Corollary 4.3.

Chapter 5

Pareto Approach for ℓ_p-norm Minimization

Problems (P_τ), (P_σ) and (P_λ) are equivalent for some pair (τ, σ, λ) [FR13] and each optimization problem can be considered as a bi-criterion problem with the objectives $\|\mathbf{x}\|_p$ and $\rho(\mathbf{y} - \mathrm{D}\mathbf{x})$. Pareto frontier approaches[1] are commonly used in multiobjective optimization [PMP08; SM12] and can be used to trace the optimality between these objectives.

5.1 Pareto Optimality

Definition 5.1. Pareto optimal and Pareto frontier.

(i) Pareto optimal is the minimal achievable feasible point of a feasible set. E.g., $\mathbf{p}$ is called Pareto optimal solution for (P_τ), (P_σ) and (P_λ), if there is no any $\mathbf{v}$ such that $\|\mathbf{v}\|_p \leq \|\mathbf{p}\|_p$ and $\|\mathbf{v}\|_p \neq \|\mathbf{p}\|_p$ in the feasible solution set.

(ii) The set that comprised of Pareto optimal points is called the Pareto frontier.

In this thesis, the solution of (P_σ) is sought by solving (P_τ). Thus, we are particularly interested in the optimal objective value of the (P_τ^p) for a given $\mathbf{y}$ and τ that can be expressed with the following function

$$\nu(\tau) := \inf_{\mathbf{x} \in \mathbb{R}^N} \{\rho(\mathbf{y} - \mathbf{D}\mathbf{x}) | \ \|\mathbf{x}\|_p \leq \tau\}, \tag{5.1}$$

and we define corresponding Pareto frontier as

$$\psi(\tau) := \nu(\tau) - \sigma. \tag{5.2}$$

Theorem 5.1. *Convexity of ψ.*

[1] It is named after well-known Italian economist Wilfredo Pareto (1848-1923).

(i) If ρ is a convex function (e.g. least-squares, Huber function), then so is ψ.

(ii) If ρ is a nonconvex function, convexity of ψ does not follow. When ρ is quasi-convex function, then so is ψ.

Proof. Let us consider any two solutions $\mathbf{x}_1$ and $\mathbf{x}_2$ of (P_τ^p) for any τ_1 and τ_2 respectively. Since ℓ_p-norm is convex for $1 \leq p \leq \infty$, for any $\beta \in [0, 1]$ following holds

$$\|\beta \mathbf{x}_1 + (1-\beta)\mathbf{x}_2\|_p \leq \beta \|\mathbf{x}_1\|_p + (1-\beta)\|\mathbf{x}_2\|_p = \beta\tau_1 + (1-\beta)\tau_2. \tag{5.3}$$

An immediate outcome of (5.3) is that $\beta\mathbf{x}_1 + (1-\beta)\mathbf{x}_2$ is a feasible point of (P_τ^p) with $\tau = \beta\tau_1 + (1-\beta)\tau_2$. Thus we can write the following inequality

$$\begin{aligned} \nu(\beta\tau_1 + (1-\beta)\tau_2) &\leq \rho(\mathbf{D}(\beta\mathbf{x}_1 + (1-\beta)\mathbf{x}_2) - \mathbf{y}) \\ &= \rho(\beta(\mathbf{D}\mathbf{x}_1 - \mathbf{y}) + (1-\beta)(\mathbf{D}\mathbf{x}_2 - \mathbf{y})). \end{aligned} \tag{5.4}$$

i) If ρ is convex, then

$$\begin{aligned} \rho(\beta(\mathbf{D}\mathbf{x}_1 - \mathbf{y}) + (1-\beta)(\mathbf{D}\mathbf{x}_2 - \mathbf{y})) &\leq \beta\rho(\mathbf{D}\mathbf{x}_1 - \mathbf{y}) + (1-\beta)\rho(\mathbf{D}\mathbf{x}_2 - \mathbf{y})) \\ &= \beta\nu(\tau_1) + (1-\beta)\nu(\tau_2), \end{aligned} \tag{5.5}$$

that shows ν is convex as well as ψ.
ii) If ρ is quasi-convex, then

$$\begin{aligned} \rho(\beta(\mathbf{D}\mathbf{x}_1 - \mathbf{y}) + (1-\beta)(\mathbf{D}\mathbf{x}_2 - \mathbf{y})) &\leq \max\{\rho(\mathbf{D}\mathbf{x}_1 - \mathbf{y}), \rho(\mathbf{D}\mathbf{x}_2 - \mathbf{y})\} \\ &= \max\{\nu(\tau_1), \nu(\tau_2)\}, \end{aligned} \tag{5.6}$$

that shows ν is quasi-convex as well as ψ. ☐

Pareto optimal points are unique for (P_τ^p) with convex losses ρ [PŽŽ17, Theorem 1.1, Theorem 1.2], [Mie01]. Also, the feasible set of (P_τ^p) enlarges as τ increases [Van09], thus $\psi(\tau)$ is nonincreasing for $\tau \in [0, \tau_{max}]$, where τ_{max} is the maximal τ that minimizes $\psi(\tau)$ and $\tau = 0$ is the minimal τ that maximizes $\psi(\tau)$. Under the assumption of $\mathbf{D}$ is full row-rank, one should notice that $\rho(\mathbf{y} - \mathbf{D}\mathbf{x}_{MF}) = 0$. Therefore, $\tau = 0$ and $\tau = \|\mathbf{x}_{MF}\|_p = \tau_{MF}$ are the two points that provide opposite signs of ψ. Having two points with opposite signs is required for a convergence guarantee for the bracketing type root finding algorithms [DB03].

In Figure 5.1 and 5.2 an abstract $\psi(\tau)$ is depicted for a convex and quasi-convex loss ρ respectively where the red line represents the σ level. Pareto optimal point for a given σ is at the intersection of the red line and black curve.

Obtaining the solution of (P_σ^p) by solving (P_τ^p) with the help Pareto frontier concept proceeds as follows. We start with a τ to solve (P_τ^p), and using the solution of the current τ parameter, and corresponding $\psi(\tau)$, a new τ will be found until $\tau \to \tau_\sigma$

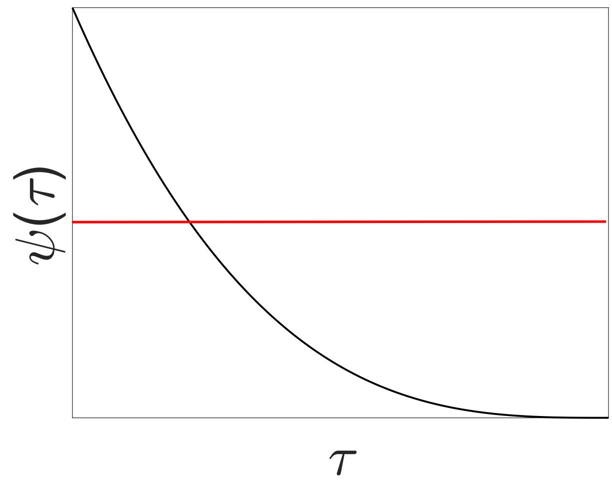

Figure 5.1: A Representative Pareto frontier for convex loss ρ.

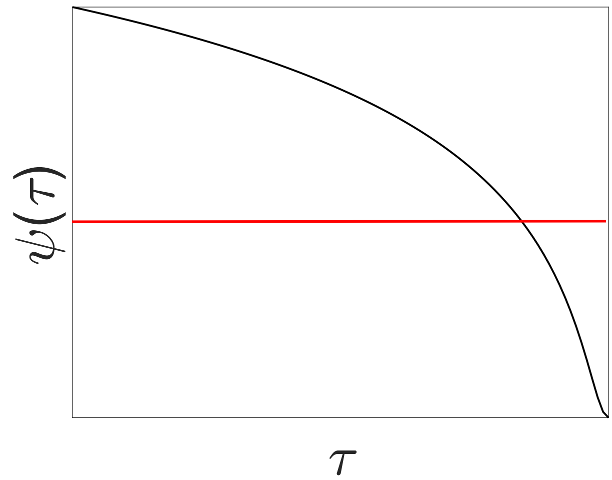

Figure 5.2: A representative Pareto frontier for quasi-convex loss ρ.

by going over Pareto frontier iteratively, where τ_σ denotes the solution of (P_σ^p), i.e. $\psi(\tau_\sigma) \to 0$ and then algorithm concludes. At this point, τ_σ, it is straightforward to remark that the solution of (P_τ^p) is also a solution of the (P_σ^p), a fact proven formally by [ABF13].

Finding τ_σ can be formulated as a non-linear equation root finding problem. We will closely investigate the solving a non-linear equation root finding problem to find τ_σ in Chapter 5.3.

Although we define a Pareto fronter for the constraint σ, we note that defining different Pareto frontiers is also an option, pleace check Figure 5.3.

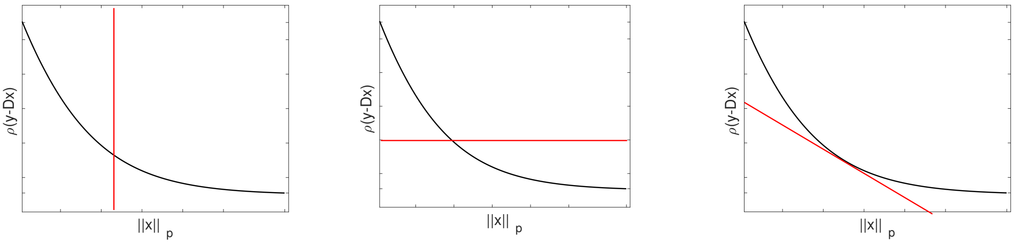

(a) Constraint on τ **(b)** Constraint on σ **(c)** Scalarization (slope $-\frac{1}{\lambda}$)

Figure 5.3: Typical Pareto frontiers for the constraints λ, τ, σ, with the objectives $\|\mathbf{x}\|_p$ and $\rho(\mathbf{y} - \mathrm{D}\mathbf{x})$.

5.2 Lagrangian Duality and the Slope of the Pareto Curve

In this subchapter, we bound the slope of the Pareto curve of the objectives $\|\mathbf{x}\|_p$ and convex $\rho(\mathbf{y} - \mathbf{D}\mathbf{x})$. In that purpose, Lagrangian duality of the problems (P_τ^p), (P_σ^p) are inspected.

5.2.1 Lagrangian Dual of the Problems ($\mathbf{P}_\tau^p$) and ($\mathbf{P}_\sigma^p$)

5.2.1.1 Lagrangian Dual of ($\mathbf{P}_\tau^p$)

Let us rewrite the problem (P_τ^p) such as

$$\underset{\mathbf{x}\in\mathbb{R}^N,\mathbf{r}\in\mathbb{R}^M}{\text{minimize}} \;\; \rho(\mathbf{r}) \;\; \text{s.t.} \;\; \mathbf{D}\mathbf{x} + \mathbf{r} - \mathbf{y} = 0, \;\; \|\mathbf{x}\|_p \leq \tau, \tag{5.7}$$

where $\mathbf{r}$ is the residual term. The Lagrange dual associated with the (5.7) can be written as

$$\mathcal{L}(\mathbf{z}_\tau, \lambda) := \inf_{\mathbf{x}\in\mathbb{R}^N,\mathbf{r}\in\mathbb{R}^M} \{\rho(\mathbf{r}) - \mathbf{z}_\tau^T(\mathbf{D}\mathbf{x} + \mathbf{r} - \mathbf{y}) + \lambda(\|\mathbf{x}\|_p - \tau)\}, \tag{5.8}$$

where $\mathbf{z}_\tau$ and λ are the Lagrange multipliers. Let us rewrite (5.8) such

$$\mathcal{L}(\mathbf{z}_\tau, \lambda) = \mathbf{y}^T\mathbf{z}_\tau - \tau\lambda - \sup_{\mathbf{r}\in\mathbb{R}^M} \{\mathbf{z}_\tau^T\mathbf{r} - \rho(\mathbf{r})\} - \sup_{\mathbf{x}\in\mathbb{R}^N} \{\mathbf{z}_\tau^T\mathbf{D}\mathbf{x} - \lambda\,\|\mathbf{x}\|_p\}. \tag{5.9}$$

Using the Lagrange dual given in (5.9), the Lagrange dual problem of (5.7) can be written as

$$(\mathrm{P}_\tau^{p,d}) \qquad \underset{\mathbf{z}_\tau\in\mathbb{R}^M,\lambda\in\mathbb{R}}{\text{maximize}} \;\; \mathbf{y}^T\mathbf{z}_\tau - \tau\lambda \;\; \text{s.t.} \;\; \rho^\circ(\mathbf{z}_\tau) \leq 1, \;\; \left\|\mathbf{D}^T\mathbf{z}_\tau\right\|_{p^*} \leq \lambda$$

5.2.1.2 Lagrangian Dual of $(\mathbf{P}_\sigma^p)$

Lagrangian dual problem of (P_σ^p) is straightforward [Ara+18] and can be written as

$$(\mathrm{P}_\sigma^{p,d}) \qquad \underset{\mathbf{z}_\sigma \in \mathbb{R}^M}{\text{maximize}} \;\; \mathbf{y}^T\mathbf{z}_\sigma - \sigma\rho^\circ(\mathbf{z}_\sigma) \;\; \text{s.t.} \;\; \mathbf{D}^T\mathbf{z}_\sigma \in \mathcal{B}_{p^*}^N,$$

Lemma 5.1. *Consider fixed s and assume that DD^T is non-singular (i.e. D is a frame) and satisfies the matrix condition* (4.1)*.*

(i) Any feasible point $\hat{\mathbf{z}}_\sigma$ of the dual problem $(P_\sigma^{p,d})$ satisfies following

$$\|\hat{\mathbf{z}}_\sigma\|_t \leq \frac{s^{\left(\frac{1}{t}-\frac{1}{p^*}\right)}}{d_t}, \tag{5.10}$$

(ii) any feasible point $\hat{\mathbf{z}}_\tau$ of the dual problem $(P_\tau^{p,d})$ satisfies following

$$\|\hat{\mathbf{z}}_\tau\|_t \leq \frac{s^{\left(\frac{1}{t}-\frac{1}{p^*}\right)}}{d_t}\lambda, \tag{5.11}$$

where $d_t = 1/(\beta_t\|(\mathbf{D}\mathbf{D}^T)^{-1}\|_{t\to t}) - \|\mathbf{D}^T\|_{t\to t}$. For $t=2$ we have $d_2 = A/\beta_2 - \sqrt{B}$.

Proof. Let us define a vector $\mathbf{v} = \mathbf{D}^T\hat{\mathbf{z}}$ and partition it into s-size j disjoint subsets (i.e. each of them has the cardinality of s), $\{T_i\}_{i\geq 1}$, in such a way that T_1 corresponds to the s largest entries of $\mathbf{v}$, T_2 corresponds to the second largest s entries of $\mathbf{v}$, and same rule continues until to the last subset. With the help of this partitioning arrangement, following can be written

$$\|\mathbf{D}\mathbf{v}\|_t = \left\|\mathbf{D}\sum_{i\geq 1}\mathrm{P}_{T_i}\mathbf{v}\right\|_t \leq \sum_{i\geq 1}\|\mathbf{D}\mathrm{P}_{T_i}\mathbf{v}\|_t \tag{5.12}$$

where P_{T_i} is the projection matrix onto the set T_i. Since it is assumed that D satisfies the eq. (4.1), eq. (5.12) can be written with β_t such that

$$\|\mathbf{D}\mathbf{v}\|_t \leq \sum_{i\geq 1}\|\mathbf{D}\mathrm{P}_{T_i}\mathbf{v}\|_t \leq \sum_{i\geq 1}\beta_t\|\mathrm{P}_{T_i}\mathbf{v}\|_t = \beta_t\|\mathrm{P}_{T_1}\mathbf{v}\|_t + \sum_{i\geq 2}\beta_t\|\mathrm{P}_{T_i}\mathbf{v}\|_t\,. \tag{5.13}$$

Let us denote $\mathbf{v}_i$ as the vector projected onto the set T_i, following inequality can be written for $i \geq 2$ and any $p^* \geq 1$,

$$\|\mathrm{P}_{T_i}\mathbf{v}\|_\infty = \max_{l\in T_i}|\mathbf{v}_l| \leq \min_{l\in T_{i-1}}|\mathbf{v}_l| \leq \left(\frac{1}{s}\sum_{l\in T_{i-1}}|\mathbf{v}_l|^{p^*}\right)^{\frac{1}{p^*}} = s^{-\frac{1}{p^*}}\left\|\mathrm{P}_{T_{i-1}}\mathbf{v}\right\|_{p^*} \tag{5.14}$$

since $\|\mathrm{P}_{T_i}\mathbf{v}\|_t \leq s^{\frac{1}{t}} \|\mathrm{P}_{T_i}\mathbf{v}\|_\infty$,

$$\|\mathrm{P}_{T_i}\mathbf{v}\|_t \leq s^{\left(\frac{1}{t}-\frac{1}{p^*}\right)} \left\|\mathrm{P}_{T_{i-1}}\mathbf{v}\right\|_{p^*}. \tag{5.15}$$

Merging eq. (5.15) and eq. (5.13) leads us to

$$\begin{aligned}\|\mathrm{D}\mathbf{v}\|_t &\leq \beta_t \|\mathrm{P}_{T_1}\mathbf{v}\|_t + \sum_{i\geq 2}\beta_t \|\mathrm{P}_{T_i}\mathbf{v}\|_t \leq \beta_t \|\mathrm{P}_{T_1}\mathbf{v}\|_t + \sum_{i\geq 2}\beta_t s^{\left(\frac{1}{t}-\frac{1}{p^*}\right)} \left\|\mathrm{P}_{T_{i-1}}\mathbf{v}\right\|_{p^*} \\ &\leq \beta_t \|\mathrm{P}_{T_1}\mathbf{v}\|_t + \sum_{i\geq 1}\beta_t s^{\left(\frac{1}{t}-\frac{1}{p^*}\right)} \left\|\mathrm{P}_{T_i}\mathbf{v}\right\|_{p^*}.\end{aligned} \tag{5.16}$$

(i) For any feasible point $\hat{\mathbf{z}}_\sigma$ of $(\mathrm{P}_\sigma^{p,d})$, $\mathbf{v} = \mathbf{D}^T\hat{\mathbf{z}}_\sigma \in \mathcal{B}_{p^*}^N$. Thus eq. (5.16) can be concluded as

$$\|\mathbf{D}\mathbf{v}\|_t \leq \beta_t \|\mathrm{P}_{T_1}\mathbf{v}\|_t + \beta_t s^{\left(\frac{1}{t}-\frac{1}{p^*}\right)}. \tag{5.17}$$

Furthermore, $\|\mathrm{P}_{T_1}\mathbf{v}\|_t$ can be bounded as

$$\|\mathrm{P}_{T_1}\mathbf{v}\|_t \leq \|\mathbf{v}\|_t = \left\|\mathbf{D}^T\hat{\mathbf{z}}_\sigma\right\|_t \leq \|\mathbf{D}^T\|_{t\to t} \|\hat{\mathbf{z}}_\sigma\|_t. \tag{5.18}$$

$\|\hat{\mathbf{z}}_\sigma\|_t = \left\|(\mathbf{D}\mathbf{D}^T)^{-1}\mathbf{D}\mathbf{D}^T\hat{\mathbf{z}}_\sigma\right\|_t \leq \|(\mathbf{D}\mathbf{D}^T)^{-1}\|_{t\to t} \left\|\mathbf{D}\mathbf{D}^T\hat{\mathbf{z}}_\sigma\right\|_t = \|(\mathbf{D}\mathbf{D}^T)^{-1}\|_{t\to t} \|\mathbf{D}\mathbf{v}\|_t$. Therefore, with the help of eq. (5.17) and eq. (5.18), following can be derived

$$\|\hat{\mathbf{z}}_\sigma\|_t \leq \|(\mathbf{D}\mathbf{D}^T)^{-1}\|_{t\to t} \left(\beta_t\|\mathbf{D}^T\|_{t\to t} \|\hat{\mathbf{z}}_\sigma\|_t + \beta_t s^{\left(\frac{1}{t}-\frac{1}{p^*}\right)}\right) \tag{5.19}$$

which can be simplified as

$$\|\hat{\mathbf{z}}_\sigma\|_t \leq \frac{s^{\left(\frac{1}{t}-\frac{1}{p^*}\right)}}{d_t}. \tag{5.20}$$

where $d_t = 1/(\beta_t\|(\mathbf{D}\mathbf{D}^T)^{-1}\|_{t\to t}) - \|\mathrm{D}^T\|_{t\to t}$.

(ii) For any feasible point $\hat{\mathbf{z}}_\tau$ of $(\mathrm{P}_\tau^{p,d})$, $\mathbf{v} = \mathbf{D}^T\hat{\mathbf{z}}_\tau$ and since $\left\|\mathbf{D}^T\hat{\mathbf{z}}_\tau\right\|_{p^*} \leq \lambda$, eq. (5.16) can be concluded as

$$\|\mathbf{D}\mathbf{v}\|_t \leq \beta_t \|\mathbf{P}_{T_1}\mathbf{v}\|_t + \beta_t s^{\left(\frac{1}{t}-\frac{1}{p^*}\right)}\lambda. \tag{5.21}$$

Let us follow similar steps that are applied for $\hat{\mathbf{z}}_\sigma$ and bound $\|\mathrm{P}_{T_1}\mathbf{v}\|_t$ as

$$\|\mathrm{P}_{T_1}\mathbf{v}\|_t \leq \|\mathbf{v}\|_t = \left\|\mathbf{D}^T\hat{\mathbf{z}}_\tau\right\|_t \leq \|\mathbf{D}^T\|_{t\to t} \|\hat{\mathbf{z}}_\tau\|_t \tag{5.22}$$

Since, $\|\hat{\mathbf{z}}_\tau\|_t = \left\|(\mathbf{D}\mathbf{D}^T)^{-1}\mathbf{D}\mathbf{D}^T\hat{\mathbf{z}}_\tau\right\|_t \leq \|(\mathbf{D}\mathbf{D}^T)^{-1}\|_{t\to t} \left\|\mathbf{D}\mathbf{D}^T\hat{\mathbf{z}}_\tau\right\|_t = \|(\mathbf{D}\mathbf{D}^T)^{-1}\|_{t\to t} \|\mathbf{D}\mathbf{v}\|_t$, with the help of eq. (5.17) and eq. (5.18), following can be derived

$$\|\hat{\mathbf{z}}_\tau\|_t \leq \|(\mathbf{D}\mathbf{D}^T)^{-1}\|_{t\to t} \left(\beta_t\|\mathbf{D}^T\|_{t\to t} \|\hat{\mathbf{z}}_\tau\|_t + \beta_t s^{\left(\frac{1}{t}-\frac{1}{p^*}\right)}\lambda\right) \tag{5.23}$$

which can be simplified as

$$\|\hat{\mathbf{z}}_\tau\|_t \leq \frac{s^{\left(\frac{1}{t}-\frac{1}{p^*}\right)}}{d_t}\lambda. \tag{5.24}$$

where $d_t = 1/(\beta_t \|(\mathbf{D}\mathbf{D}^T)^{-1}\|_{t\to t}) - \|\mathbf{D}^T\|_{t\to t}$.

□

5.2.2 Slope of The Pareto Curve

Subdifferential of the Pareto frontier is related with the Lagrange multipliers of dual problem formulation ($\mathrm{P}_\tau^{p,d}$) and explicitly given in [ABF13, Theorem 5.2], and we accommodate it with the Theorem 5.2.

Theorem 5.2. *For all $\tau \in [0, \tau_{MF})$, subdifferential of the ν with respect to τ is given $\partial_\tau \nu(\tau) \neq \emptyset$ with*

$$\partial_\tau \nu(\tau) = \{-\lambda |\ \lambda \in \{\underset{\lambda \geq 0}{arg\ min}\ \ \tau\lambda + \left\|\mathbf{D}^T \mathbf{z}_\tau\right\|_{p^*}\}\} \tag{5.25}$$

As long as $\tau > 0$, λ is compelled to be at its lower bound, i.e. $\lambda = \left\|\mathbf{D}^T \mathbf{z}_\tau\right\|_{p^*}$, otherwise the objective can increase. Thus, an immediate outcome of Theorem 5.2 is

$$\partial_\tau \nu(\tau) = -\left\|\mathbf{D}^T \mathbf{z}_\tau\right\|_{p^*}. \tag{5.26}$$

Proposition 5.1. *Under the conditions of Lemma 5.1, subdifferential of the ν with respect to $\tau \in [0, \tau_{max})$ satisfies following*

$$-\frac{\left\|\mathbf{D}^T \boldsymbol{y}\right\|_{p^*}}{\rho^\circ(\mathbf{y})} \leq \partial_\tau \nu(\tau) \leq -\frac{\|\mathbf{r}_\tau\|_t}{\rho^\circ(\mathbf{r}_\tau)} \times \frac{d_t}{s^{\left(\frac{1}{t}-\frac{1}{p^*}\right)}} \tag{5.27}$$

where $\mathbf{r}_\tau = \mathbf{y} - \mathbf{D}\mathbf{x}_\tau$, $\mathbf{x}_\tau$ is the optimal solution of (P_τ^p).

For ρ is ℓ_2-norm and $t = 2$, (5.27) becomes

$$-\frac{\left\|\mathbf{D}^T \boldsymbol{y}\right\|_{p^*}}{\|\boldsymbol{y}\|_2} \leq \partial_\tau \nu(\tau) \leq \left(\frac{\beta_2 \sqrt{B} - A}{\beta_2 s^{\left(\frac{1}{2}-\frac{1}{p^*}\right)}}\right) \tag{5.28}$$

Proof. Let us take $\mathbf{z}_\tau = \mathbf{r}_\tau/\rho^\circ(\mathbf{r}_\tau)$, it is feasible for ($\mathrm{P}_\tau^{p,d}$) since ρ is positive homogeneous. Then with the help of (5.11) and (5.26), upper bound of $\partial_\tau \nu(\tau)$ can be found. Since $\nu(\tau)$ is convex decreasing in τ, the minimum of $\partial_\tau \nu(\tau)$ occurs where the $\nu(\tau)$ is maximum, i.e. $\nu(\tau = 0)$. For $\tau = 0$, $\mathbf{x}_\tau$ is also a vector with zeros. In that case $\mathbf{r}_0 = \mathbf{y}$, and taking $\mathbf{r}_0 = \mathbf{y}$ provides the lower bound of $\partial_\tau \nu(\tau)$. For ρ is ℓ_2-norm, ρ° is also ℓ_2-norm and for $t = 2$ we can directly employ d_2 and obtain (5.28). □

5.3 Nonlinear Equation Root Finding

In the pursuit of the solution of (P_σ^p) with the help Pareto frontier approach, our aim is to

$$\text{find} \quad \tau \quad \text{such that} \quad \psi(\tau) = 0, \tag{5.29}$$

which is a nonlinear equation root finding problem indeed.

There are various problems in different fields require to find a solution of a nonlinear equation [TCS19] Hence, there have been numerous works on this topic. Depending on the properties of the function to be analyzed (e.g. the differentiability), and the requirements of the application itself (e.q. convergence order), several methods are introduced in the literature to deal with the nonlinear equation root finding problems.

Root finding problems generally can be classified into two categories: *open-type root finding methods* and *bracketing-type root finding methods* as follows

I) Open-type root finding methods

   i) *Newton's method* (also known as the Newton Raphson method) is very commonly used and mostly very efficient. It is derived from [New11], requires a differentiable function, mostly converges faster if the starting point lies near the root.

   ii) *Halley's method* is similar to Newton's method in terms of using a variable with continuous derivative and requires first and second derivative of a function [Hal07].

   iii) *Steffensen's method* is similar to Newton's method in terms of using a variable with continuous derivative. However, instead of the derivative of a function, it uses the first-order divided difference of the function between two points [Ste33].

   iv) *Secant method* uses the secant through the last two calculated points in contrast to tangent of a single point. It needs two starting points and does not require a differentiable function.

   v) *Müller's method* [Mul56] is similar to the secant method, however requires three starting points. It does not require a differentiable function.

II) Bracketing-type root finding methods

   i) *Bisection method* repeatedly halves the given interval that contains the root. It is a simple and robust method, requires two starting points with opposite signs and does not require a differentiable function. It always converges.

   ii) *Regula falsi (false position) method* repeatedly splits the interval that contains the root by using linear interpolation. It is an old, simple and efficient method, requires two starting points with opposite signs and does not require a differentiable function. It retains the last two points that bracket the root and always converges. It has several modified versions. The well-known versions are

- Illinois,
- Pegasus,
- Anderson-Björk.

We summarized major open and bracketing type root finding methods above. There are more methods proposed, however they are mostly hybrid models or modified versions of the existing methods. For example, improved and modified versions of the Newton's and secant methods are proposed in [Kou07; Hom03; RAS+21; Xin99; Sah+16] and [Tir19; MT13; Bar65; Tek19] respectively. Similarly, [Chh14; OT20; MR16] introduced versions of bisection method. Many modified versions of Regula falsi have been proposed as well, such as [Gal; For; SM15; Che07; Kin73].

The difference between the open and bracketing type root finding methods is that, in contrast to bracketing methods, open-type methods require only a single starting value or two starting values which do not have to bracket a root while bracketing-type root finding methods necessitate two starting points which bracket a root. Unlike the open-type methods, bracketing-type methods divides the root searching interval into two and continues over the one that contains the root in each iteration.

Each of the existing nonlinear equation root finding methods have their own advantages and disadvantages. The applicability and the efficiency of these methods depend on the function. Thus, chosing one of them is function dependent. Comparison of the open-type and bracketing-type root finding methods is given in Table 5.1.

In this thesis, we solve (5.29) with some of the open-type and bracketing-type methods. We employ Newton's method as open-type and several Regula falsi versions as bracketing-type methods. We also introduce an approach called *one-point retention* (OPR) method which is inspired from Regula falsi however does not necessarily bracket the root searching interval, does not require differentiable function, applicable for nonconvex losses and is flexible about the starting point choice.

5.3.1 Open-type Root Finding Methods

In order to solve (P_σ^p) with the Pareto frontier approach introduced in Chapter 5.1, (5.29) needs to be solved. For that purpose, Newton's and OPR methods are employed as open-type root finders.

5.3.1.1 Newton's Method

Newton's method is a simple and a very commonly utilized approach in many nonlinear equation root finding problems. Nevertheless, it might have some drawbacks though.

Table 5.1: Comparison of the open-type and bracketing-type root finding methods.

	Advantages	Disadvantages
Open-type root finding methods	- Usually converges fast.	- Convergence depends on the starting point and is not guaranteed, i.e. may diverge. - Most of its versions require differentiable functions. - Not flexible about starting points. - Usually can not handle nonconvex losses.
Bracketing-type root finding methods	- **Always converges** if two starting points with opposite signs is given. - Applicable for nonconvex losses. - Does not require differentiable functions. - Flexible about starting points.	- May convergence slowly if the function has significant curvature.

First of all, the derivative of a nonlinear equation needs to be calculated. Depending on the problem, derivative calculation of a nonlinear equation may bring extra computational cost to the algorithm or it may not be possible. Another drawback of the Newton's method or alternative secant variants is that if ρ is nonconvex they are not guaranteed to solve (5.29). In particular, the tangent lines may cross the feasible region and can end up at a negative τ. The reason of why Newton's method can not offer convergence guarantee for the nonconvex ρ is explained more detailed in Chapter 5.4.

The recursion formula of the Newton's method to solve (5.29) is

$$g_N(\tau_n) = \tau_{n+1} = \tau_n - \frac{\psi(\tau_n)}{\partial_\tau \psi(\tau_n)} \quad \text{for} \quad n = 0, 1, \ldots, \tau_\sigma \tag{5.30}$$

where $\tau_0 = 0$. Newton's method starts with $\tau = 0$ and move along the Pareto frontier $\psi(\tau)$ with tangent lines. Iterations are depicted in Figure 5.4 for a convex decreasing ρ.

5.3.1.2 One-Point Retention (OPR) Method

OPR is a derviative-free approach with simple iterations intoduced in this thesis. Derivative-freeness can be very favorable and preferable when derivative calculation

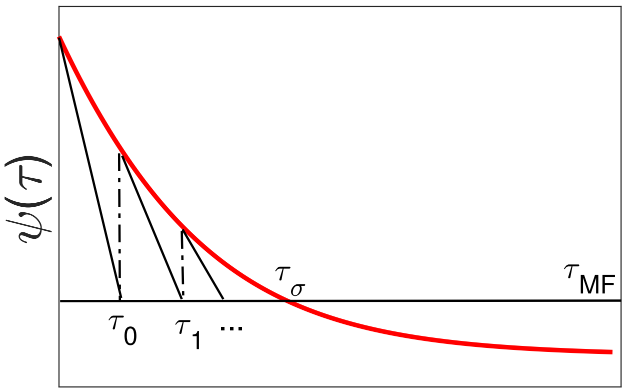

Figure 5.4: Newton's method iterations over the Pareto frontier $\psi(\tau)$, i.e. g_N steps in (5.30).

of the Pareto frontier $\psi(\tau)$ costly or not possible. Except necessity of differentiable $\psi(\tau)$, OPR differs from Newton's method in starting points as well. Newton's method starts with $\tau = 0$ and trace the root over the Pareto frontier with tangent lines, while the OPR starts with $\tau = \mu \left\|\mathbf{x}_{MF}\right\|_p$ and draws secant line between $\psi(\tau = 0)$ and $\psi(\tau = \mu \left\|\mathbf{x}_{MF}\right\|_p)$ then continues drawing secant lines between $\psi(\tau = 0)$ and several $\psi(\tau)$ values until it converges. OPR can handle nonconvex losses also unlike the Newton's method or Newton's method like variants. OPR retains one point and update the other point of the bracket.

The recursion formula for the OPR method to solve (5.29) is

$$g_O(\tau_n) = \tau_{n+1} = \tau_n \times \frac{\psi_{max}}{\psi_{max} - \psi(\tau_n)}, \quad \text{for} \quad n = 0, 1, \ldots, \tau_\sigma \tag{5.31}$$

where $\tau_0 = \mu\tau_{MF}$ with $0 < \mu \leq 1$, ψ_{max} is the maximum value of the function ψ. By the definition of ψ, i.e eq. (7.49), it can be inferred that ψ_{max} occurs for $\tau = 0$.

Iterations to solve (P^p_σ) with the OPR method for a convex decreasing ρ is shown in Figure 5.5 and 5.6 for $\tau_\sigma < \tau_0$ and $\tau_0 < \tau_\sigma$ respectively.

5.3.2 Bracketing-Type Root Finding Methods

It is necessary to solve (5.29) in order to solve (P^p_σ) using the Pareto frontier approach described in Section 5.1. Bisection and regula falsi type methods such as Illinois, Pegasus and Anderson-Björk are presented as bracketing-type root finders.

If one knows two values of a function with opposite signs, then there must be some value between these two points at which the function is zero, follows by the Bolzano's theorem [Bol17] which is a corollary of the intermediate value theorem.

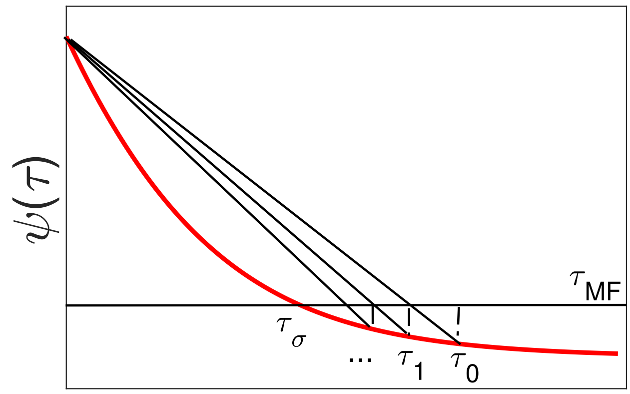

Figure 5.5: OPR iterations over the Pareto frontier $\psi(\tau)$, i.e. g_O steps in (5.31) when $\tau_\sigma < \tau_0$.

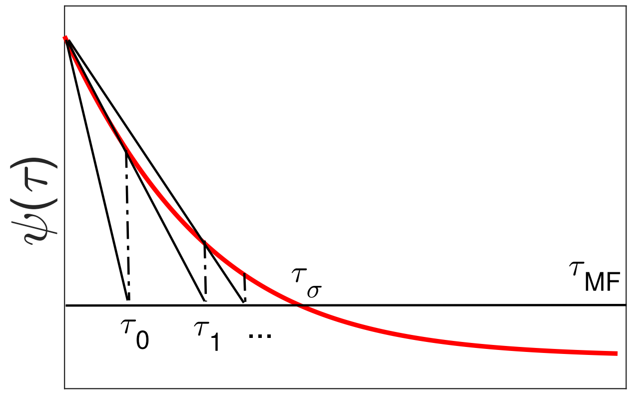

Figure 5.6: OPR iterations over the Pareto frontier $\psi(\tau)$, i.e. g_O steps in (5.31) when $\tau_0 < \tau_\sigma$.

5.3.2.1 Bisection Method

Bracketing the root of a function between two values with opposite sign enables to use a very simple and efficient method called bisection as root finder. Bisection method repeatedly halves the given interval that contains the root, always converges and does not require a differentiable function.

Let us denote the solution of a nonlinear equation of f with the x^*, i.e $f(x^*) = 0$, bisection method starting with the points a and b can be demonstrated with following steps

1. Calculate the midpoint of a and b, that is $c = (a + b)/2$.

2. Calculate $f(c)$. If $f(c)$ is equal to zero or sufficiently small for convergence then $x^* = c$, otherwise continue.

3. Adjust the new interval: if $f(c)f(b) < 0$, x^* should be in between b and c. Set $a = b,\ b = c$, if $f(c)f(b) > 0$, x^* should be in between a and c, set $b = c$, go back to 1.

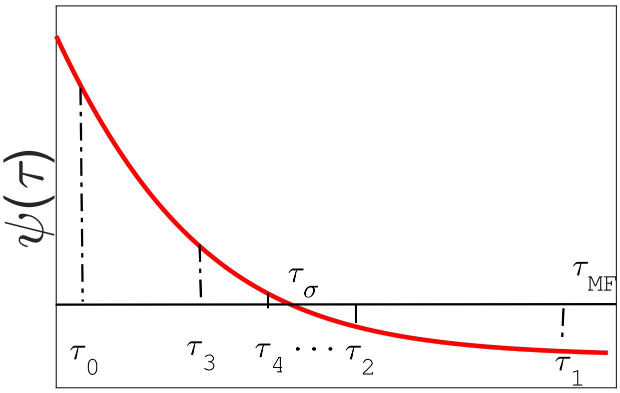

Figure 5.7: Bisection iterations over the Pareto frontier $\psi(\tau)$.

Iterations to solve (P_σ^ρ) with the bisecton method for a convex decreasing ρ is shown in Figure 5.7 where $\tau_0 = a$, $\tau_1 = b$ and $\psi = f$.

5.3.2.2 Regula Falsi-Type Root finding Methods

Similar to bisection method, Regula falsi-type methods offer convergence guarantee if two values of a function with opposite signs given. They are derivative free and repeatedly splits the interval that contains the root by using linear interpolation.

Let us denote the solution of a nonlinear equation of f by x^*, i.e $f(x^*) = 0$. With this notation, Regula falsi type methods starting with the points a and b proceed as follows.

1. Calculate the secant line between a and b,

$$s_{ab} = \frac{f(b) - f(a)}{b - a}, \tag{5.32}$$

   and find the point where (5.32) intersects the x-axis, which is $c = b - \frac{f(b)}{s_{ab}}$.

2. Calculate $f(c)$. If $f(c) = 0$ then $x^* = c$, otherwise continue.

3. Adjust the new interval: if $f(c)f(b) < 0$, x^* should be in between b and c. Set

$$a = b,\ b = c, \quad \text{and} \quad f(a) = f(b),\ f(b) = f(c), \tag{5.33}$$

if $f(c)f(b) > 0$, x^* should be in between a and c. Set

$$b = c, \quad \text{and} \quad f(a) = \mu f(a), \; f(b) = f(c), \tag{5.34}$$

where μ is the scaling factor.

4. Check the ending condition: if $|b - a| \le \epsilon$, stop the iteration. Take

$$x^* = \begin{cases} b, & \text{if } \; |f(b)| \le |f(a)| \\ a, & \text{if } \; |f(b)| > |f(a)| \end{cases}, \tag{5.35}$$

if $|b - a| > \epsilon$, continue the iteration, go back to 1) with the values a, b and $f(a), f(b)$ from 3).

Regula falsi-type methods differ from each other in the choice of the scaling factor μ. Several commonly considered μ in the literature is summarized in Table 5.2. Additional options for μ are studied in [Gal], [For].

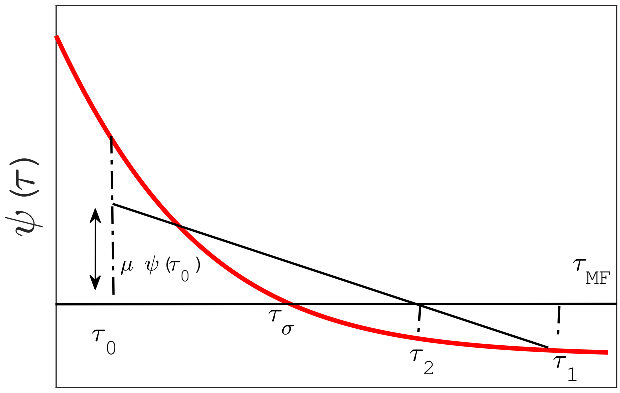

Figure 5.8: Iterations of the Regula falsi-type methods over the Pareto frontier $\psi(\tau)$.

Iterations to solve (P_σ^p) with the regula falsi-type root finding methods for a convex decreasing ρ is shown in Figure 5.8 where $\tau_0 = a$, $\tau_1 = b$ and $\psi = f$.

Table 5.2: Regula falsi-type methods with different μ values.

Method	μ
Regula Falsi	1
Illinois	0.5
Pegasus	$\frac{f(b)}{f(b)+f(c)}$
Anderson-Björck	$1 - \frac{f(c)}{f(b)}$, and in case $1 \le \frac{f(c)}{f(b)}$ set $\mu = 0.5$.

5.3.3 Newton's and OPR Methods as Fixed-Point Iterations

In this subchapter, we express the fixed-point iteration and mention some properties of Newton's and OPR methods with it.

5.3.3.1 Fixed-Point Iteration

Fixed-point iteration is a method for calculating a function's fixed points in numerical analysis. Some nonlinear equation root finding methods can also be a fixed point iteration under some conditions.

Let us assume a function $f(x)$ is equal to zero at x^*, if we rearrange the function so that $f(x) = x - g(x)$. Then, g is called the fixed-point iteration function with following recursion formula

$$x_{n+1} = g(x_n), \quad \text{for} \quad n = 0, 1, \ldots \tag{5.36}$$

x_0 represents a first guess at x^*. At x^*, $x^* = g(x^*)$.

Following can be remarked about a fixed point iteration,

- if $x^* = g(x^*)$, then a function $g(x)$ has a fixed point at $x = x^*$,
- if a function $g(x)$ has a fixed point at $x = x^*$, then the function $f(x) = x^* - g(x^*)$ has a root at $x = x^*$,
- if a function $f(x)$ has a root at $x = x^*$, then the function $g(x) = x - f(x)$ has a fixed point at $x = x^*$.

5.3.3.2 Convergence of a Fixed-Point Iteration

Let us take (5.36), consider x^* as fixed-point of g and define $e_n = x_n - x^*$ to be the error between x_n and x^* for any n. Assume that the derivative of g exists and continuous, then we can write following

$$\begin{aligned} e_{n+1} &= x_{n+1} - x^* \\ &= g(x_n) - g(x^*) \\ &= g'(x_u) \cdot (x_n - x^*) \\ &= g'(x_u) \cdot e_n \end{aligned} \tag{5.37}$$

where $g'(x_u)$ is some point between $x_n - x^*$. Equation (5.37) derived with the help of *the mean value theorem.*

An iteration in (5.36) comes closer to the fixed point x^* if and only if $| e_{n+1} | < | e_n |$ which occurs if and only if $| g'(x_u) | < 1$. It can easily be seen that the smaller value of the $g'(x_u)$ causes faster convergence.

Theorem 5.3. *(Mean Value Theorem) Assume $f(x)$ is continous on $[a, c]$ and differentiable on (a, b), then there exists a b such that $a < b < c$ and*

$$f'(b) = \frac{f(c) - f(a)}{c - a} \tag{5.38}$$

The fixed point method has four main types of convergence and divergence depending on g' which are

- *monotonic convergence*, if $0 < g' < 1$,
- *oscillating convergence*, if $-1 < g' < 0$
- *monotonic divergence*, if $g' > 1$,
- *oscillating divergence*, if $g' < -1$,

and shown in Figure 5.9.

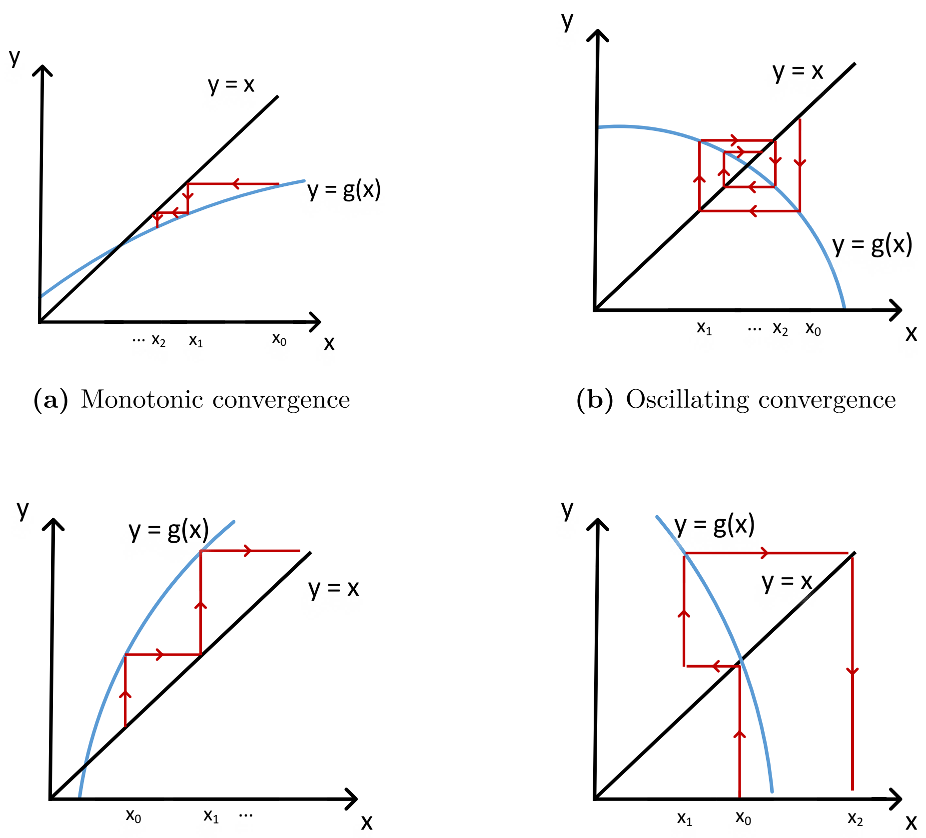

(a) Monotonic convergence **(b)** Oscillating convergence

(c) Monotonic divergence **(d)** Oscillating divergence

Figure 5.9: Convergence and divergence of a fixed point iteration.

Theorem 5.4. *Let $g(x)$ be a fixed point iteration function on $x \in [a, c]$. Suppose that g' exists on (a, c) and satisfies following*

$$|g'(x)| \leq k < 1, \quad \forall x \in [a, c]. \tag{5.39}$$

Then by taking any initial value $x_0 \in [a, c]$, the sequence $x_{n+1} = g(x_n)$ converges to a unique fixed point x^* in $[a, c]$, and satisfies following

(i) a-posteriori error estimate bounds

$$|x_{n+1} - x^*| \leq k|x_n - x^*|, \tag{5.40}$$

$$|x_{n+1} - x^*| \leq \frac{k}{1-k}|x_{n+1} - x_n|. \tag{5.41}$$

(ii) a-priori error estimate bound

$$|x_{n+1} - x^*| \leq \frac{k^{n+1}}{1-k}|x_1 - x_0|. \tag{5.42}$$

Proof. By using the *mean value theorem*, it is possible obtain the eq. (5.40) directly from following inequalities

$$\begin{aligned} |x_{n+1} - x^*| &= |g(x_n) - g(x^*)| \\ &= |g'(x_u)||x_n - x^*| \\ &\leq k|x_n - x^*|, \end{aligned} \tag{5.43}$$

where x_u is any point between x^* and x_n, therefore $|x_{n+1} - x^*| \leq k^{n+1}|x_0 - x^*|$. Since $\lim\limits_{n\to\infty}|x_{n+1} - x^*| \leq \lim\limits_{n\to\infty} k^{n+1}|x_0 - x^*| = 0$, the sequence $x_{n+1} = g(x_n)$ converges to the fixed point b^*.

In order to show the uniqueness of the fixed point let us assume we have two fixed points f_1 and f_2, with the help of the *mean value theorem* there should be a value d such $g(f_1) - g(f_2) = g'(d)(f_1 - f_2)$. So $|f_1 - f_2| = |g(f_1) - g(f_2)| = |g'(d)||f_1 - f_2| \leq k|f_1 - f_2| < |f_1 - f_2|$, which is a contradiction. Therefore, it shows the uniqueness of the fixed point.

To get the bound (5.41), by using the *mean value theorem* again we have following inequality $|x_{n+1} - x_n| \leq k|x_n - x_{n-1}|$. By induction $|x_{n+l} - x_{n+l-1}| \leq k^l|x_n - x_{n-1}|$, so $|x_{n+m} - x_n| \leq (k + k^2 + ... + k^m)|x_n - x_{n-1}| = \left(\sum_{m=0}^{\infty} k^m - 1\right)|x_n - x_{n-1}|$. By letting $m \to \infty$, we obtain (5.41).

With a focus on how to obtain the bound (5.42), note that $|x_0 - x^*| = |x^* - g(x_0) + x_1 - x_0| \leq |g(x^*) - g(x_0)| + |x_1 - x_0| \leq k|x_0 - x^*| + |x_1 - x_0|$ from which it can be written that $|x_0 - x^*| \leq \frac{1}{1-k}|x_1 - x_0|$. Finally, bound (5.42) can be deduced as $|x_{n+1} - x^*| \leq k^{n+1}|x_0 - x^*| \leq \frac{k^{n+1}}{1-k}|x_1 - x_0|$.

$\square$

5.3.3.3 Newton's and OPR Methods as Fixed Point Iterations

Newton's and OPR methods are fixed point iterations.

Corollary 5.1. *Assume τ_s is the root of the function ψ, while $\partial_\tau \psi(\tau_s) \neq 0$, g_N (5.30) and g_O (5.31) are fixed point iterations for the function ψ.*

Proof. It can be easily deduced $g_N(\tau_s) = \left(\tau_n - \frac{\psi(\tau_n)}{\partial_\tau \psi(\tau_n)}\right) = \tau_s$ and $g_O(\tau_s) = \left(\tau_s \times \frac{\psi_{max}}{\psi_{max} - \psi(\tau_s)}\right) = \tau_s$. $\square$

Proposition 5.2. *Some properties of the Newton's and OPR Methods:*

(i) $g_N(\tau_n)$ and $g_O(\tau_n)$ satisfies the convergence bounds indicated in (5.40), (5.41) and (5.42) as fixed point iterations.

(ii) If $g_N(\tau_n)$ starts with $\tau_0 = 0$, then $\psi(\tau) \geq 0$ and $\psi(\tau)$ monotonically decreases until convergence ($\tau \to \tau_\sigma$) while τ monotonically increases in every iteration ($\tau_0 = 0 < \ldots < \tau_n$).

(iii) For $g_O(\tau_n)$, if $\tau_\sigma < \tau_0$, $\psi(\tau) < 0$ until convergence ($\tau \to \tau_\sigma$) and τ monotonically decreases in every iteration ($\tau_0 > \ldots > \tau_n$).

(iv) For $g_O(\tau_n)$, if $\tau_0 < \tau_\sigma$, $0 < \psi(\tau)$ until convergence ($\tau \to \tau_\sigma$) and τ monotonically increases in every iteration ($\tau_0 < \ldots < \tau_n$).

Proof.

(i) $g_N(\tau_n)$ and $g_O(\tau_n)$ satisfies the convergence bounds indicated in (5.40), (5.41) and (5.42) as fixed point iterations.

(ii) $\psi(0) = \psi_{max} > 0$ by the definition of ψ. A convex function always lies above any of its tangent lines. So, $(\tau_{n+1}, \psi(\tau_{n+1}))$ is above than $(\tau_{n+1}, \psi(\tau_\sigma) = 0)$ which is on the tangent line. Thus, $\psi(\tau_n) \geq 0$ for all n. $\partial_\tau \psi(\tau_n)$ is negative since ψ is a convex nonincreasing function and $(\tau_n, \psi(\tau_n))$ lies above the x-axis. Therefore any τ_{n+1} must be on the left of (τ_n, τ_σ).

(iii) Since ψ is convex function, satisfies the following inequality

$$\forall \tau_1, \tau_2 \in [0, \tau_{MF}], \forall t \in [0,1]: \quad \psi(t\tau_1 + (1-t)\tau_2) \leq t\psi(\tau_1) + (1-t)\psi(\tau_2), \quad (5.44)$$

Eq. (5.31) simply produce the insersection point of the x-axis and the line between $\psi(0) = \psi_{max}$ and τ_n. Assume $\tau_1 = \tau_n$, $\tau_2 = 0$, and $t\tau_n + (1-t)\tau_2 = \tau_{n+1}$ then it has to be $t\psi(\tau_n) + (1-t)\psi(\tau_2) = 0$ that leads $\psi(\tau_{n+1}) < 0$ until $\tau \to \tau_\sigma$ where $\psi(\tau_\sigma) = 0$ (Since (5.31) is a fixed point, according to fixed point theorem except the root τ_σ, ψ

can not be equal to 0). Consider the τ_0, since $\psi(\tau_0) < 0$, $\left(0 < \frac{\psi_{max}}{\psi_{max}-\psi(\tau_0)} < 1\right)$ which resulting $\tau_0 > \tau_1$ and $\psi(\tau_0) < \psi(\tau_1)$ (since ψ is convex decreasing function). In a similar way, if we consider the $\tau_2 = \tau_1 \times \frac{\psi_{max}}{\phi_{max}-\psi(\tau_2)} = \tau_0 \times \frac{\psi_{max}}{\psi_{max}-\psi(\tau_1)} \times \frac{\psi_{max}}{\psi_{max}-\psi(\tau_2)}$ leads that $\tau_0 > \tau_1 > \tau_2$. It goes on until τ_σ, which leads us to conclude that $\tau_0 > \tau_1 > ... > \tau_\sigma$.

(iv) Following the similar steps in (iii), (iv) can be shown.

□

5.3.4 A Warm-Start Strategy for (P_σ^p)

A warm-start strategy provides an initial starting point to an algorithm instead a random one. It is mostly about finding a point nearby the solution and it is possible to gain some benefits in any algorithm if a priori information about the solution is known. Therefore there has ben many works investigated algorithms with a warm-start strategy such as [YW02; JY08; SKC10; CGG11; CPT17] to gain some benefits like faster convergence and less iterations etc.

In Chapter 3, the relation between the ℓ_p-norm representation and the concept n-widths is studied. There is a clear and direct link between n-widths and the optimal ℓ_p-norm representations. The n-widths provide insight about the order of the projection of the ℓ_p-ball onto a subspace.

In this subchapter, we introduce an ℓ_p-norm representation level based on n-widths and matrix properties presented in Chapter 4.1. We also offer a warm-start strategy for any algorithm which seeks the solution of (P_σ^p) based on this representation level.

5.3.4.1 An ℓ_p-norm Representation Level Based on n-widths and the Matrix Properties

The solution of (P_σ^p) satisfies some inequalities. Proposition 5.3 exhibits the relation between the solution of (P_σ^p) and the solution of $(\mathrm{P}_\sigma^{p,d})$ for a given signal $\mathbf{y}$.

Proposition 5.3. *For all* $\mathbf{y}$ *the solution of* (P_σ^p)*, i.e.* $\mathbf{x}_\sigma$*, satisfies following*

$$\|\mathbf{x}_\sigma\|_p \leq \rho^\circ(\hat{\mathbf{z}}_\sigma)\,(\rho(\mathbf{y}) - \sigma) \tag{5.45}$$

where $\hat{\mathbf{z}}_\sigma$ *is the solution of* $(P_\sigma^{p,d})$*.*

Proof. When there is no duality gap between (P_σ^p) and $(\mathrm{P}_\sigma^{p,d})$, following has to be satisfied

$$\|\mathbf{x}_\sigma\|_p = \mathbf{y}^T\hat{\mathbf{z}}_\sigma - \sigma\rho^\circ(\hat{\mathbf{z}}_\sigma). \tag{5.46}$$

Furthermore since ρ and its polar ρ° satisfies $\mathbf{y}^T\hat{\mathbf{z}}_\sigma \leq \rho(\mathbf{y})\rho^\circ(\hat{\mathbf{z}}_\sigma)$ [Ara+18], (5.45) simply can be derived. □

With the help of Proposition 5.3, an ℓ_p-norm representation level based on n-widths and the matrix property (4.1) introduced in Proposition 5.4

Proposition 5.4. *(ℓ_p-norm Representation Level Based on n-widths and the Matrix Properties) For all* $\mathbf{y}$ *there exists a solution of* (P_σ^p)*, i.e.* $\mathbf{x}_\sigma$*, satisfies* $\|\mathbf{x}_\sigma\|_p \leq K_p \|\mathbf{y}\|_2$*, with the representation level*

$$K_p = \frac{\beta_2 s^{\left(\frac{1}{2}-\frac{1}{p^*}\right)}}{A - \beta_2\sqrt{B}}, \tag{5.47}$$

for a frame matrix $\mathbf{D}$ *that satisfies (4.1).*

Proof. Reminding that if ρ is an ℓ_p-norm then ρ° is the dual norm [ROC70]. For ρ is ℓ_2-norm then (5.45) becomes $\|\mathbf{x}_\sigma\|_p \leq \|\hat{\mathbf{z}}_\sigma\|_2 (\|\mathbf{y}\|_2 - \sigma)$, and since $\|\hat{\mathbf{z}}_\sigma\|_2 \leq s^{\left(\frac{1}{2}-\frac{1}{p^*}\right)}/d_2$ where $d_2 = A/\beta_2 - \sqrt{B}$ from the Lemma 5.1, there is a

$$\|\mathbf{x}_\sigma\|_p \leq \frac{\beta_2 s^{\left(\frac{1}{2}-\frac{1}{p^*}\right)}}{(A - \beta_2\sqrt{B})} \left(\|\mathbf{y}\|_2 - \sigma\right), \tag{5.48}$$

and for $\sigma = 0$, (5.47) can be derived.

□

Corollary 5.2. *[Studer, [Stu+14]]. For all* $\mathbf{y}$ *there exists an* $\mathbf{x}_\sigma$ *satisfies,* $\|\mathbf{x}_\sigma\|_\infty \leq K_\infty \|\mathbf{y}\|_2$*, with the representation level* $K_\infty = \frac{\eta}{(A-\eta\sqrt{B})\sqrt{\delta N}}$*, for a frame matrix* $\mathbf{D}$ *that satisfies UP.*

Proof. K_∞ can be written by using equation (5.47) with $\beta_2 = \eta$, $s_2 = \delta N$ and $p^* = 1$. Remark that $K_\infty\sqrt{N}$ is called Kashin level and for a given $\mathbf{D}$, it only depends on η and δ. □

5.3.4.2 A Warm-Start Strategy

ℓ_p-norm representation level can help us to introduce a warm-start strategy for the problem (P_σ^p). For a decent warm start strategy, it is needed to find a point that is close to the solution. Let us introduce an upper bound for the solution of (P_σ^p) in Proposition 5.5.

Proposition 5.5. *For all* $\mathbf{y}$ *there exists an* $\mathbf{x}_\sigma$ *satisfies*

$$\|\mathbf{x}_\sigma\|_p \leq K_p \times \left(\frac{N^{\max\{0,(1/2-1/p)\}} \|\mathbf{x}_{MF}\|_p}{A^{\frac{3}{2}}} - \sigma \right), \tag{5.49}$$

for a frame matrix $\mathbf{D}$ *that satisfies (4.1).*

Proof. By using the frame inequalities following can be written

$$\|\mathbf{y}\|_2 \leq \frac{1}{A^{\frac{1}{2}}} \left\|\mathbf{D}^T\mathbf{y}\right\|_2 \leq \frac{1}{A^{\frac{3}{2}}} \left\|\mathbf{D}^T(\mathbf{D}\mathbf{D}^T)^{-1}\mathbf{y}\right\|_2. \tag{5.50}$$

Since $\left\|\mathbf{D}^T(\mathbf{D}\mathbf{D}^T)^{-1}\mathbf{y}\right\|_2 \leq N^{\max\{0,(1/2-1/p)\}}\left\|\mathbf{D}^T(\mathbf{D}\mathbf{D}^T)^{-1}\mathbf{y}\right\|_p$ and $\|\mathbf{x}_{MF}\|_p = \left\|\mathbf{D}^T(\mathbf{D}\mathbf{D}^T)^{-1}\mathbf{y}\right\|_p$, using representation level of ℓ_p-norms, (5.49) can be derived. □

With the help of Proposition 5.5, following warm start strategy is introduced for the algorithms that searches the solution of (P_σ^p).

Proposition 5.6. *For all* $\mathbf{y}$ *there exists an* τ_σ*, satisfies* $\tau_\sigma \leq \mu_p \tau_{MF}$ *where*

$$\mu_p = K_p \times \left(\frac{N^{\max\{0,(1/2-1/p)\}}}{A^{\frac{3}{2}}} - \frac{\sigma}{\tau_{MF}}\right). \tag{5.51}$$

Proof. Reminding $\tau_\sigma = \|\mathbf{x}_\sigma\|_p$, $\tau_{MF} = \|\mathbf{x}_{MF}\|_p$, and using Proposition 5.5, (5.51) can be obtained. □

Numerically K_p is not known, however its order depending on N, M and p is given in Corollary 3.2. One can try to seek a decent starting point for the root finding methods with a better understanding of K_p.

5.3.5 Bracketing the Root of the Nonlinear Equation

The bracketing type root finding methods require two points with opposing signs to assure convergence. [DB03]. In order to choose the root searching interval, we consider the MOF given in Chapter 2.2. Many common loss functions ρ are nonnegative and vanish at the origin, including gauges like Huber, least-squares and nonconvex losses such as Student's t. For these kind of losses, under the assumption that $\mathbf{D}$ is full row-rank, $\rho(\mathbf{y} - \mathbf{D}\mathbf{x}_{MF}) = 0$ and $\psi(\tau_{MF}) = -\sigma$ with $\tau_{MF} = \|\mathbf{x}_{MF}\|_p$. For the left endpoint, we consider $\mathbf{x} = 0$, and $\tau = 0$, with loss equal to $\rho(\mathbf{y})$. Bracketing the root searching interval between the points $\mathbf{x}_{MF}$ and 0 ensures finding a solution for (5.29) since they provide two initial points with opposite signs for ψ, as long as $\rho(\mathbf{y}) > \sigma$.

5.4 Nonconvexity and the Pareto Curve

In this subchapter, we investigate the ℓ_p-norm level-set formulations ((P_σ^p), (P_λ^p) and (P_τ^p)) with a nonconvex ρ. All of the root finding methods given in thesis can find a solution of (P_σ^p) if ρ is convex. However, if the ρ is nonconvex, some of the methods may not offer a solution for (P_σ^p).

Moving outside of the convex class is an appealing property since the loss functions can be more likely to be nonconvex in real world applications [GBC16] and opens the way for using many useful nonconvex models in (P_σ) formulations. For example, [SBV10] and [BG11] consider mixture models whose negative log-likelihood are nonconvex, with applications to high-dimensional inhomogeneous data where number of covariates could be larger than sample size. It is much harder to deal with the nonconvex losses since they may have multiple local optimal points in multiple feasible regions and nonconvex optimization problems can not be solved adequately [Dan+20]. However, they can achieve better performances than the convex ones [MBM18; VAS21]. For instance, [ABP12; ABP13; Ara+12] use nonconvex Student's t likelihoods to develop outlier-robust approaches.

5.4.1 Open-type Root Finding Methods and Nonconvexity

In order to solve the (P_σ^p), (5.29) needed to be solved. One possible approach to solve (5.29) is to deploy an open-type root finding method. In general, they are known with their speed and efficiency and mainly they do not assure convergence. In this subsection, Newton's and OPR methods are inspected.

5.4.1.1 Newton's Method and Nonconvex Pareto Frontiers

Newton's method can not maintain a convergence guarantee for the (P_σ^p) with a nonconvex ρ. An example of Newton's method divergence for nonconvex Pareto curves is shown in Figure 5.10. Green lines represent the tangent line for ψ at some τ. For some τ the tangent line can leave the feasible area, can be negative or equal to zero. In these conditions, it is not possible for Newton's method iterations to proceed further. Same situation is valid for secant method and its variants as well.

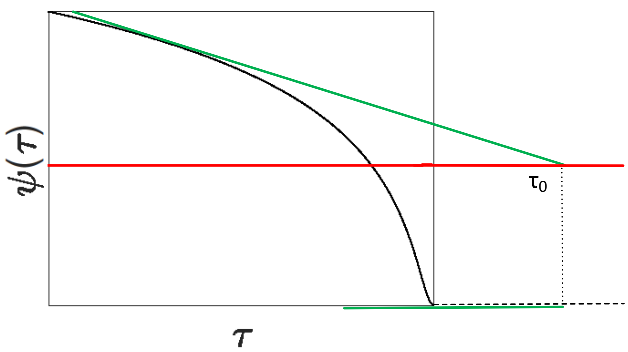

Figure 5.10: An example of Newton's divergence for nonconvex Pareto curves.

5.4.1.2 OPR and Nonconvex Pareto Frontiers

Although the OPR is an open-type root finding method and does not necessarily bracket the root, it ensures convergence guarantee for the Pareto frontier (7.49) for the (P_σ^p) even with a nonconvex ρ.

An example of OPR method convergence for nonconvex Pareto curves is shown in Figure 5.11. Green lines represent the secant line for ψ at some τ. The OPR draws a secant line between $\psi(\tau = 0)$ and any $\psi(\tau)$ until it converges. τ can not be negative for the OPR since the secant can not leave the feasible area. Thus, the OPR ensures convergence to solve (P_σ^p) with both convex and nonconvex loss ρ.

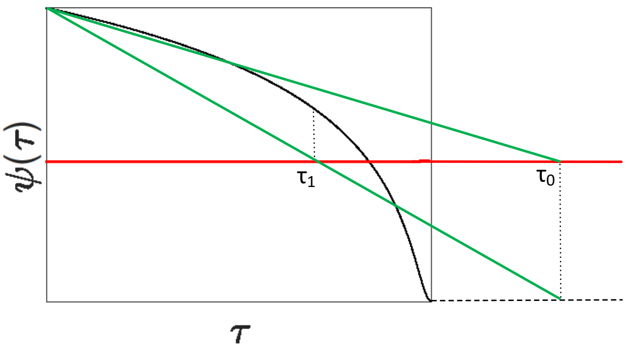

Figure 5.11: An example of OPR convergence for nonconvex Pareto curves.

5.4.2 Bracketing-type Root Finding Methods and Nonconvexity

The bracketing-type root finding methods must have two points with opposing signs in order to guarantee convergence [DB03] and as long as it is provided they are compelled to find a solution. Bracketing the root of (5.29) as it is introduced in 5.3.5 ensures convergence for the bracketing-type root finding methods to solve (P_σ^p).

5.5 Error Bounds for the Fixed Point Root Finding Methods

Newton's and OPR are deployed to solve (5.29) as fixed point iterations. In this subchapter, convergence of the these methods are analyzed with the matrix properties given in Chapter 4.1.

5.5.1 Error Estimate Bounds for the Newton's Method Iterations

The error bound for Newton's method iterations of solving (5.29) is derived in Proposition 5.7.

Proposition 5.7. *(Convergence with g_N Iterations) For $\tau_0 = 0$, error bound of the Pareto curve method with (5.30), i.e. $\tau_{n+1} - \tau_\sigma$, satisfies (5.40), (5.41) and (5.42) for ℓ_p-norm minimization where*

$$k = \left(1 - \frac{\psi_{max}}{\tau_\sigma} \times \frac{\rho^\circ(\boldsymbol{y})}{\|\mathbf{D}^T\mathbf{y}\|_{p^*}}\right). \tag{5.52}$$

Proof. Let us consider the relation between $\tau_1 - \tau_\sigma$ and $\tau_0 - \tau_\sigma$ for $\tau_0 = 0$,

$$\begin{aligned}\frac{\tau_1 - \tau_\sigma}{\tau_0 - \tau_\sigma} = 1 - \frac{\tau_0 - \tau_1}{\tau_0 - \tau_\sigma} = 1 - \frac{\tau_0 - \left(\tau_0 - \frac{\psi(\tau_0)}{\partial_\tau \nu(\tau_0)}\right)}{\tau_0 - \tau_\sigma} &= 1 + \frac{\psi_{max}}{\tau_\sigma \partial_\tau \nu(\tau_0)} \\ &= 1 - \frac{\psi_{max}}{\tau_\sigma} \times \frac{\rho^\circ(\mathbf{y})}{\|\mathbf{D}^T \mathbf{y}\|_{p^*}}.\end{aligned} \tag{5.53}$$

From (5.43), it can be inferred that $\tau_1 - \tau_\sigma \leq k(\tau_0 - \tau_\sigma)$ where $k < 1$. Equation (5.53) shows that there exists a $k = \left(1 - \frac{\psi_{max}}{\tau_\sigma} \times \frac{\rho^\circ(\mathbf{y})}{\|\mathbf{D}^T\mathbf{y}\|_{p^*}}\right)$. ☐

5.5.2 Error Estimate Bounds for the OPR Iterations

The error bound for the OPR method iterations of solving (5.29) is derived in Proposition 5.8.

Proposition 5.8. *(Convergence with g_O Iterations) Under the conditions of Lemma 5.1, and for $\tau_0 = \mu\tau_{MF}$, error bound of the Pareto curve method with (5.31), i.e. $\tau_{n+1} - \tau_\sigma$, satisfies (5.40), (5.41) and (5.42) for ℓ_p-norm minimization where*

$$k = \left(1 - \frac{d_t}{s^{\left(\frac{1}{t} - \frac{1}{p^*}\right)}} \times \frac{\|\mathbf{y}\|_t}{\|\mathbf{D}\mathbf{D}^T\|_{t\to t} N^{\max\{0,(1/p^* - 1/p)\}}} \times \frac{\mu}{\psi_{max} + \sigma} \times \left|\frac{\psi(\mu\tau_{MF})}{(\mu\tau_{MF} - \tau_\sigma)}\right|\right) \tag{5.54}$$

if $\beta_t < \|\mathbf{D}^T\|_{t\to t} / \left\|\mathbf{D}\mathbf{D}^T\right\|_{t\to t}$ and $0 < s < N$.

For $t = 2$, (5.54) becomes

$$k = \left(1 - \left(\frac{A - \beta_2\sqrt{B}}{\beta_2 s^{\left(\frac{1}{2} - \frac{1}{p^*}\right)}}\right) \times \frac{\|\mathbf{y}\|_2}{B N^{\max\{0,(1/p^* - 1/p)\}}} \times \frac{\mu}{\psi_{max} + \sigma} \times \left|\frac{\psi(\mu\tau_{MF})}{(\mu\tau_{MF} - \tau_\sigma)}\right|\right). \tag{5.55}$$

For $t = 2$ and if ρ is ℓ_2-norm, (5.54) becomes

$$k = \left(1 - \left(\frac{A - \beta_2\sqrt{B}}{\beta_2 s^{\left(\frac{1}{2} - \frac{1}{p^*}\right)}}\right) \times \frac{\mu}{B N^{\max\{0,(1/p^* - 1/p)\}}} \times \left|\frac{\psi(\mu\tau_{MF})}{(\mu\tau_{MF} - \tau_\sigma)}\right|\right). \tag{5.56}$$

Proof. Let us consider the relation between $\tau_1 - \tau_\sigma$ and $\tau_0 - \tau_\sigma$ for $\tau_0 = \mu\tau_{MF}$,

$$\begin{aligned}\frac{\tau_1 - \tau_\sigma}{\tau_0 - \tau_\sigma} = 1 - \frac{\tau_0 - \tau_1}{\tau_0 - \tau_\sigma} &= 1 - \frac{\mu\tau_{MF} - \frac{\mu\tau_{MF}\psi_{max}}{\psi_{max} - \psi(\mu\tau_{MF})}}{\mu\tau_{MF} - \tau_\sigma} \\ &= 1 + \frac{\mu\tau_{MF}\psi(\mu\tau_{MF})}{(\psi_{max} - \psi(\mu\tau_{MF}))(\mu\tau_{MF} - \tau_\sigma)}.\end{aligned} \tag{5.57}$$

The term $\psi(\mu\tau_{MF}) / (\mu\tau_{MF} - \tau_\sigma)$ is always negative since $0 < \psi(\mu\tau_{MF})$, if $\mu\tau_{MF} > \tau_\sigma$ and $0 > \psi(\mu\tau_{MF})$, if $\mu\tau_{MF} < \tau_\sigma$, and $\mu\tau_{MF} / (\psi_{max} - \psi(\mu\tau_{MF}))$ is always positive. We know that $(\psi_{max} - \psi(\mu\tau_{MF})) \leq \psi_{max} - (\nu(\mu\tau_{MF}) - \sigma) \leq \psi_{max} + \sigma$. Then, following inequality can be deduced

$$\begin{aligned} \frac{\tau_1 - \tau_\sigma}{\tau_0 - \tau_\sigma} &= 1 - \frac{\mu\tau_{MF}}{(\psi_{max} - \psi(\mu\tau_{MF}))} \left| \frac{\psi(\mu\tau_{MF})}{(\mu\tau_{MF} - \tau_\sigma)} \right| \\ &\leq 1 - \frac{\mu\tau_{MF}}{\psi_{max} + \sigma} \left| \frac{\psi(\mu\tau_{MF})}{(\mu\tau_{MF} - \tau_\sigma)} \right| . \end{aligned} \tag{5.58}$$

Reminding that $\tau_{MF} = \|\mathbf{x}_{MF}\|_p = \left\|\mathbf{D}^T(\mathbf{D}\mathbf{D}^T)^{-1}\mathbf{y}\right\|_p$, with the help of Lemma 5.1, $\left\|\mathbf{D}^T(\mathbf{D}\mathbf{D}^T)^{-1}\mathbf{y}\right\|_p$ can be bounded. Let us consider the point $\hat{\mathbf{z}}_\sigma = (\mathbf{D}\mathbf{D}^T)^{-1}\mathbf{y} / \left\|\mathbf{D}^T(\mathbf{D}\mathbf{D}^T)^{-1}\mathbf{y}\right\|_{p^*}$, which is a feasible point of $(\mathrm{P}_\sigma^{p,d})$, then it should satisfies following

$$\frac{d_t}{s^{\left(\frac{1}{t} - \frac{1}{p^*}\right)}} \leq \frac{\left\|\mathbf{D}^T(\mathbf{D}\mathbf{D}^T)^{-1}\mathbf{y}\right\|_{p^*}}{\|(\mathbf{D}\mathbf{D}^T)^{-1}\mathbf{y}\|_t} \leq \frac{\left\|\mathbf{D}^T(\mathbf{D}\mathbf{D}^T)^{-1}\mathbf{y}\right\|_{p^*}\left\|\mathbf{D}\mathbf{D}^T\right\|_{t\to t}}{\|\mathbf{y}\|_t}, \tag{5.59}$$

then since $\left\|\mathbf{D}^T(\mathbf{D}\mathbf{D}^T)^{-1}\mathbf{y}\right\|_{p^*} \leq N^{\max\{0,(1/p^*-1/p)\}} \left\|\mathbf{D}^T(\mathbf{D}\mathbf{D}^T)^{-1}\mathbf{y}\right\|_p$, $\left\|\mathbf{D}^T(\mathbf{D}\mathbf{D}^T)^{-1}\mathbf{y}\right\|_p$ can be bounded as

$$\frac{d_t}{s^{\left(\frac{1}{t} - \frac{1}{p^*}\right)}} \times \frac{\|\mathbf{y}\|_t}{\|\mathbf{D}\mathbf{D}^T\|_{t\to t} N^{\max\{0,(1/p^*-1/p)\}}} \leq \left\|\mathbf{D}^T(\mathbf{D}\mathbf{D}^T)^{-1}\mathbf{y}\right\|_p \tag{5.60}$$

and eq. (5.57) can be induced as

$$\frac{\tau_1 - \tau_\sigma}{\tau_0 - \tau_\sigma} \leq 1 - \frac{d_t}{s^{\left(\frac{1}{t} - \frac{1}{p^*}\right)}} \times \frac{\|\mathbf{y}\|_t}{\|\mathbf{D}\mathbf{D}^T\|_{t\to t} N^{\max\{0,(1/p^*-1/p)\}}} \times \frac{\mu}{\psi_{max} + \sigma} \left| \frac{\psi(\mu\tau_{MF})}{(\mu\tau_{MF} - \tau_\sigma)} \right| \tag{5.61}$$

From (5.43), it can be inferred that $\tau_1 - \tau_\sigma \leq k(\tau_{MF} - \tau_\sigma)$ where $k < 1$. Eq. (5.61) shows that there exists a $k = \left(1 - \frac{d_t}{s^{\left(\frac{1}{t} - \frac{1}{p^*}\right)}} \times \frac{\|\mathbf{y}\|_t}{\|\mathbf{D}\mathbf{D}^T\|_{t\to t} N^{\max\{0,(1/p^*-1/p)\}}} \times \frac{\mu}{\psi_{max}+\sigma} \left| \frac{\psi(\mu\tau_{MF})}{(\mu\tau_{MF}-\tau_\sigma)} \right| \right)$.

For ρ is ℓ_2-norm $\psi_{max} = \|\mathbf{y}\|_2 - \sigma$ and by taking $t = 2$, (5.55) can be derived. □

5.5.2.1 Error Bounds of the ℓ_1-norm Minimization via OPR Iterations with the Matrix Properties

Corollary 5.3. *Convergence of* (P_σ^1)*: Assume* $\frac{1}{\sqrt{M}}\mathbf{D}$ *is a* $M \times N$ *matrix with i.i.d zero mean sub-Gaussian random variable entries with parameter* ς *and satisfies the UUP. Error bound of the Pareto curve method with* g_O *iterations satisfies (5.40), (5.41) and (5.42) for* ℓ_1*-norm minimization with*

$$k = \left(1 - \frac{\left(A - (1+\epsilon)\sqrt{B}\right)}{B(1+\epsilon)\sqrt{s}} \times \frac{\mu\|\mathbf{y}\|_2}{\psi_{max} + \sigma} \times \left| \frac{\psi(\mu\tau_{MF})}{(\mu\tau_{MF} - \tau_\sigma)} \right| \right) \tag{5.62}$$

and for ρ is ℓ_2-norm,

$$k = \left(1 - \frac{\left(A - (1+\epsilon)\sqrt{B}\right)}{B(1+\epsilon)\sqrt{s}} \times \mu \times \left|\frac{\psi(\mu\tau_{MF})}{(\mu\tau_{MF} - \tau_\sigma)}\right|\right) \tag{5.63}$$

provided (with the assumption of) $M > C_\varsigma \epsilon^{-2} s \log(N/s)$ and C_ς is a constant depending on ς.

Proof. Consider $t = 2$ for (4.1). With $p = 1$ (i.e. $p^* = \infty$), (5.62) can be obtained by using (5.55). If ρ is ℓ_2-norm then $\psi_{max} = \|\mathbf{y}\|_2 - \sigma$. Reminding that for a matrix that satisfies UUP, $\beta_2 = 1 + \epsilon$. □

5.5.2.2 Error Bounds of the ℓ_∞-norm Minimization via OPR Iterations with the Matrix Properties

Corollary 5.4. *Convergence of (P_σ^∞): Assume $\frac{1}{\sqrt{N}}\mathbf{D}$ is a $M \times N$ ξ-Parseval frame with i.i.d zero mean sub-Gaussian random variable entries with parameter ς and satisfies the UP. Error bound of the Pareto curve method with g_O iterations satisfies (5.40), (5.41) and (5.42) for ℓ_∞-norm minimization with*

$$k = \left(1 - \frac{\left(A - \eta\sqrt{B}\right)\delta\,\|\mathbf{y}\|_2}{\eta B\sqrt{N}} \times \frac{\mu}{\psi_{max} + \sigma} \times \left|\frac{\psi(\mu\tau_{MF})}{(\mu\tau_{MF} - \tau_\sigma)}\right|\right) \tag{5.64}$$

and for ρ is ℓ_2-norm,

$$k = \left(1 - \frac{\left(A - \eta\sqrt{B}\right)\delta}{\eta B\sqrt{N}\mu} \times \mu \times \left|\frac{\psi(\mu\tau_{MF})}{(\mu\tau_{MF} - \tau_\sigma)}\right|\right) \tag{5.65}$$

where $A = 1 - \xi, B = 1 + \xi$ frame bounds with small $\xi > 0$.
If

- *$\frac{1}{\sqrt{N}}\mathbf{D}$ is a $M \times N$ ξ-Parseval frame with i.i.d zero mean sub-Gaussian random variable entries with parameter ς and satisfies the UP, then* (5.65) *holds for*

$$\eta = \varsigma c_6 \sqrt{\frac{\log(\omega)}{\omega}}, \tag{5.66}$$

$$\delta = \frac{c_7}{\omega} \tag{5.67}$$

where c_6 and c_7 are the positive constants.

- *$\mathbf{D}$ is a $M \times N$ random orthogonal matrix satisfies the UP, then* (5.65) *holds for*

$$\eta = 1 - \frac{c_1}{4}, \tag{5.68}$$

$$\delta = \frac{c_2 c_1^2}{\log\left(\frac{1}{c_1}\right)}, \tag{5.69}$$

where $0 < c_1 = \omega - 1$ *and* $0 < c_2$ *is an absolute constant.*

- $\mathbf{D}$ *is a* $M \times N$ *random partial Fourier matrix as it is described in Theorem 4.3 and satisfies the UP, then* (5.65) *holds for*

$$\eta = 1 - \frac{c_4}{4}, \tag{5.70}$$

$$\delta = \frac{c_5 c_4^2}{\log^4(N)}, \tag{5.71}$$

where $c_4 = \omega - 1$ *for some* $c_4 \in (0, 1]$ *and* $0 < c_5$.

Proof. Consider $t = 2$ for (4.1). With $p = \infty$ (i.e. $p^* = 1$), (5.64) can be obtained by using (5.55). If ρ is ℓ_2-norm then $\psi_{max} = \|\mathbf{y}\|_2 - \sigma$. Reminding that for a matrix that satisfies UP, $\beta_2 = \eta$, $s = \delta N$. Using the UP parameters given Section 4.2.2 for several random matrices, η and δ can be written.

□

Chapter 6

Solving (P_σ)

In order to solve (P_σ^p), (P_τ^p) needs to be repeatedly solved. In this thesis, two methods are introduced to solve (P_τ^p). First one is the well-known, simple and efficient *projected gradient method* and the second one is the projection-free Frank-Wolfe method.

6.1 ($\mathbf{P}_\tau$) Solver

(P_τ) can be solved using the simple projected gradient method

6.1.1 Projected Gradient Method to Solve ($\mathbf{P}_\tau$)

Let us reformulate the optimization problem (P_τ) as Nesterov's first-order method for smooth convex functons

$$\underset{\|\mathbf{x}\|_p \leq \tau}{\text{minimize}} \quad f(\mathbf{x}), \tag{6.1}$$

where $f(\mathbf{x}) = \rho(\mathbf{y} - \mathbf{D}\mathbf{x})$. Eq. (6.1) can be solved with the well known basic gradient descent method, which requires computing

$$\mathbf{x}^{(k)} = \mathbf{x}^{(k-1)} - \gamma \nabla f(\mathbf{x}^{(k-1)}) \tag{6.2}$$

iteratively until the stopping criteria is met, where k is the iteration number and γ is a suitable step size. Although γ has key importance to the speed of the algorithm itself, in this study, we avoid applying any acceleration methods regarding γ to solve (6.2) for the sake of analysis simplicity.

For mathemaical convenience, eq. (6.2) can be interpreted via an approximation scheme which replaces the original problem with a quadratic approximation function of the objective function such as $f(\mathbf{x}) \approx f(\mathbf{v}) + \langle \nabla f(\mathbf{v}), \mathbf{x} - \mathbf{v} \rangle + \frac{1}{2\gamma} \|\mathbf{x} - \mathbf{v}\|_2^2$. Then for a fixed point $\mathbf{x}^{(k-1)}$, a minimizer $\mathbf{x}^{(k)}$ to solve (6.1) for $\mathbf{v} = \mathbf{x}^{(k-1)}$ is going to be

$$\mathbf{x}^{(k)} = \arg \min_{\|\mathbf{x}\|_p \leq \tau} \{ f(\mathbf{x}^{(k-1)}) + \langle \nabla f(\mathbf{x}^{(k-1)}), \mathbf{x} - \mathbf{x}^{(k-1)} \rangle + \frac{\gamma}{2} \left\| \mathbf{x} - \mathbf{x}^{(k-1)} \right\|_2^2 \}, \tag{6.3}$$

by ignoring the constant term and after some simplifications, (6.3) can be written as

$$\mathbf{x}^{(k)} = \underset{\|\mathbf{x}\|_p \le \tau}{\arg\min} \ \frac{1}{2} \left\| \mathbf{x} - \left(\mathbf{x}^{(k-1)} - \gamma \nabla f(\mathbf{x}^{(k-1)}) \right) \right\|_2^2 . \tag{6.4}$$

With the problem definition of (P_τ), it can be easily deduced that (6.4) is just the orthogonal projection of the vector $\left(\mathbf{x}^{(k-1)} - \gamma \nabla f(\mathbf{x}^{(k-1)})\right)$ onto the ℓ_p-ball of radius τ, which will be denoted as

$$\mathbf{x}^{(k)} = \mathrm{proj}_{\mathcal{B}_p} \left(\mathbf{x}^{(k-1)} - \gamma \nabla f(\mathbf{x}^{(k-1)}), \tau \right), \tag{6.5}$$

that is

$$\mathbf{x}^{(k)} = \mathrm{proj}_{\mathcal{B}_p} \left(\mathbf{x}^{(k-1)} + \gamma \mathbf{D}^T \nabla \rho(\mathbf{y} - \mathbf{D}\mathbf{x}^{(k-1)}), \tau \right). \tag{6.6}$$

6.1.1.1 Projection onto the ℓ_1-ball

Projection of a vector $\mathbf{a} = [a_1, a_2, ..., a_N]$ onto the ℓ_1-ball can be written as following

$$\mathrm{proj}_{\tau\mathcal{B}_1}(\mathbf{a}) = \begin{cases} \mathbf{a}, & \text{if} \ \ \|\mathbf{a}\|_1 \le 1 \\ \mathrm{sgn}(a_i)\max\{|a_i| - \kappa, 0\}, & \text{else} \end{cases} \tag{6.7}$$

where κ is the Lagrangian multiplier of $\mathrm{proj}_{\tau\mathcal{B}_1}(\mathbf{a})$ [Duc+08]. The tricky part of the projection is to find the κ that satisifes Karush-Kuhn-Tucker optimality condition $\sum_{i=1}^{N}(|a_i| - \kappa) = \tau$ in an efficient way.

In order to find κ, we utilized the simple, sorting based approach introduced in [HWC74]. Additional variations of this method are described in [Con16].

To find κ:

- Sort $|\mathbf{a}|$ as: $c_1 \ge c_2 \ge ... \ge c_N$,
- Find $K = \max\limits_{1 \le k \le N} \left\{ k \mid \left(\sum_{j=1}^{k} c_j - \tau \right) / k \le c_k \right\}$,
- Calculate $\kappa = \left(\sum_{k=1}^{K} c_k - \tau \right) / K$.

6.1.1.2 Projection onto the ℓ_∞-ball

Projection onto the ℓ_∞-ball is a simple thresholding operation and with the help of Moreau Decomposition and *soft thresholding operator* can be written as:

$$\mathrm{proj}_{\mathcal{B}_\infty}(\mathbf{a}, \tau) = \begin{cases} \tau\mathrm{sgn}(\tau), & \text{if} \ \ |a_i| \ge \tau \\ a_i, & \text{if} \ \ |a_i| < \tau \end{cases} . \tag{6.8}$$

6.1.1.3 A Duality Gap

Since Pareto curve depicts the optimal solution, duality of (P_τ^p) is important to bound the accuracy of the calculated ψ. Let us consider a feasible solution $\bar{\mathbf{x}}_\tau$ and corresposing residual vector $\bar{\mathbf{r}_\tau} = \mathbf{y} - \mathrm{D}\bar{\mathbf{x}}_\tau$ for a τ. Pareto curve is convex decreasing in τ and a given has to be higher than the optimal. Similarly a residual for a feasible point has to be higher than the optimal residual, thus we can write

$$0 < \rho\left(\mathbf{r}_\tau\right) \leq \rho\left(\bar{\mathbf{r}_\tau}\right) \tag{6.9}$$

where $\mathbf{r}_\tau = \mathbf{y} - \mathbf{D}\mathbf{x}_\tau$ and $\mathbf{x}_\tau$ is the optimal solution for a given τ.

Remember the Lagrangian dual of (P_σ^p). The objective of ($\mathrm{P}_\tau^{p,d}$) should satisfy

$$\mathbf{y}^T\mathbf{z}_\tau - \tau\lambda \leq \rho\left(\mathbf{r}_\tau\right) \leq \rho\left(\bar{\mathbf{r}_\tau}\right) \tag{6.10}$$

Let us take $\mathbf{z}_\tau = \bar{\mathbf{r}_\tau}/\rho^\circ(\bar{\mathbf{r}_\tau})$, it is feasible for ($\mathrm{P}_\tau^{p,d}$) since ρ is positive homogeneous and $\lambda = \left\|\mathbf{D}^T\mathbf{z}_\tau\right\|_{p^*}$. Then

$$\frac{\mathbf{y}^T\bar{\mathbf{r}_\tau} - \tau\left\|\mathbf{D}^T\bar{\mathbf{r}_\tau}\right\|_{p^*}}{\rho^\circ(\bar{\mathbf{r}_\tau})} \leq \rho\left(\mathbf{r}_\tau\right) \leq \rho\left(\bar{\mathbf{r}_\tau}\right). \tag{6.11}$$

By using (6.11), following duality gap g_τ can be defined.

$$g_\tau := \frac{\mathbf{y}^T\bar{\mathbf{r}_\tau} - \tau\left\|\mathbf{D}^T\bar{\mathbf{r}_\tau}\right\|_{p^*}}{\rho^\circ(\bar{\mathbf{r}_\tau})} - \rho\left(\bar{\mathbf{r}_\tau}\right). \tag{6.12}$$

6.1.1.4 Fast Iterative Shrinkage Thresholding Algorithm

(P_τ) can be solved with the projected gradeient method *Fast Iterative Shrinkage Thresholding Algorithm* (FISTA) with the steps given in Algorithm 1.

Algorithm 1 FISTA (τ)

Input: $\mathbf{y}$, $\mathbf{D}$, τ, ζ,
Initialization: $\mathbf{x}^{(0)} = \mathbf{x}$, $\mathbf{z}^{(1)} = \mathbf{x}$, $t_1 = 1$,

1: **for** k=1,2,3,...,iter **do**
2: $\quad \mathbf{x}^{(k)} = \mathrm{proj}_{\mathcal{B}_p}\left(\mathbf{z}^{(k)} - \gamma\mathbf{D}^T\nabla\rho(\mathbf{y} - \mathbf{D}\mathbf{z}^{(k)}), \tau\right)$
3: $\quad t_{k+1} = \frac{1+\sqrt{1+4t_k^2}}{2}$
4: $\quad \mathbf{z}^{(k+1)} = \mathbf{x}^{(k)} + \frac{t_k - 1}{t_{k+1}}(\mathbf{x}^{(k)} - \mathbf{x}^{(k-1)})$
5: $\quad$ **if** $g_\tau \leq \zeta$ **then**
6: $\qquad$ return $\mathbf{x}_\tau = \mathbf{z}^{(k+1)}$
7: $\quad$ **end if**
8: **end for**

Output: $\mathbf{x}_\tau = \arg\min$ (P_τ^p).

6.1.2 Projection-Free Frank-Wolfe to Solve ($\mathbf{P}_\tau$)

(P_τ^p) can be solved with the projected gradient methods. However, especially in big data sets projection steps could be notably costly [HK12]. There is a simple projection-free algorithm called Frank-Wolfe that performs linear optimization over the constraint set has been introduced in [FW+56]. The Frank-Wolfe algorithm can be a very preferable alternative to projection gradient methods since linear optimization over the ℓ_p-ball constraint is much faster and simpler than projection onto it [DU18].

Algorithm 2 Frank-Wolfe(τ) to Solve (P_τ^p)

Input: $\mathbf{y}$, $\mathbf{D}$, τ, ζ,
Initialization: Let $\left\|\mathbf{x}^{(0)}\right\|_p \leq \tau$,

1: **repeat**
2: **for** $k = 0, \ldots$ **do**
3: $\mathbf{s}^{(k-1)} = \underset{\|\mathbf{s}\|_p \leq \tau}{\arg\min} \ \langle \mathbf{s}, \mathbf{D}^T \nabla \rho(\mathbf{y} - \mathbf{D}\mathbf{x}^{(k)}) \rangle$
4: $\mathbf{x}^{(k+1)} = (1-\gamma)\,\mathbf{x}^{(k)} + \gamma \mathbf{s}$, with $\gamma = \frac{2}{k+2}$
5: **end for**
6: **until** $g_\tau \leq \zeta_1$

Output: $\mathbf{x}_\tau = \arg\min\ (\mathrm{P}_\tau^p)$.

6.1.2.1 Duality Gap for the Frank-Wolfe Iterations

Pareto curve depicts the optimal solution, therefore stopping criteria is important for (P_τ^p). Frank-Wolfe iterations most oftenly enforces a duality gap as a stopping condition that is given in [Jag13] such

$$g_\tau := \max_{\|\mathbf{s}\|_p \leq \tau} \ \langle \mathbf{x} - \mathbf{s}, \mathbf{D}^T \nabla \rho(\mathbf{y} - \mathbf{D}\mathbf{x}) \rangle. \tag{6.13}$$

(7.52) can be simplified as

$$g_\tau := \max_{\|\mathbf{s}\|_p \leq \tau} \ \langle \mathbf{x} - \mathbf{s}, \mathbf{D}^T \nabla \rho(\mathbf{y} - \mathbf{D}\mathbf{x}) \rangle = \langle \mathbf{x}, \nabla \mathbf{D}^T \nabla \rho(\mathbf{y} - \mathbf{D}\mathbf{x}) \rangle + \tau \left\| \mathbf{D}^T \nabla \rho(\mathbf{y} - \mathbf{D}\mathbf{x}) \right\|_{p^*}. \tag{6.14}$$

6.2 Solving ($\mathbf{P}_\sigma^p$)

(P_σ^p) can be solved by combining the root finding methods presented in Section 5.3 with a (P_τ^p) solver as follows:

- Choose initial τ values.

  Some root finding approaches require one single starting point like Newton's method while some require two like the bracketing-type methods. Choose two initial values with opposite signs to ensure convergence of bracketing-type methods. The default choice can given by $\tau = 0$ and $\tau = \tau_{MF}$ to secure two points with opposite signs as it is explained in Section 5.3.5.

- Apply the steps of a nonlinear equation root finding step to solve (5.29).

  Different root finding methods come with different computational costs. Solving (5.29) is more expensive for Newton's method than for bracketing-type methods since the derivative calculation of the nonlinear equation is required along with the function evaluation, while bracketing-type methods need only the function evaluation which does not required for the points $\tau = 0$ and $\tau = \tau_{MF}$ since we can already calculate $\nu(\tau = 0)$ and $\nu(\tau = \tau_{MF})$ without solving (P_τ^p).

- Terminate once the stopping criteria are met.

The steps above are algoritmized in Algorithm 3.

Algorithm 3 Solving (P_σ^p)

Input: $\mathbf{y}$, $\mathbf{D}$, σ, ζ,
Initialization: Choose initial τ,

repeat
  for $k = 1, \ldots$ **do**
    $\mathbf{x}^{(k-1)} :=$ The solution of ($\mathrm{P}_{\tau-1}^p$)
    $\tau_k :=$ The solution of (5.29)
  end for
until $\rho(\mathbf{y} - \mathrm{D}\mathbf{x}^{(k-1)}) - \sigma \leq \zeta_2$

Output: $\mathbf{x}_\sigma = \arg\min\ (\mathrm{P}_\sigma^p)$.

6.3 Solving ($\mathbf{P}_\sigma^1$) and ($\mathbf{P}_\sigma^\infty$) with the OPR and Newton's Method Iterations

In this subchapter, numerical experiments are exhibited for solving (P_σ^1) and (P_σ^∞) by using the Algorithm 3. g_O is compared to g_N in terms of the results accuracy and the iteration number (*iter*) which is the number of required (P_τ^p) solving steps to have the solution of (P_σ^p). Performances of the g_O and g_N iterations are investigated for three different loss functions ρ which are

$$\text{Least squares} \quad \rho_l(\mathbf{x}) = \|\mathbf{x}\|_2\,, \tag{6.15}$$

$$\text{Huber} \quad \rho_h(\mathbf{x})_i = \sum_{i=1}^{N} \begin{cases} \frac{x_i^2}{2}, & \text{if } |x_i| \leq \Gamma \\ \Gamma|x_i| - \frac{\Gamma^2}{2}, & \text{otherwise} \end{cases}\,, \tag{6.16}$$

$$\text{Student's t} \quad \rho_s(\mathbf{x})_i = \sum_{i=1}^{N} \kappa \log\left(1 + x_i^2/\kappa\right), \tag{6.17}$$

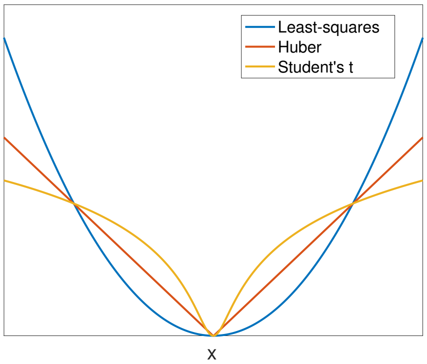

Figure 6.1: Illustration of the loss functions *least-squares*, *Huber* and *Student's t*.

where Γ and κ are the tunning parameters for ρ_h and ρ_s respectively; we take Γ and κ 0.1 for the simulations. Behaviours of the ρ_l, ρ_h and ρ_s are depicted in Figure 6.1.

ρ_l and ρ_h are employed as gauge penalties while ρ_s is utilized as a nonconvex penalty. While ρ_l is the most commonly used loss function in numerous optimziation problems, ρ_h is less sensitive to outliers in the data than ρ_l. ρ_s is also utilized to develop outlier-robust approaches [ABP12; ABP13; Ara+12]. Thus, we include ρ_s for the simulations as well.

For the g_N iterations, $\partial_\tau \nu(\tau)$ is needed to be calculated. $\partial_\tau \nu(\tau)$ calculation requires the feasible solution of ($\mathrm{P}_\tau^{p,d}$) which can be found in [Ara+19] for several loss functions.

6.3.1 Using the Warm-Start Strategy for ($\mathbf{P}_\sigma^1$) and ($\mathbf{P}_\sigma^\infty$)

From the Proposition 5.6, it is known that for all $\mathbf{y}$ there exists an τ_σ, satisfies $\tau_\sigma \leq \mu \tau_{MF}$ where

$$\mu = K_1 \left(\frac{1}{A^{\frac{3}{2}}} - \frac{\sigma}{\tau_{MF}} \right), \tag{6.18}$$

$$\mu = K_\infty \left(\frac{\sqrt{N}}{A^{\frac{3}{2}}} - \frac{\sigma}{\tau_{MF}} \right), \tag{6.19}$$

for (P_σ^1) and (P_σ^∞) respectively. Having a decent bound on $C_{2,1}$ and $C_{2,\infty}$ could assist us to adopt a μ that makes τ_{MF} close to τ_σ which inherently leads less g_O iterations.

In the literature $C_{p,q}$ is upper bounded to assure $d^n(\mathcal{B}_p^N)_{\ell_q^N} \leq 1$ in [Kas77; GG84; Glu81; Glu84] for the corresponding K_p. In the simulations, we observed that these bounds on $C_{2,1}$ and $C_{2,\infty}$ are not very tight, especially for $C_{2,\infty}$. Therefore, instead of using the upper bounds of $C_{2,1}$ and $C_{2,\infty}$, we introduce and choose experimental constants $C_{2,1}^e$ and $C_{2,\infty}^e$ to generate a corresponding experimental μ^e for (P_σ^1) and (P_σ^∞) respectively. μ^e is generated to satisfy $\tau_\sigma = \mu^e \tau_{MF}$.

6.3.1.1 Simulation Settings

For the simulations, different $\omega = N/M$ values such $2, 4, 8$ and 16 are taken into account. $\mathbf{y}$ is created as a normally distributed signal with a variance of 1 and D is constructed as to be a *Parseval frame*.

In order to employ μ values for the g_O iterations, (P_σ^1) and (P_σ^∞) are solved 100 times and experimental μ values, denoted with μ^e, are obtained for several $\sigma/\rho(\mathbf{y})$ and ω. Averaged μ^e values are used for the simulations and shown in Table 6.1 and 6.2 for the (P_σ^1) and (P_σ^∞) respectively. Corresponding $C_{2,1}^e$ and $C_{2,\infty}^e$ values are depicted in Figure 6.2 and 6.3.

We also want to mention the bound on $C_{2,1}$ and $C_{2,\infty}$. $C_{2,1} = 0.088$, for $M = 128$ while $C_{2,\infty}$ is equal to 10.79, 21.2886, 34.2876 and 51.4282 for N/M is equal to 256/128, 512/128, 1024/128 and 2048/128 respectively.

Table 6.1: Chosen μ^e values for the (P_σ^1) experiments.

		(N,M)					
ρ	$\sigma/\rho(\mathbf{y})$	$(256, 512)$	$(256, 1024)$	$(256, 2048)$	$(512, 1024)$	$(512, 2048)$	$(1024, 2048)$
	0.5	0.3599	0.3143	0.2791	0.36	0.3139	0.3601
ρ_l	0.05	0.783	0.6715	0.5873	0.7834	0.6705	0.7831
	0.005	0.8284	0.7095	0.6199	0.8287	0.7085	0.8285
	0.5	0.286	0.252	0.2261	0.2879	0.2521	0.2871
ρ_h	0.05	0.7434	0.6364	0.5594	0.7439	0.6379	0.7437
	0.005	0.8105	0.6945	0.6071	0.8123	0.6949	0.8129
	0.5	0.3459	0.299	0.2656	0.3451	0.2991	0.3452
ρ_s	0.05	0.7404	0.635	0.5559	0.7408	0.6344	0.7408
	0.005	0.8098	0.6938	0.6063	0.8103	0.6929	0.8099

Table 6.2: Chosen μ^e values for the (P_σ^∞) experiments.

		(N,M)					
ρ	$\sigma/\rho(\mathbf{y})$	$(256, 512)$	$(256, 1024)$	$(256, 2048)$	$(512, 1024)$	$(512, 2048)$	$(1024, 2048)$
	0.5	0.2142	0.1917	0.1756	0.1976	0.1839	0.1931
ρ_l	0.05	0.4421	0.3766	0.3444	0.41	0.3601	0.3927
	0.005	0.4673	0.396	0.3618	0.4336	0.3785	0.4153
	0.5	0.1754	0.1612	0.1433	0.1675	0.153	0.1598
ρ_h	0.05	0.4161	0.3627	0.3261	0.3981	0.3446	0.3774
	0.005	0.4544	0.3924	0.3528	0.5345	0.3702	0.4103
	0.5	0.2013	0.1774	0.1592	0.1845	0.172	0.1757
ρ_s	0.05	0.4184	0.3569	0.3261	0.3904	0.338	0.3676
	0.005	0.4588	0.3894	0.3588	0.4264	0.3699	0.374

6.3.1.2 Simulations

(P_σ^1) and (P_σ^∞) are solved 100 times with g_0 and g_N iterations. μ is taken as $\mu = 1$ and $\mu = \mu^e$ from Table 6.1 and 6.2. Averaged results are shown in Table 6.3 and Table 6.4 for (P_σ^1) and (P_σ^∞) respectively. Several σ values are chosen relative to $\rho(\mathbf{y})$, in particular $5 \times 10^{-1}\rho(\mathbf{y})$, $5 \times 10^{-2}\rho(\mathbf{y})$ and $5 \times 10^{-3}\rho(\mathbf{y})$. Residual $\rho(\mathbf{r}_\sigma)$ and $\|\mathbf{x}_\sigma\|_p$ values are depicted at the solution point $\mathbf{x}_\sigma$.

Newton's method requires fewer (P_τ^p) solves (see Table 6.1 and 6.2). However, solving (5.29) is more expensive for Newton's method than for OPR since the derivative

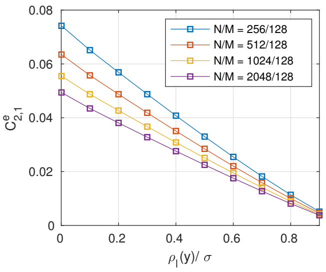

(a) $\rho_l(\mathbf{y})/\sigma$ vs. $C^e_{2,1}$

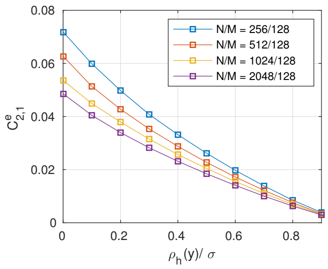

(b) $\rho_h(\mathbf{y})/\sigma$ vs. $C^e_{2,1}$

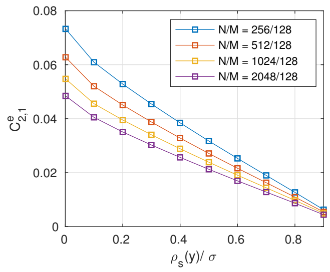

(c) $\rho_s(\mathbf{y})/\sigma$ vs. $C^e_{2,1}$

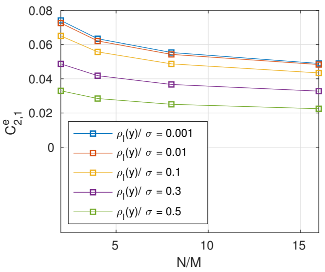

(d) N/M vs. $C^e_{2,1}$

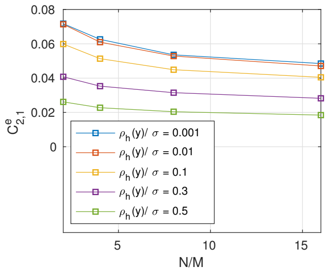

(e) N/M vs. $C^e_{2,1}$

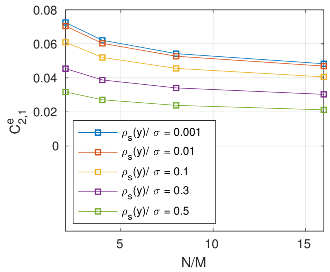

(f) N/M vs. $C^e_{2,1}$

Figure 6.2: $C^e_{2,1}$ values for several $\rho(\mathbf{y})/\sigma$ and N/M.

calculation of the nonlinear equation is required along with the function evaluation, while OPR need only the function evaluation. Also, Newton's method does not ensure convergence guarantee for nonconvex ρ_s.

Table 6.3: Simulation results for (P_σ^1) with ρ_l, ρ_h and ρ_s.

			least squares				*Huber* ($\Gamma = 0.1$)				*Students t* ($\kappa = 0.1$)			
(N, M)	$\sigma/\rho(\mathbf{y})$	Methods	$\rho_l(\mathbf{r}_\sigma)$	$\lVert\mathbf{x}_\sigma\rVert_1$	$\frac{\tau_\sigma}{\tau_{MF}}$	*iter*	$\rho_h(\mathbf{r}_\sigma)$	$\lVert\mathbf{x}_\sigma\rVert_1$	$\frac{\tau_\sigma}{\tau_{MF}}$	*iter*	$\rho_s(\mathbf{r}_\sigma)$	$\lVert\mathbf{x}_\sigma\rVert_1$	τ_σ/τ_{MF}	*iter*
		$g_O, (\mu = 1)$	8.005	104.15	0.36	6.94	9.63	83.2	0.287	6.06	11.14	100.2	0.3463	5.77
	0.5	$g_O, (\mu = \mu^e)$	8.005	104.15	0.36	3.78	9.63	83.2	0.287	2.39	11.14	100.2	0.3463	3.32
		g_N	8.005	104.15	0.36	3.09	9.63	83.2	0.287	3.05	–	–	–	–
		$g_O, (\mu = 1)$	0.8	226.49	0.783	9.06	0.963	215.5	0.7441	10.09	1.114	214.24	0.7406	13.02
$(512, 256)$	0.05	$g_O, (\mu = \mu^e)$	0.8	226.48	0.783	3.99	0.963	215.5	0.7441	2.61	1.114	214.23	0.7405	5.81
		g_N	0.8	226.48	0.783	3.8	0.963	215.5	0.7441	4.15	–	–	–	–
		$g_O, (\mu = 1)$	0.08	239.63	0.8285	40.57	0.09	236.2	0.8165	42.9	0.1114	234.3	0.81	53.85
	0.005	$g_O, (\mu = \mu^e)$	0.08	239.62	0.8284	4.22	0.09	236.2	0.8165	2.62	0.1114	234.28	0.81	11.04
		g_N	0.08	239.62	0.8284	3.8	0.09	236.2	0.8165	4.08	–	–	–	–
		$g_O, (\mu = 1)$	8.012	128.62	0.3144	6.86	9.65	103.4	0.2526	6.07	11.16	122.55	0.2994	5.7
	0.5	$g_O, (\mu = \mu^e)$	8.012	128.62	0.3143	3.79	9.65	103.4	0.2523	2.42	11.16	122.54	0.2994	3.2
		g_N	8.012	128.62	0.3143	3.01	9.65	103.4	0.252	3.07	–	–	–	–
		$g_O, (\mu = 1)$	0.801	274.75	0.6715	11.93	0.965	262.53	0.6397	12.93	1.116	259.88	0.6351	15.91
$(1024, 256)$	0.05	$g_O, (\mu = \mu^e)$	0.801	274.74	0.6715	3.93	0.965	262.51	0.6395	2.7	1.116	259.87	0.635	5.99
		g_N	0.801	274.73	0.6715	3.43	0.965	262.5	0.6395	4	–	–	–	–
		$g_O, (\mu = 1)$	0.08	290.29	0.7095	71.38	0.09	286.06	0.6994	73.77	0.112	283.93	0.6939	84.52
	0.005	$g_O, (\mu = \mu^e)$	0.08	290.28	0.7095	4.32	0.09	285.94	0.6963	3.039	0.112	283.9	0.6939	11.77
		g_N	0.08	290.27	0.7095	3.57	0.09	286.02	0.699	4	–	–	–	–
		$g_O, (\mu = 1)$	7.997	161.24	0.2791	6.71	9.45	129.3	0.2267	6	11.136	153.74	0.266	5.6
	0.5	$g_O, (\mu = \mu^e)$	7.997	161.24	0.2791	3.64	9.45	129.01	0.2265	2.35	11.136	153.74	0.2659	2.99
		g_N	7.997	161.24	0.2791	3	9.45	128.95	0.2263	3	–	–	–	–
		$g_O, (\mu = 1)$	0.8	339.35	0.5874	14.32	0.95	321.083	0.5608	15.5	1.113	321.28	0.556	18.2
$(2048, 256)$	0.05	$g_O, (\mu = \mu^e)$	0.8	339.35	0.5874	3.81	0.95	320.45	0.5597	2.938	1.114	321.27	0.556	5.67
		g_N	0.8	339.35	0.5874	3.07	0.95	320.575	0.5599	4	–	–	–	–
		$g_O, (\mu = 1)$	0.08	358.16	0.6199	98.23	0.09	351.02	0.609	101.3	0.111	349.23	0.6059	111.46
	0.005	$g_O, (\mu = \mu^e)$	0.08	358.15	0.6199	4.19	0.09	350.39	0.608	3.14	0.111	349.19	0.6058	11.28
		g_N	0.08	358.14	0.6199	3.22	0.09	351.76	0.61	4.143	–	–	–	–
		$g_O, (\mu = 1)$	11.317	208.21	0.36	7	19.28	165.84	0.2866	6.56	22.23	199.81	0.3454	6.02
	0.5	$g_O, (\mu = \mu^e)$	11.317	208.2	0.36	3.84	19.28	165.68	0.2864	2.61	22.23	199.81	0.3454	3.55
		g_N	11.317	208.2	0.36	3.44	19.28	165.54	0.2861	3.833	–	–	–	–
		$g_O, (\mu = 1)$	1.132	453.05	0.7834	9.14	1.92	427.4	0.7413	11.46	2.223	428.49	0.7409	13.73
$(1024, 512)$	0.05	$g_O, (\mu = \mu^e)$	1.132	453.04	0.7833	4.11	1.92	427.22	0.741	3.09	2.223	428.49	0.7409	6.24
		g_N	1.132	453.04	0.7833	3.99	1.92	427.9	0.7423	5.1	–	–	–	–
		$g_O, (\mu = 1)$	0.113	479.29	0.8288	40.64	0.19	469.9	0.8126	45	0.2223	469.56	0.8102	55.625
	0.005	$g_O, (\mu = \mu^e)$	0.113	479.28	0.8287	4.23	0.19	469.4	0.8117	3.2	0.2223	469.53	0.8102	12.96
		g_N	0.113	479.28	0.8287	4	0.19	470.5	0.8113	5.4	–	–	–	–
		$g_O, (\mu = 1)$	11.31	256.36	0.3139	7	19.05	203.58	0.2501	6.7	22.2	244.41	0.2992	5.97
	0.5	$g_O, (\mu = \mu^e)$	11.31	256.35	0.3139	3.73	19.05	203.45	0.2499	2.4	22.2	244.41	0.2992	3.33
		g_N	11.31	256.34	0.3139	3.01	19.05	203.19	0.2496	3.5	–	–	–	–
		$g_O, (\mu = 1)$	1.13	547.6	0.6705	12.03	1.91	520.88	0.637	14	2.22	518.2	0.6348	16.44
$(2048, 512)$	0.05	$g_O, (\mu = \mu^e)$	1.13	547.6	0.6705	3.85	1.91	520.42	0.6365	2.83	2.22	518.2	0.6348	6.11
		g_N	1.13	547.6	0.6705	3.85	1.91	520.9	0.6373	5	–	–	–	–
		$g_O, (\mu = 1)$	0.113	578.6	0.7085	71.85	0.19	563.45	0.6932	75.77	0.222	566.52	0.6932	86.44
	0.005	$g_O, (\mu = \mu^e)$	0.113	578.6	0.7085	4.09	0.19	563.1	0.6927	2.875	0.222	566.5	0.6932	12.41
		g_N	0.113	578.6	0.7085	3.9	0.19	564.15	0.6937	5	–	–	–	–
		$g_O, (\mu = 1)$	15.99	416.22	0.3601	7.02	38.36	333.67	0.2884	7	44.48	400.55	0.346	6.1395
	0.5	$g_O, (\mu = \mu^e)$	15.99	416.21	0.3601	3.75	38.36	333.52	0.2882	2.5	44.48	400.55	0.346	3.86
		g_N	15.99	416.21	0.3601	3.89	38.36	333.01	0.2878	4.167	–	–	–	–
		$g_O, (\mu = 1)$	1.599	904.97	0.7831	9.51	3.8	847.17	0.7443	11.75	4.448	857.33	0.7407	14.31
$(2048, 1024)$	0.05	$g_O, (\mu = \mu^e)$	1.599	904.95	0.7831	3.9	3.8	846.46	0.7437	3.5	4.448	857.32	0.7407	6.43
		g_N	1.599	904.95	0.7831	4	3.8	855.62	0.7517	7.26	–	–	–	–
		$g_O, (\mu = 1)$	0.16	957.45	0.8285	40.83	0.38	941.03	0.8135	45.2	0.445	934.37	0.8095	57.78
	0.005	$g_O, (\mu = \mu^e)$	0.16	957.43	0.8285	3.95	0.38	941.2	0.8135	3.52	0.445	934.35	0.8095	13.5
		g_N	0.16	957.43	0.8285	4	0.38	941	0.8135	14.5	–	–	–	–

Table 6.4: Simulation results for $(\mathrm{P}_\sigma^\infty)$ with ρ_l, ρ_h and ρ_s.

			least squares				*Huber* $(\Gamma = 0.1)$				*Students t* $(\kappa = 0.1)$			
(N, M)	$\sigma/\rho(\mathbf{y})$	Methods	$\rho_l(\mathbf{r}_\sigma)$	$\Vert\mathbf{x}_\sigma\Vert_\infty$	$\frac{\tau_\sigma}{\tau_{MF}}$	*iter*	$\rho_h(\mathbf{r}_\sigma)$	$\Vert\mathbf{x}_\sigma\Vert_\infty$	$\frac{\tau_\sigma}{\tau_{MF}}$	*iter*	$\rho_s(\mathbf{r}_\sigma)$	$\Vert\mathbf{x}_\sigma\Vert_\infty$	τ_σ/τ_{MF}	*iter*
(512, 256)	0.5	$g_O, (\mu = 1)$	8.005	0.4808	0.2126	6.34	9.63	0.397	0.1755	6.6	11.14	0.453	0.2002	5.11
		$g_O, (\mu = \mu^e)$	8.005	0.4808	0.2126	3.92	9.63	0.397	0.1754	3.64	11.14	0.453	0.2002	2.62
		g_N	8.005	0.4808	0.2126	3	9.63	0.397	0.1754	3	–	–	–	–
	0.05	$g_O, (\mu = 1)$	0.8	0.999	0.4418	20.2	0.96	0.9503	0.4205	22.72	1.11	0.945	0.418	21.88
		$g_O, (\mu = \mu^e)$	0.8	0.999	0.4418	5.33	0.96	0.9503	0.4202	6.65	1.11	0.945	0.418	5.65
		g_N	0.8	0.999	0.4418	3	0.96	0.9503	0.4203	3.7	–	–	–	–
	0.005	$g_O, (\mu = 1)$	0.08	1.057	0.4674	165.7	0.09	1.04	0.4602	162.2	0.11	1.038	0.459	167.99
		$g_O, (\mu = \mu^e)$	0.08	1.057	0.4674	13.16	0.09	1.04	0.4596	12.96	0.11	1.037	0.4583	16.57
		g_N	0.08	1.057	0.4674	4.03	0.09	1.04	0.4599	5.37	–	–	–	–
(1024, 256)	0.5	$g_O, (\mu = 1)$	8.013	0.3263	0.191	5.99	9.647	0.2721	0.1592	6.34	11.16	0.3038	0.1777	4.97
		$g_O, (\mu = \mu^e)$	8.013	0.3263	0.191	3.43	9.647	0.272	0.1592	3.32	11.16	0.3038	0.1777	2.57
		g_N	8.013	0.3263	0.191	2	9.647	0.272	0.1592	2.89	–	–	–	–
	0.05	$g_O, (\mu = 1)$	0.801	0.6438	0.3768	22.36	0.96	0.615	0.3604	24.94	1.116	0.6099	0.3569	24.59
		$g_O, (\mu = \mu^e)$	0.801	0.6438	0.3768	4.35	0.96	0.615	0.3601	5.95	1.116	0.6096	0.3568	5.29
		g_N	0.801	0.6438	0.3768	3	0.96	0.615	0.3602	3.39	–	–	–	–
	0.005	$g_O, (\mu = 1)$	0.08	0.6772	0.4002	195.3	0.09	0.6661	0.3951	191.6	0.112	0.663	0.388	195.13
		$g_O, (\mu = \mu^e)$	0.08	0.6772	0.4002	10.14	0.09	0.6654	0.3947	11.8	0.112	0.663	0.3877	14.91
		g_N	0.08	0.6772	0.4002	3	0.09	0.6662	0.3952	19.88	–	–	–	–
(2048, 256)	0.5	$g_O, (\mu = 1)$	7.997	0.227	0.1797	5.51	9.62	0.1892	0.1497	6.22	11.14	0.2095	0.1657	4.97
		$g_O, (\mu = \mu^e)$	7.997	0.227	0.1797	2.99	9.62	0.1891	0.1496	3.19	11.14	0.2095	0.1657	2.71
		g_N	7.997	0.227	0.1797	2	9.62	0.189	0.1496	2.79	–	–	–	–
	0.05	$g_O, (\mu = 1)$	0.7997	0.4369	0.3458	23.5	0.96	0.4187	0.3316	26.25	1.114	0.4131	0.327	26.07
		$g_O, (\mu = \mu^e)$	0.7997	0.4369	0.3458	3.8	0.96	0.4184	0.3314	5.46	1.114	0.4131	0.3269	5.08
		g_N	0.7997	0.4369	0.3458	2.71	0.96	0.4185	0.3315	3.412	–	–	–	–
	0.005	$g_O, (\mu = 1)$	0.08	0.4592	0.3635	207.52	0.09	0.4513	0.3553	212.5	0.111	0.448	0.355	212.73
		$g_O, (\mu = \mu^e)$	0.08	0.459	0.3633	10.96	0.09	0.4508	0.3549	13.125	0.111	0.448	0.355	14.72
		g_N	0.08	0.4587	0.3631	3.43	0.09	0.4515	0.3554	50.75	–	–	–	–
(1024, 512)	0.5	$g_O, (\mu = 1)$	11.317	0.4805	0.1973	6.82	19.22	0.396	0.1626	7.08	22.23	0.4518	0.1855	5.43
		$g_O, (\mu = \mu^e)$	11.317	0.4805	0.1973	4.05	19.22	0.396	0.1626	4	22.23	0.4517	0.1854	2.77
		g_N	11.317	0.4805	0.1973	3	19.22	0.396	0.1626	3.13	–	–	–	–
	0.05	$g_O, (\mu = 1)$	1.132	0.9988	0.41	21.85	1.922	0.9538	0.3942	24.76	2.223	0.945	0.3879	24.1
		$g_O, (\mu = \mu^e)$	1.132	0.9988	0.41	5.51	1.922	0.9534	0.3941	7.56	2.223	0.945	0.3878	6.29
		g_N	1.132	0.9988	0.41	3	1.922	0.9535	0.3941	4	–	–	–	–
	0.005	$g_O, (\mu = 1)$	0.1132	1.057	0.4338	171.74	0.19	1.041	0.4281	177.72	0.222	1.033	0.4242	179.38
		$g_O, (\mu = \mu^e)$	0.1132	1.057	0.4338	12.16	0.19	1.041	0.4279	14	0.222	1.033	0.4239	16.8
		g_N	0.1132	1.057	0.4338	3.96	0.19	1.041	0.4278	7.635	–	–	–	–
(2048, 512)	0.5	$g_O, (\mu = 1)$	11.31	0.3255	0.1828	6	19.2	0.271	0.1518	6.95	22.19	0.3026	0.1698	5
		$g_O, (\mu = \mu^e)$	11.31	0.3255	0.1828	3.42	19.2	0.271	0.1518	3.65	22.19	0.3026	0.1698	2.7
		g_N	11.31	0.3255	0.1827	2	19.2	0.271	0.1518	2.98	–	–	–	–
	0.05	$g_O, (\mu = 1)$	1.13	0.6418	0.3603	23.3	1.92	0.6139	0.3403	26.87	2.22	0.6076	0.3411	26.11
		$g_O, (\mu = \mu^e)$	1.13	0.6418	0.3603	4.29	1.92	0.6138	0.3402	6.47	2.22	0.6075	0.3411	5.67
		g_N	1.13	0.6418	0.3603	3	1.92	0.6138	0.3402	3.6	–	–	–	–
	0.005	$g_O, (\mu = 1)$	0.113	0.6785	0.3777	199.38	0.192	0.663	0.3807	199.3	0.22	0.6596	0.3707	205.69
		$g_O, (\mu = \mu^e)$	0.113	0.6785	0.3776	11.175	0.192	0.663	0.3805	8.33	0.22	0.6592	0.3704	14.85
		g_N	0.113	0.6785	0.3775	3.5	0.192	0.663	0.3805	23.67	–	–	–	–
(2048, 1024)	0.5	$g_O, (\mu = 1)$	15.995	0.4802	0.1883	6.99	38.43	0.3956	0.1553	7.4545	44.41	0.4511	0.1777	5.828
		$g_O, (\mu = \mu^e)$	15.995	0.4802	0.1883	4.05	38.43	0.3956	0.1553	4.273	44.41	0.4511	0.1777	2.88
		g_N	15.995	0.4802	0.1883	3	38.43	0.3956	0.1552	3.3	–	–	–	–
	0.05	$g_O, (\mu = 1)$	1.599	0.9974	0.391	22.96	3.84	0.9515	0.3662	27.14	4.44	0.9449	0.3717	25.566
		$g_O, (\mu = \mu^e)$	1.599	0.9974	0.391	5.44	3.84	0.9514	0.3662	8.21	4.44	0.9448	0.3717	6.55
		g_N	1.599	0.9974	0.391	3	3.84	0.9514	0.3662	4.07	–	–	–	–
	0.005	$g_O, (\mu = 1)$	0.159	1.0553	0.4068	184.7	0.38	1.0523	0.3747	206.5	0.44	1.031	0.3985	193.47
		$g_O, (\mu = \mu^e)$	0.159	1.0552	0.4068	12.39	0.38	1.0523	0.3747	14.23	0.44	1.031	0.3983	14.79
		g_N	0.159	1.0552	0.4068	4.056	0.38	1.0521	0.3747	8.5	–	–	–	–

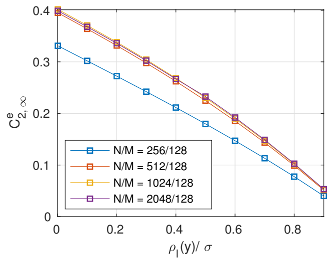

(a) $\rho_l(\mathbf{y})/\sigma$ vs. $C^e_{2,\infty}$

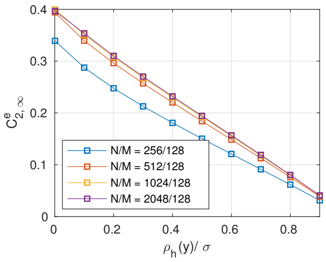

(b) $\rho_h(\mathbf{y})/\sigma$ vs. $C^e_{2,\infty}$

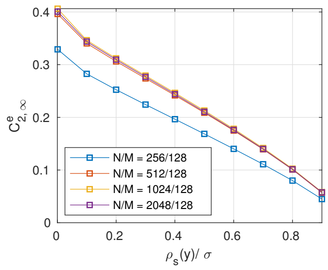

(c) $\rho_s(\mathbf{y})/\sigma$ vs. $C^e_{2,\infty}$

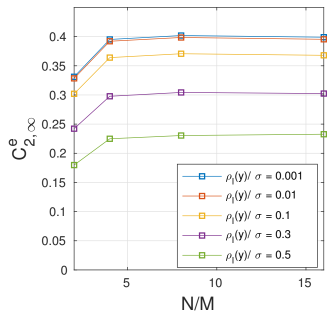

(d) N/M vs. $C^e_{2,\infty}$

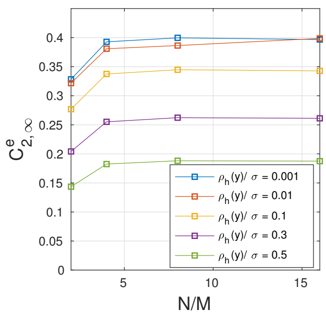

(e) N/M vs. $C^e_{2,\infty}$

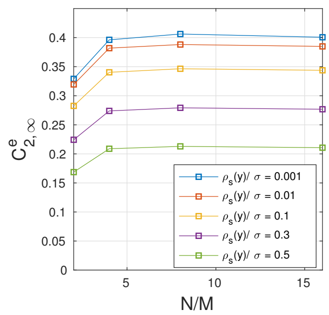

(f) N/M vs. $C^e_{2,\infty}$

Figure 6.3: $C^e_{2,\infty}$ values for several $\rho(\mathbf{y})/\sigma$ and N/M.

Chapter 7

$(\mathbf{P}_\sigma)$ Related Applications

7.1 ℓ_1-norm Minimization

ℓ_1-norm minimization plays a major role in many signal processing applications. The minimal ℓ_1-norm solution is also the sparsest solution under certain conditions, as outlined in compressive sensing theory.

7.1.1 ℓ_1-norm Minimization using a Test Benchmark

In order to create the testing environment and benchmark for comparison of proposed nonlinear equation root finding methods for solving (P_σ^1), Sparco [Ber+09] framework is utilized. Newton and main Regula falsi methods are deployed as the nonlinear equation root finders. Real-valued problems are chosen from Sparco for the simulations among the collection of test problems that include problems compiled from the literature as well. Details about the problems and related publications can be found in [Ber+09].

Simulation results are shown in Table 7.2, 7.3, and 7.4. Different σ values from high to low are set to solve (P_σ^1) such $5 \times 10^{-1}\rho(\mathbf{y})$, $10^{-1}\rho(\mathbf{y})$, $5 \times 10^{-2}\rho(\mathbf{y})$, $10^{-2}\rho(\mathbf{y})$, $5 \times 10^{-3}\rho(\mathbf{y})$ and $10^{-3}\rho(\mathbf{y})$. Residual vector $\rho(\mathbf{r}_\sigma) = \rho(\mathbf{y} - \mathrm{D}\mathbf{x}_\sigma)$, $\|\mathbf{x}_\sigma\|_1$ and the number of nonzero (nnz) for each solution point $\mathbf{x}_\sigma$ are depicted. N, M and $\rho(\mathbf{y})$ values for the chosen problems are given in Table 7.1.

The optimal objective values of the (P_τ^1), $\nu(\tau)$, for a given $\mathbf{y}$ and τ is shown in Figure 7.1, reminding that Pareto frontier $\psi(\tau)$ is the σ shifted from $\nu(\tau)$.

Problems	id	M	N	$\rho_l(\mathbf{y})$	$\rho_h(\mathbf{y})$	$\rho_s(\mathbf{y})$
cos-spike	3	1024	2048	102.2423	2378.8	25.09
gauss-cos	5	300	2048	83.6987	1140.3	9.7146
gauss-en	11	256	1024	99.9055	1272.5	8.957
hdr	12	2000	8192	2327.5	83057	112.5971
jitter	902	200	1000	0.4476	4.6881	0.0901
sign-spike	7	600	2560	2.1934	41.6002	1.3892

Table 7.1: N, M, $\rho(\mathbf{y})$ values for the problem setups.

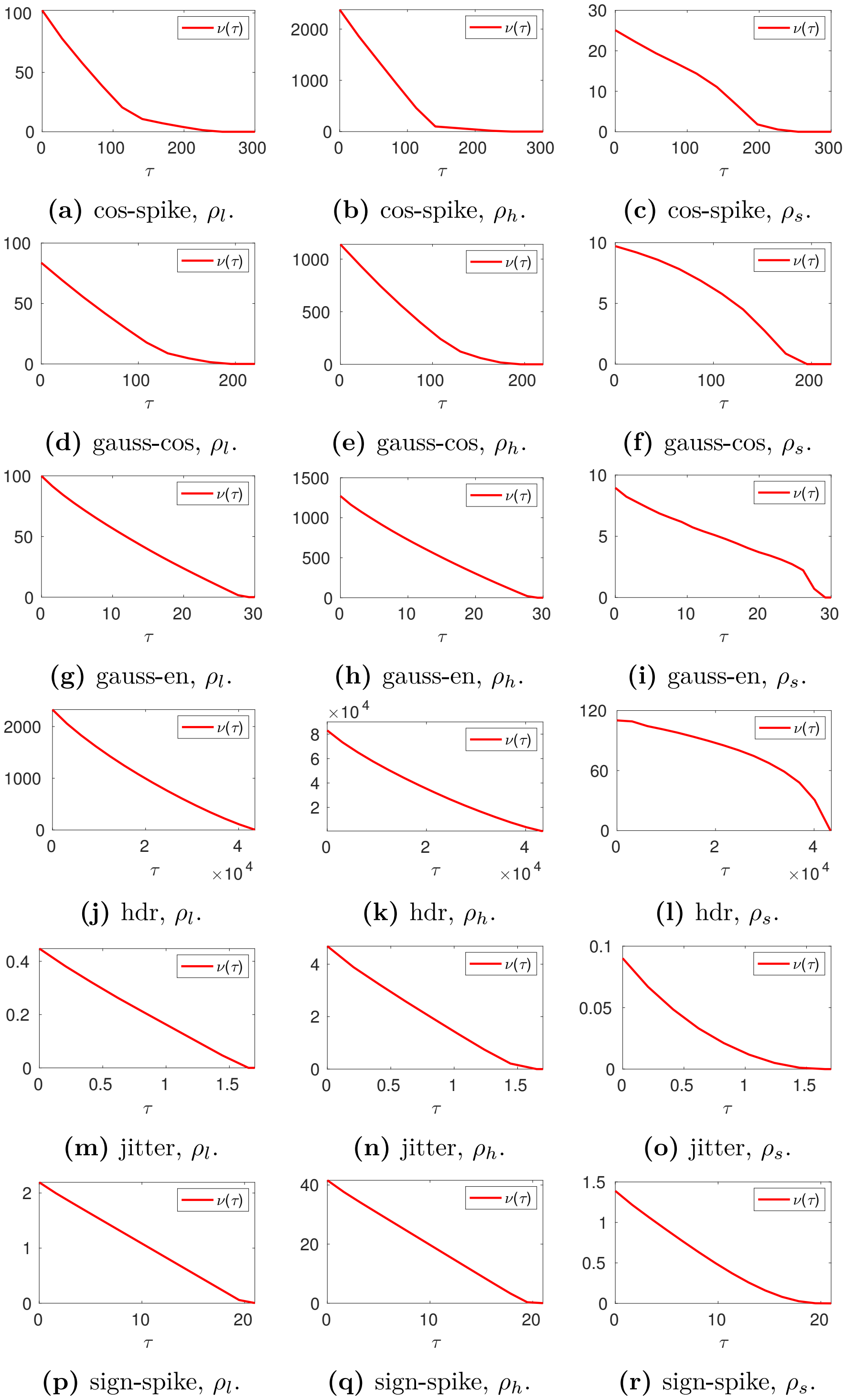

(a) cos-spike, ρ_l. **(b)** cos-spike, ρ_h. **(c)** cos-spike, ρ_s.

(d) gauss-cos, ρ_l. **(e)** gauss-cos, ρ_h. **(f)** gauss-cos, ρ_s.

(g) gauss-en, ρ_l. **(h)** gauss-en, ρ_h. **(i)** gauss-en, ρ_s.

(j) hdr, ρ_l. **(k)** hdr, ρ_h. **(l)** hdr, ρ_s.

(m) jitter, ρ_l. **(n)** jitter, ρ_h. **(o)** jitter, ρ_s.

(p) sign-spike, ρ_l. **(q)** sign-spike, ρ_h. **(r)** sign-spike, ρ_s.

Figure 7.1: Optimal objective function $\nu(\tau)$ for the problems.

Table 7.2: Simulation results for solving (P_σ^1).

			least squares				*Huber* ($\delta = 5 \times 10^{-3}$)				*Student's t* ($\nu = 10^{-2}$)			
Problems	$\sigma/\rho(\mathbf{y})$	Methods	$\rho_l(\mathbf{r}_\sigma)$	$\lVert\mathbf{x}_\sigma\rVert_1$	*nnz*	*iter*	$\rho_h(\mathbf{r}_\sigma)$	$\lVert\mathbf{x}_\sigma\rVert_1$	*nnz*	*iter*	$\rho_s(\mathbf{r}_\sigma)$	$\lVert\mathbf{x}_\sigma\rVert_1$	*nnz*	*iter*
cos-spike	0.5	Regula Falsi	51.12	66.24	2	10	1189.4	68.328	2	8	12.545	129.52	55	12
		Illinois	51.12	66.24	2	7	1189.4	68.328	2	7	12.545	129.52	55	9
		Pegasus	51.12	66.24	2	7	1189.4	68.328	3	6	12.545	129.52	55	7
		And.-Björck	51.12	66.24	2	9	1189.4	68.328	3	9	12.545	129.52	55	9
		Newton	51.12	66.24	2	3	1189.4	68.328	2	3	–	–	–	–
	0.1	Regula Falsi	10.2242	144.82	26	67	237.852	126.92	2	29	2.509	190.74	81	24
		Illinois	10.2242	144.82	26	10	237.852	126.92	2	10	2.509	190.74	81	19
		Pegasus	10.2242	144.82	26	9	237.852	126.92	2	10	2.509	190.74	81	15
		And.-Björck	10.2242	144.82	26	30	237.852	126.92	2	10	2.509	190.74	81	29
		Newton	10.2242	144.82	26	6	237.852	126.92	2	3	–	–	–	–
	0.05	Regula Falsi	5.112	188.4	75	85	118.702	134.72	2	68	1.2545	207.66	95	57
		Illinois	5.112	188.4	75	13	118.702	134.72	2	17	1.2545	207.66	95	20
		Pegasus	5.112	188.4	75	12	118.702	134.72	2	15	1.2545	207.66	95	18
		And.-Björck	5.112	188.4	75	46	118.702	134.72	2	17	1.2545	207.66	95	41
		Newton	5.112	188.4	75	5	118.702	134.72	2	4	–	–	–	–
	0.01	Regula Falsi	1.0224	230	118	219	23.783	217.134	125	279	0.2509	234.171	123	196
		Illinois	1.0224	230	118	16	23.783	217.133	125	12	0.2509	234.171	123	19
		Pegasus	1.0224	230	118	15	23.783	217.133	125	12	0.2509	234.171	123	19
		And.-Björck	1.0224	230	118	185	23.783	217.133	125	12	0.2509	234.171	123	164
		Newton	1.0224	230	118	5	23.783	217.133	125	3	–	–	–	–
	0.005	Regula Falsi	0.5112	235.6	123	393	11.89	229.03	125	443	0.1254	237.044	126	372
		Illinois	0.5112	235.6	123	17	11.89	229.03	125	15	0.1254	237.044	126	22
		Pegasus	0.5112	235.6	123	16	11.89	229.03	125	15	0.1254	237.044	126	22
		And.-Björck	0.5112	235.6	123	327	11.89	229.03	125	15	0.1254	237.044	126	316
		Newton	0.5112	235.6	123	5	11.89	229.03	125	3	–	–	–	–
	0.001	Regula Falsi	0.1022	240.01	125	441	2.3745	238.542	125	662	0.0251	239.62	1024	799
		Illinois	0.1022	240.01	125	27	2.3745	238.542	125	26	0.0251	239.62	1024	32
		Pegasus	0.1022	240.01	125	27	2.3745	238.542	125	25	0.0251	239.62	1024	31
		And.-Björck	0.1022	240.01	125	397	2.3745	238.542	125	25	0.0251	239.62	1024	762
		Newton	0.1022	240.01	125	5	2.3745	238.542	125	3	–	–	–	–
gauss-cos	0.5	Regula Falsi	41.8493	65.6144	3	9	570.139	64.51	3	10	4.8573	124.76	73	9
		Illinois	41.8493	65.6144	3	7	570.14	64.51	3	8	4.8573	124.76	73	11
		Pegasus	41.8493	65.6144	3	7	570.14	64.51	3	7	4.8573	124.76	73	7
		And.-Björck	41.8493	65.6144	3	9	570.14	64.51	3	7	4.8573	124.76	73	8
		Newton	41.8493	65.6144	3	3	570.14	64.51	3	3	–	–	–	–
	0.1	Regula Falsi	8.3698	132.0913	12	42	114.018	132.336	12	40	0.9716	172.51	163	25
		Illinois	8.3698	132.0913	12	13	114.018	132.336	12	13	0.9716	172.51	163	18
		Pegasus	8.3698	132.0913	12	11	114.018	132.336	12	11	0.9716	172.51	163	16
		And.-Björck	8.3698	132.0913	12	28	114.018	132.336	12	13	0.9716	172.51	162	23
		Newton	8.3698	132.0913	12	5	114.018	132.336	12	4	–	–	–	–
	0.05	Regula Falsi	4.1849	154.764	52	66	56.97	153.284	66	64	0.4855	178.36	186	42
		Illinois	4.1849	154.764	52	14	56.97	153.284	66	18	0.4855	178.36	186	20
		Pegasus	4.1849	154.764	52	13	56.97	153.284	66	14	0.4855	178.36	186	19
		And.-Björck	4.1849	154.764	52	51	56.97	153.284	66	14	0.4855	178.36	184	29
		Newton	4.1849	154.764	52	5	56.97	153.284	66	5	–	–	–	–
	0.01	Regula Falsi	0.8370	179.2257	127	210	11.2807	177.6979	161	215	0.0969	183.82	237	183
		Illinois	0.8370	179.2257	127	17	11.2812	177.6976	161	19	0.0969	183.82	237	29
		Pegasus	0.8370	179.2257	127	17	11.2812	177.6976	161	17	0.0969	183.82	237	24
		And.-Björck	0.8370	179.2257	127	174	11.2812	177.6976	161	20	0.0969	183.82	237	32
		Newton	0.8370	179.2252	127	5	11.2812	177.69	161	5	–	–	–	–
	0.005	Regula Falsi	0.4185	182.9291	156	385	5.539	181.912	192	391	0.0487	184.82	252	364
		Illinois	0.4185	182.9291	156	22	5.54	181.912	192	20	0.0487	184.82	252	31
		Pegasus	0.4185	182.9291	156	20	5.54	181.912	192	19	0.0487	184.82	252	30
		And.-Björck	0.4185	182.9291	156	340	5.54	181.912	192	23	0.0487	184.82	257	77
		Newton	0.4185	182.9288	156	6	5.54	181.912	192	6	–	–	–	–
	0.001	Regula Falsi	0.0837	186.068	173	502	0.9534	185.7096	212	691	0.0097	185.99	352	792
		Illinois	0.0837	186.068	173	25	0.9534	185.7096	212	26	0.0097	185.99	352	41
		Pegasus	0.0837	186.068	173	25	0.9534	185.7096	212	26	0.0097	185.99	352	44
		And.-Björck	0.0837	186.068	173	433	0.9534	185.7096	212	85	0.0097	185.99	352	70
		Newton	0.0837	186.068	173	5	0.9579	185.7055	212	6	–	–	–	–

Table 7.3: Simulation results for solving (P_σ^1).

Problems	$\sigma/\rho(\mathbf{y})$	Methods	*least squares* $\rho_l(\mathbf{r}_\sigma)$	$\Vert\mathbf{x}_\sigma\Vert_1$	*nnz*	*iter*	*Huber* ($\delta = 5\times10^{-3}$) $\rho_h(\mathbf{r}_\sigma)$	$\Vert\mathbf{x}_\sigma\Vert_1$	*nnz*	*iter*	*Student's t* ($\nu = 10^{-2}$) $\rho_s(\mathbf{r}_\sigma)$	$\Vert\mathbf{x}_\sigma\Vert_1$	*nnz*	*iter*
gauss-en		Regula Falsi	49.9527	11.9	16	9	636.264	11.966	19	8	4.4784	22.56	97	8
		Illinois	49.9527	11.9	16	7	636.265	11.966	19	6	4.4784	22.56	97	8
	0.5	Pegasus	49.9527	11.9	16	5	636.265	11.966	19	5	4.4784	22.56	97	7
		And.-Björck	49.9527	11.9	16	7	636.265	11.966	19	5	4.4784	22.56	97	10
		Newton	49.9527	11.9	16	4	636.267	11.97	19	3	–	–	–	–
		Regula Falsi	9.9905	24.69	34	17	127.218	24.644	46	9	0.8956	27.651	102	15
		Illinois	9.9906	24.69	34	9	127.218	24.644	46	9	0.8958	27.651	102	14
	0.1	Pegasus	9.9905	24.69	34	9	127.218	24.644	46	9	0.8961	27.651	102	14
		And.-Björck	9.9905	24.69	34	14	127.218	24.644	46	9	0.8958	27.651	102	17
		Newton	9.9905	24.69	34	4	127.218	24.644	46	4	–	–	–	–
		Regula Falsi	4.995	26.453	35	26	63.586	26.4067	50	27	0.4482	27.905	102	24
		Illinois	4.992	26.453	35	11	63.586	26.4067	50	13	0.4482	27.904	102	17
	0.05	Pegasus	4.995	26.453	35	11	63.586	26.4067	50	12	0.4482	27.905	102	16
		And.-Björck	4.995	26.453	35	24	63.586	26.4067	50	12	0.4482	27.905	104	23
		Newton	4.995	26.453	35	4	63.586	26.4067	50	4	–	–	–	–
		Regula Falsi	0.999	27.877	35	105	12.6864	27.8557	45	106	0.0897	28.114	110	107
		Illinois	0.999	27.877	35	14	12.6864	27.8557	45	16	0.0899	28.114	110	27
	0.01	Pegasus	0.999	27.877	35	14	12.6864	27.8557	45	16	0.0895	28.113	110	23
		And.-Björck	0.999	27.877	35	43	12.6864	27.8557	45	19	0.0897	28.114	112	57
		Newton	0.999	27.877	35	3	12.6864	27.8557	45	4	–	–	–	–
		Regula Falsi	0.4995	28.055	35	205	6.314	28.038	46	207	0.0444	28.151	118	211
		Illinois	0.4995	28.055	35	16	6.314	28.038	46	16	0.0444	28.151	118	28
	0.005	Pegasus	0.4995	28.055	35	16	6.314	28.038	46	16	0.0445	28.151	118	26
		And.-Björck	0.4995	28.055	35	88	6.314	28.038	46	16	0.0445	28.151	116	47
		Newton	0.4995	28.055	35	3	6.314	28.038	46	4	–	–	–	–
		Regula Falsi	0.0999	28.2	35	701	1.183	28.185	39	443	0.0009	28.197	221	805
		Illinois	0.0999	28.2	35	30	1.183	28.185	39	31	0.0009	28.197	221	36
	0.001	Pegasus	0.0999	28.2	35	30	1.183	28.185	39	31	0.0009	28.197	221	44
		And.-Björck	0.0999	28.2	35	67	1.183	28.185	39	44	0.0009	28.197	221	29
		Newton	0.0999	28.2	35	3	1.183	28.185	39	4	–	–	–	–
hdr		Regula Falsi	1163.8	16864	56	14	41529	16806	56	12	56.379	39452	2684	22
		Illinois	1163.8	16864	56	8	41529	16806	56	16	56.41	39447	2684	17
	0.5	Pegasus	1163.8	16864	56	7	41529	16806	56	13	56.22	39469	2684	18
		And.-Björck	1163.8	16864	56	8	41529	16806	56	10	56.36	39476	2684	13
		Newton	1163.8	16864	56	4	41529	16806	56	4	–	–	–	–
		Regula Falsi	232.75	36691	139	29	8305.6	36573	152	29	11.251	47038	7966	41
		Illinois	232.75	36691	139	12	8305.6	36573	152	13	11.164	47047	7966	30
	0.1	Pegasus	232.75	36691	139	10	8305.6	36573	152	14	11.39	46883	7966	24
		And.-Björck	232.75	36691	139	19	8305.6	36573	152	13	11.568	47002	7963	28
		Newton	232.75	36691	139	5	8305.6	36573	152	5	–	–	–	–
		Regula Falsi	116.377	39905	177	43	4152.7	39831	224	44	5.6424	106753	8192	51
		Illinois	116.377	39905	177	13	4152.7	39831	224	13	5.614	106739	8192	25
	0.05	Pegasus	116.377	39905	177	11	4152.7	39831	224	12	5.6389	106792	8192	16
		And.-Björck	116.377	39905	177	25	4152.7	39831	225	17	5.6163	106722	8192	16
		Newton	116.377	39905	177	5	4152.7	39831	225	5	–	–	–	–
		Regula Falsi	23.2754	42877	287	147	830.2	42831	418	147	1.126	148920	8192	43
		Illinois	23.2754	42877	287	20	830.2	42831	418	25	1.126	148920	8192	14
	0.01	Pegasus	23.2754	42877	287	18	830.2	42831	418	18	1.126	148920	8192	18
		And.-Björck	23.2754	42877	287	38	830.2	42831	417	21	1.126	148920	8192	11
		Newton	23.2754	42877	287	5	830.2	42831	417	5	–	–	–	–
		Regula Falsi	11.6377	43301	347	215	414.84	43268	526	278	0.563	151560	8192	33
		Illinois	11.6377	43268	347	23	414.84	43268	526	27	0.563	151560	8192	8
	0.005	Pegasus	11.6377	43268	347	21	414.84	43268	526	22	0.563	151560	8192	12
		And.-Björck	11.6377	43268	347	40	414.84	43268	526	33	0.563	151560	8192	10
		Newton	11.6377	43301	347	6	414.84	43268	526	6	–	–	–	–
		Regula Falsi	2.3275	43655	375	411	82.5367	43644	596	502	0.1126	153500	8192	44
		Illinois	2.3275	43655	375	31	82.5367	43644	596	37	0.1126	153500	8192	8
	0.001	Pegasus	2.3275	43655	375	32	82.5367	43644	596	36	0.1126	153500	8192	7
		And.-Björck	2.3275	43655	375	44	82.5367	43644	596	43	0.1126	153500	8192	7
		Newton	2.3275	43655	375	5	82.5367	43644	596	5	–	–	–	–

Table 7.4: Simulation results for solving (P^1_σ).

			least squares				*Huber* ($\delta = 5 \times 10^{-3}$)				*Student's t* ($\nu = 10^{-2}$)			
Problems	$\sigma/\rho(\mathbf{y})$	Methods	$\rho_l(\mathbf{r}_\sigma)$	$\\|\mathbf{x}_\sigma\\|_1$	*nnz*	*iter*	$\rho_h(\mathbf{r}_\sigma)$	$\\|\mathbf{x}_\sigma\\|_1$	*nnz*	*iter*	$\rho_s(\mathbf{r}_\sigma)$	$\\|\mathbf{x}_\sigma\\|_1$	*nnz*	*iter*
jitter	0.5	Regula Falsi	0.2238	0.7664	3	7	2.3279	0.7012	3	7	0.0451	0.4548	2	9
		Illinois	0.2238	0.7664	3	6	2.3279	0.7012	3	7	0.0451	0.4548	2	7
		Pegasus	0.2238	0.7664	3	6	2.3279	0.7012	3	7	0.0451	0.4548	2	6
		And.-Björck	0.2238	0.7664	3	8	2.3279	0.7012	3	7	0.0451	0.4548	2	6
		Newton	0.2238	0.7664	3	3	2.3279	0.7012	3	2	–	–	–	–
	0.1	Regula Falsi	0.0448	1.4517	3	21	0.3499	1.3849	3	22	0.009	1.1063	3	31
		Illinois	0.0448	1.4517	3	11	0.3499	1.3849	3	13	0.009	1.1062	3	10
		Pegasus	0.0448	1.4517	3	11	0.3499	1.3849	3	12	0.009	1.1062	3	10
		And.-Björck	0.0448	1.4517	3	25	0.3499	1.3849	3	12	0.009	1.1062	3	10
		Newton	0.0448	1.4517	2	5	0.3499	1.3849	3	4	–	–	–	–
	0.05	Regula Falsi	0.0224	1.5373	3	39	0.1460	1.4762	3	41	0.0045	1.2588	3	54
		Illinois	0.0224	1.5373	3	12	0.1460	1.4762	3	16	0.0045	1.2586	3	14
		Pegasus	0.0224	1.5373	3	12	0.1460	1.4762	3	15	0.0045	1.2586	3	13
		And.-Björck	0.0224	1.5373	3	34	0.1460	1.4762	3	15	0.0045	1.2586	3	13
		Newton	0.0224	1.5373	3	2	0.1460	1.4762	3	3	–	–	–	–
	0.01	Regula Falsi	0.0045	1.6059	3	186	0.0235	1.5642	3	194	$9e-4$	1.4609	3	216
		Illinois	0.0045	1.6059	3	19	0.0235	1.5642	3	17	$9e-4$	1.4604	3	14
		Pegasus	0.0045	1.6059	3	19	0.0235	1.5642	3	16	$9e-4$	1.4604	3	14
		And.-Björck	0.0045	1.6059	3	48	0.0235	1.5642	3	16	$9e-4$	1.4604	3	14
		Newton	0.0045	1.6059	3	2	0.0235	1.5642	3	4	–	–	–	–
	0.005	Regula Falsi	0.0022	1.6144	3	371	0.0118	1.5814	3	382	$4.46e-4$	1.5087	3	410
		Illinois	0.0022	1.6144	3	20	0.0118	1.5814	3	14	$4.5e-4$	1.5081	3	16
		Pegasus	0.0022	1.6144	3	22	0.0118	1.5814	3	19	$4.5e-4$	1.5081	3	16
		And.-Björck	0.0022	1.6144	3	74	0.0118	1.5814	3	19	$4.5e-4$	1.5081	3	15
		Newton	0.0022	1.6144	3	2	0.0118	1.5814	3	3	–	–	–	–
	0.001	Regula Falsi	0.0004	1.6213	3	912	0.0024	1.6044	3	307	$9e-5$	1.5716	3	511
		Illinois	0.0004	1.6213	3	34	0.0024	1.6044	3	31	$9e-5$	1.5716	3	28
		Pegasus	0.0004	1.6213	3	34	0.0024	1.6044	3	30	$9e-5$	1.5716	3	28
		And.-Björck	0.0004	1.6213	3	92	0.0024	1.6044	3	30	$9e-5$	1.5716	3	30
		Newton	0.0004	1.6213	3	3	0.0024	1.6044	3	4	–	–	–	–
sign-spike	0.5	Regula Falsi	1.0967	9.8766	20	6	20.763	9.5133	20	6	0.6946	7.4109	20	7
		Illinois	1.0967	9.8766	20	3	20.763	9.5133	20	5	0.6946	7.4109	20	7
		Pegasus	1.0967	9.8766	20	3	20.763	9.5133	20	5	0.6946	7.4109	20	6
		And.-Björck	1.0967	9.8766	20	5	20.763	9.5133	20	5	0.6946	7.4109	20	6
		Newton	1.0967	9.8766	20	2	20.763	9.5133	20	2	–	–	–	–
	0.1	Regula Falsi	0.2193	17.975	20	17	3.961	17.507	20	17	0.1389	14.99	20	25
		Illinois	0.2193	17.975	20	7	3.961	17.507	20	12	0.1389	14.99	20	12
		Pegasus	0.2193	17.975	20	7	3.961	17.507	20	12	0.1389	14.99	20	10
		And.-Björck	0.2193	17.975	20	15	3.961	17.507	20	12	0.1389	14.99	20	11
		Newton	0.2193	17.975	20	2	3.961	17.5027	20	3	–	–	–	–
	0.05	Regula Falsi	0.1097	18.988	20	30	1.7787	18.599	20	32	0.0695	16.514	20	44
		Illinois	0.1097	18.988	20	10	1.7787	18.599	20	13	0.0695	16.514	20	14
		Pegasus	0.1097	18.988	20	10	1.7787	18.599	20	13	0.0695	16.514	20	13
		And.-Björck	0.1097	18.988	20	21	1.7787	18.599	20	13	0.0695	16.514	20	14
		Newton	0.1097	18.988	20	2	1.7787	18.599	20	5	–	–	–	–
	0.01	Regula Falsi	0.0219	19.7975	20	142	0.2115	19.5754	20	145	0.0139	18.46	20	172
		Illinois	0.0219	19.7975	20	19	0.2115	19.5754	20	21	0.0139	18.46	20	21
		Pegasus	0.0219	19.7975	20	19	0.2115	19.5754	20	20	0.0139	18.46	20	19
		And.-Björck	0.0219	19.7975	20	32	0.2115	19.5754	20	20	0.0139	18.46	20	20
		Newton	0.0219	19.7975	20	2	0.2115	19.5754	20	3	–	–	–	–
	0.005	Regula Falsi	0.011	19.899	20	282	0.1041	19.7022	20	288	0.0069	18.914	20	323
		Illinois	0.011	19.899	20	23	0.1041	19.7022	20	25	0.0069	18.914	20	24
		Pegasus	0.011	19.899	20	23	0.1041	19.7022	20	24	0.0069	18.914	20	22
		And.-Björck	0.011	19.899	20	39	0.1041	19.7022	20	25	0.0069	18.914	20	23
		Newton	0.011	19.899	20	2	0.1041	19.7022	20	4	–	–	–	–
	0.001	Regula Falsi	0.0022	19.9798	20	496	0.0208	19.8668	20	353	0.0014	19.515	20	921
		Illinois	0.0022	19.9798	20	37	0.0208	19.8668	20	32	0.0014	19.515	20	27
		Pegasus	0.0022	19.9798	20	37	0.0208	19.8668	20	32	0.0014	19.515	20	26
		And.-Björck	0.0022	19.9798	20	62	0.0208	19.8668	20	32	0.0014	19.515	20	26
		Newton	0.0022	19.9798	20	2	0.0208	19.8668	20	5	–	–	–	–

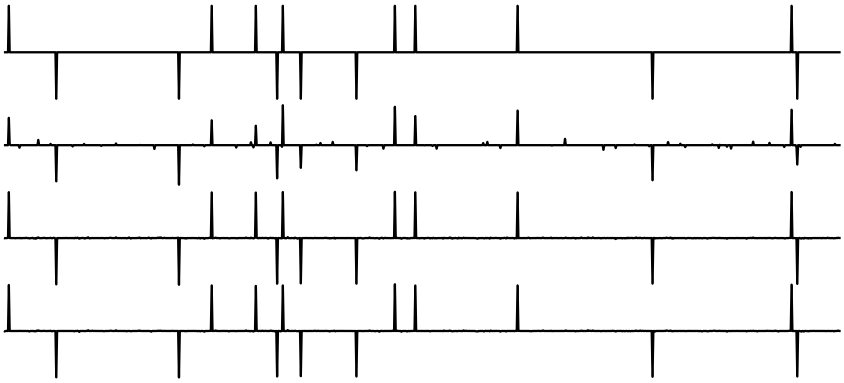

Figure 7.2: Top to bottom: true signal, reconstructions with *least squares*, *Huber* and *Student's t* losses

7.1.2 A Typical Compressed Sensing Example

We also considered a typical compressed sensing example. A 15-sparse vector, $\mathbf{x}_0$, is recovered using a normally distributed Parseval frame $\mathbf{D} \in \mathbb{R}^{512\times1024}$. Measurements are generated according to $\mathbf{y} = \mathbf{D}\mathbf{x} + \mathbf{w} + \zeta$, where the noise $\mathbf{w}$ is zero mean normal error with the variance of 0.005 and ζ has five randomly placed outliers with a zero mean normal distribution variance of 1. (P^1_σ) solved with the $\sigma = \rho(\zeta)$ for a fair comparison of ρ_l, ρ_h and ρ_s. Averaged recovery error variances, i.e. $\frac{1}{N}\|\mathbf{x}_0 - \mathbf{x}_\sigma\|_2^2$, over 100 simulations are calculated as $0.0019, 2.015\times10^{-5}$ and 1.589×10^{-5} for the ρ_l, ρ_h and ρ_s respectively. An instance of these simulations is shown in Figure 7.2. Huber loss is less sensitive to outliers in measurement data than least-squares, and Student's t marginally outperforms Huber based on error results; the residuals in Figure 7.3 show Student's t more cleanly identifies outliers. The performance gap increases with prevalence and size of outliers.

7.2 ℓ_∞-norm Minimization

In this subchapter, applications related to the ℓ_∞-norm minimization are probed.

7.2.1 A New Communication Scheme Based on ℓ_∞-norm Representations

As it is already mentioned in Chapter 2.2, MOF has already plentiful applications for several benefits. Since the presented warm-start strategy in Chapter 5.3.4 uses the MOF, one can try to get some extra gains that MOF has already offered by solving (P^p_σ). In this thesis, that idea is cultivated and an ℓ_∞-norm representations based

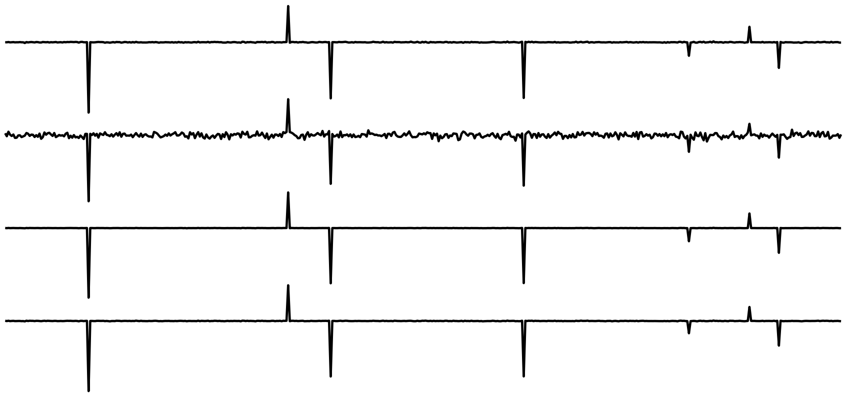

Figure 7.3: Top to bottom: true errors, *least squares*, *Huber* and *Student's t* residuals.

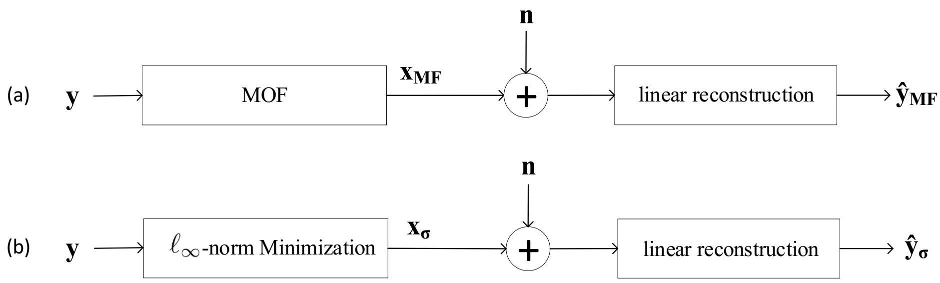

Figure 7.4: a) MOF based communication architecture, b) Proposed ℓ_∞-norm representations based communication architecture.

communication architecture as an approximate overcomplete representation alternative to the MOF based one for noisy channels is presented. The proposed approximate overcomplete representation is based on ℓ_∞-norm minimization problem. The most important feature of that optimization problem is enforcing the signal to be spread evenly [Fuc11]. Proposed scheme is demonstrated in Figure 7.4b while the state-of-art is depicted Figure 7.4a that is detailed investigated in [GKV99].

One of the most common noise for any communication architecture is the quantization noise. Thus, the universal (randomized) quantizer is utilized for a fair comparison of the proposed communication scheme with the MOF based one.

7.2.1.1 Universal Quantizer (Unbounded Uniform Subtractive Entropy Coded Dithered Quantizer)

The idea behind the universal quantizer is to breaking up the pattern of quantization noise and make it statistically independent of the quantizer source. Most common and accepted way of doing that is to add a random signal which is called dither to the source. Theoretical analysis of the dithering is studied by Schuchman [Sch64a] and it is proved that under some conditions, the quantization error is uniformly distributed and independent of the signal. The scalar universal quantizer with dither can be defined as follows:

$$q_o = \mathcal{Q}_\Delta(q_i + z) - z, \tag{7.1}$$

where q_o is the output of the quantizer, q_i is the quantizer source, z is the dither signal and $\mathcal{Q}_\Delta(.)$ is the quantizer operator which is considered as unbounded scalar uniform quantizer with a Δ quantization step size and defined as:

$$\mathcal{Q}_\Delta(t) = k\Delta \quad \text{for} \quad k\Delta - \Delta/2 \le t < k\Delta + \Delta/2 \quad . \tag{7.2}$$

In order to satisfy Schuchman's conditions [Sch64a], z is considered as uniformly distributed in the interval $[-\Delta/2, \Delta/2)$ and known at the receiver. With the introduced quantizer model, it can be assumed that each quantization noise component $n = q_i - q_o$ has zero mean with $\sigma_q^2 = \frac{\Delta^2}{12}$ variance and the components are uncorrelated.

7.2.1.2 Linear Reconstruction and the Minimum Squared Error (MSE) Analysis

For MOF and ℓ_∞-norm representation based communication architectures with a noise, the goal is to estimate $\mathbf{y} \in \mathbb{R}^M$ from given quantized representation coefficients. This can be easily done with well known Moore–Penrose inverse approach such that $\mathrm{D}^\dagger \mathbf{y}$. Note that because of the optimization problem, there will be a residual error for the proposed scheme depending σ.

MSE for the MOF Based Communication Architecture: Let us assume the received signal at the receiver is $\hat{\mathbf{x}}_{MF} \in \mathbb{R}^N$ which consists the quantization noise $\mathbf{n} \in \mathbb{R}^N$, ($\hat{\mathbf{x}}_{MF} = \mathbf{x}_{MF} + \mathbf{n}$), and the reconstructed signal denoted $\hat{\mathbf{y}}_{MF} \in \mathbb{R}^M$ for the frame expansion based communication scheme. Then regarding *minimum squared error* (MSE) is going to be

$$\mathrm{MSE}_{MF} = \frac{1}{M}\mathbb{E}\left\|\mathbf{y} - \hat{\mathbf{y}}_{MF}\right\|_2^2 . \tag{7.3}$$

By using $\mathbf{y} = \mathrm{D}\mathbf{x}_{MF}$, $\hat{\mathbf{y}}_{MF} = \mathrm{D}(\mathbf{x}_{MF} + \mathbf{n})$ and trace properties, (7.3) can be rewritten as follows

$$\mathrm{MSE}_{MF} = \frac{1}{M}\mathbb{E}\left\|\mathrm{D}\mathbf{n}\right\|_2^2 = \frac{1}{M}\mathrm{tr}\left(\mathrm{D}\mathbb{E}[\mathbf{n}\mathbf{n}^T]\mathrm{D}^T\right) = \frac{\mathbb{E}[\mathbf{n}\mathbf{n}^T]}{M}\mathrm{tr}\left(\mathrm{D}\mathrm{D}^T\right) = \frac{\mathbb{E}[\mathbf{n}\mathbf{n}^T]}{M}\sum_{i=1}^{M} m_i. \tag{7.4}$$

where sum of eigenvalues of DD^T equal to $\sum_{i=1}^{M} m_i$. Since $A \leq m_i \leq B$, MSE_{MF} becomes

$$A\sigma_q^2 \leq \mathrm{MSE}_{MF} \leq B\sigma_q^2. \tag{7.5}$$

For the tight frames MSE_{MF} will be equal to $A\sigma_q^2$, while σ_q^2 for Parseval frames.

MSE for the ℓ_∞-norm Representation Based Communication Architecture: Because of the optimization problem definition itself, there will be a residual error, related with the choice of the parameters σ, λ and τ. With the consideration of that, MSE for the proposed scheme can be written as

$$\mathrm{MSE}_\sigma = \frac{1}{M}\mathbb{E}\left\|\mathbf{y} - \hat{\mathbf{y}}_\sigma\right\|_2^2 = \frac{1}{M}\mathbb{E}\left\|\mathbf{y} - (\mathrm{DD}^T)^{-1}\mathrm{D}(\mathbf{x}_\sigma + \mathbf{n})\right\|_2^2. \tag{7.6}$$

In order to derive the relation between MSE_σ and MSE_{MF}, let us rewrite the (7.6) such

$$\begin{aligned}
\mathrm{MSE}_\sigma &= \frac{1}{M}\mathbb{E}\left\|\mathbf{y} - \hat{\mathbf{y}}_\sigma\right\|_2^2 \\
&= \frac{1}{M}\mathbb{E}\left\|\mathbf{y} - (\mathrm{DD}^T)^{-1}\mathrm{D}(\mathbf{x}_\sigma + \mathbf{n})\right\|_2^2 \\
&= \frac{1}{M}\mathbb{E}\left\|\mathbf{y} - (\mathrm{DD}^T)^{-1}\mathbf{y} + (\mathrm{DD}^T)^{-1}(\mathbf{y} - \mathrm{D}\mathbf{x}_\sigma) - (\mathrm{DD}^T)^{-1}\mathrm{D}\mathbf{n}\right\|_2^2
\end{aligned} \tag{7.7}$$

by using Minkowski's inequality following inequality can be derived for MSE_σ

$$\begin{aligned}
\sqrt{\mathrm{MSE}_\sigma} \leq \sqrt{\frac{1}{M}}\Big(\left\|\mathbf{y}\right\|_2 + \left\|(\mathrm{DD}^T)^{-1}\mathbf{y}\right\|_2 + \mathbb{E}\left\|(\mathrm{DD}^T)^{-1}\mathrm{D}(\mathbf{y} - \mathrm{D}\mathbf{x}_\sigma)\right\|_2 \\
+\mathbb{E}\left\|(\mathrm{DD}^T)^{-1}\mathrm{D}\mathbf{n}\right\|_2\Big).
\end{aligned} \tag{7.8}$$

It is possible to bound $\mathbb{E}\left\|(\mathrm{DD}^T)^{-1}\mathrm{D}(\mathbf{y} - \mathrm{D}\mathbf{x}_\sigma)\right\|_2$, since

$$\begin{aligned}
\mathbb{E}\left\|(\mathrm{DD}^T)^{-1}\mathrm{D}(\mathbf{y} - \mathrm{D}\mathbf{x}_\sigma)\right\|_2^2 &= \mathrm{tr}\left((\mathrm{DD}^T)^{-1}\mathrm{D}\mathbb{E}[(\mathbf{y} - \mathrm{D}\mathbf{x}_\sigma)(\mathbf{y} - \mathrm{D}\mathbf{x}_\sigma)^T]((\mathrm{DD}^T)^{-1}\mathrm{D})^T\right) \\
&= \mathbb{E}[(\mathbf{y} - \mathrm{D}\mathbf{x}_\sigma)(\mathbf{y} - \mathrm{D}\mathbf{x}_\sigma)^T]\mathrm{tr}\left((\mathrm{DD}^T)^{-1}\right) \\
&= \sigma^2 \sum_{i=1}^{M} \frac{1}{m_i}
\end{aligned} \tag{7.9}$$

such

$$\sigma\sqrt{\frac{M}{B}} \leq \mathbb{E}\left\|(\mathrm{DD}^T)^{-1}\mathrm{D}(\mathbf{y} - \mathrm{D}\mathbf{x}_\sigma)\right\|_2 \leq \sigma\sqrt{\frac{M}{A}}, \tag{7.10}$$

and by using similar steps $\mathbb{E}\left\|(\mathrm{DD}^T)^{-1}\mathrm{D}\mathbf{n}\right\|_2^2$ can be bounded, since

$$\begin{aligned}\mathbb{E}\left\|(\mathrm{DD}^T)^{-1}\mathrm{D}\mathbf{n}\right\|_2^2 &= \mathrm{tr}\left((\mathrm{DD}^T)^{-1}\mathrm{D}\mathbb{E}[\mathbf{nn}^T]((\mathrm{DD}^T)^{-1}\mathrm{D})^T\right)\\ &= \mathbb{E}[\mathbf{nn}^T]\mathrm{tr}\left((\mathrm{DD}^T)^{-1}\right)\\ &= \mathbb{E}[\mathbf{nn}^T]\sum_{i=1}^{M}\frac{1}{m_i}.\end{aligned} \tag{7.11}$$

such

$$\sigma_q\sqrt{\frac{M}{B}} \le \mathbb{E}\left\|(\mathrm{DD}^T)^{-1}\mathrm{D}\mathbf{n}\right\|_2 \le \sigma_q\sqrt{\frac{M}{A}}. \tag{7.12}$$

By using $\mathbb{E}\left\|(\mathrm{DD}^T)^{-1}\mathrm{D}\mathbf{n}\right\|_2 = \sqrt{\frac{M}{AB}}\sqrt{\mathrm{MSE}_{MF}}$, MSE_σ can be bounded in terms of MSE_{MF} such

$$\sqrt{\mathrm{MSE}_\sigma} \le \sqrt{\frac{1}{M}}(1-A)\left\|\mathbf{y}\right\|_2 + \frac{\sigma}{\sqrt{A}} + \sqrt{\frac{\mathrm{MSE}_{MF}}{AB}} \tag{7.13}$$

Corollary 7.1. *It is straigthforward to obtain following MSE_σ bound*

$$\sigma_q\sqrt{\frac{1}{B}} \le \sqrt{MSE_\sigma} \le \sqrt{\frac{1}{M}}(1-A)\left\|\boldsymbol{y}\right\|_2 + \frac{(\sigma+\sigma_q)}{\sqrt{A}}. \tag{7.14}$$

Proof. Upper bound of (7.14) can be found simply by inserting (7.5) into (7.13). Lower bound of MSE_σ occurs when there is no reconstruction error comes from the optimization problem itself, i.e. when $\sigma = 0$. In that case $\mathrm{MSE}_{\sigma=0}$ is going to be equal to $\frac{1}{M}\mathbb{E}\left\|(\mathrm{DD}^T)^{-1}\mathrm{D}\mathbf{n}\right\|_2^2$. With the eq. (7.12), lower bound of (7.14) can be derived. □

7.2.1.3 Quantization Levels

By using the definition of uniform quantizer in eq. (7.2), required quantization level with a symmetric source vector $\mathbf{s}$ can be written as:

$$L = 2\left\lceil \frac{\left\|\mathbf{s}\right\|_\infty}{\Delta} + 1\right\rceil, \tag{7.15}$$

where $\lceil . \rceil$ is the ceiling function.

Required quantization levels for the proposed ℓ_∞-norm and MOF based representations are denoted with L_σ and L_{MF} respectively.

Proposition 7.1. *There exists a quantization level ratio between L_σ and L_{MF} with using unifom quantizer (i.e. (7.2)) such*

$$0 < \frac{L_\sigma}{L_{MF}} \le \frac{A\eta}{\left(A-\eta\sqrt{B}\right)N\sqrt{\delta B}}\frac{(\left\|\boldsymbol{y}\right\|_2 - \sigma)}{\left\|\boldsymbol{y}\right\|_2} + \Delta. \tag{7.16}$$

Table 7.5: σ values for the simulations.

	$\sigma/\rho(\mathbf{y})$							
	5×10^{-1}		10^{-1}		5×10^{-2}		5×10^{-3}	
	$M = 256$ $N = 1024$	$M = 128$ $N = 4096$	$M = 256$ $N = 1024$	$M = 128$ $N = 4096$	$M = 256$ $N = 1024$	$M = 128$ $N = 4096$	$M = 256$ $N = 1024$	$M = 128$ $N = 4096$
Least-squares	8.3577	5.8205	1.4945	1.1641	0.7473	0.5758	0.0747	0.0561
Huber ($\Gamma = 0.1$)	91.0153	50.6534	18.2031	10.2527	9.1015	4.3262	0.9102	0.5065
Student's t ($\kappa = 0.1$)	10.7885	5.8809	2.1577	1.1952	1.0788	0.5881	0.1079	0.0588

for a frame matrix D that satisfies the UP.

Proof. By using (7.15) following can be derived

$$\frac{\|\mathbf{x}_\sigma\|_\infty}{\|\mathbf{x}_{MF}\|_\infty} \le \frac{L_\sigma}{L_{LS}} \le \frac{\|\mathbf{x}_\sigma\|_\infty}{\|\mathbf{x}_{MF}\|_\infty} + \Delta. \tag{7.17}$$

With the help of K_∞ introduced in Corollary 5.2, following can be written

$$\|\mathbf{x}_\sigma\|_\infty \le \frac{\eta}{\left(A - \eta\sqrt{B}\right)\sqrt{\delta N}}(\|\mathbf{y}\|_2 - \sigma) \tag{7.18}$$

In order to bound $\|\mathbf{x}_{MF}\|_\infty$, one can simply use following inequality $\|\mathbf{x}_{MF}\|_\infty = \left\|\mathrm{D}^T(\mathrm{D}\mathrm{D}^T)^{-1}\mathbf{y}\right\|_\infty \le \sqrt{N}\left\|\mathrm{D}^T(\mathrm{D}\mathrm{D}^T)^{-1}\mathbf{y}\right\|_2 \le \sqrt{NB}\left\|(\mathrm{D}\mathrm{D}^T)^{-1}\mathbf{y}\right\|_2 \le \frac{\sqrt{NB}}{A}\|\mathbf{y}\|_2$. □

7.2.1.4 Performance of the Proposed Communication Architecture

ℓ_∞-norm representation based communication architecture is compared with the MOF based one in terms of rate and MSE for several Δ values. By reminding that $\Delta = 12\sigma_q^2$, these comparisons answer two questions: one is what rates one can achieve, i.e what the advantage of finding more equally spread representations in terms of required quantization levels and second is what the cost is overall of spreading the signal more uniformly in terms of MSE for a same noise variance. For the simulations $\mathbf{y}$ is created as a normally distributed signal with a variance 1 and D constructed as to be a Parseval frame. Results are averaged over 100 simulations. σ values of the simulations are given in Table 7.5.

Figure 7.5, 7.6, 7.7 show the MSE_{MF} and MSE_σ values for $M = 256$, $N = 1024$. Several $\sigma/\rho(\mathbf{y})$ ratios such 5×10^{-1}, 10^{-1}, 5×10^{-2} and 5×10^{-3} are chosen for ρ_l, ρ_h and ρ_s respectively.

Figure 7.8 shows the rate for Δ values. Rate is calculated as $(N/M) \times \log(L)$. and rates for the ℓ_∞-norm representation based communication architecture inspected from high to low noise tolerances such $\sigma/\rho(\mathbf{y}) = 5 \times 10^{-1}$, $\sigma/\rho(\mathbf{y}) = 10^{-1}$, $\sigma/\rho(\mathbf{y}) = 5 \times 10^{-2}$ and $\sigma/\rho(\mathbf{y}) = 5 \times 10^{-3}$.

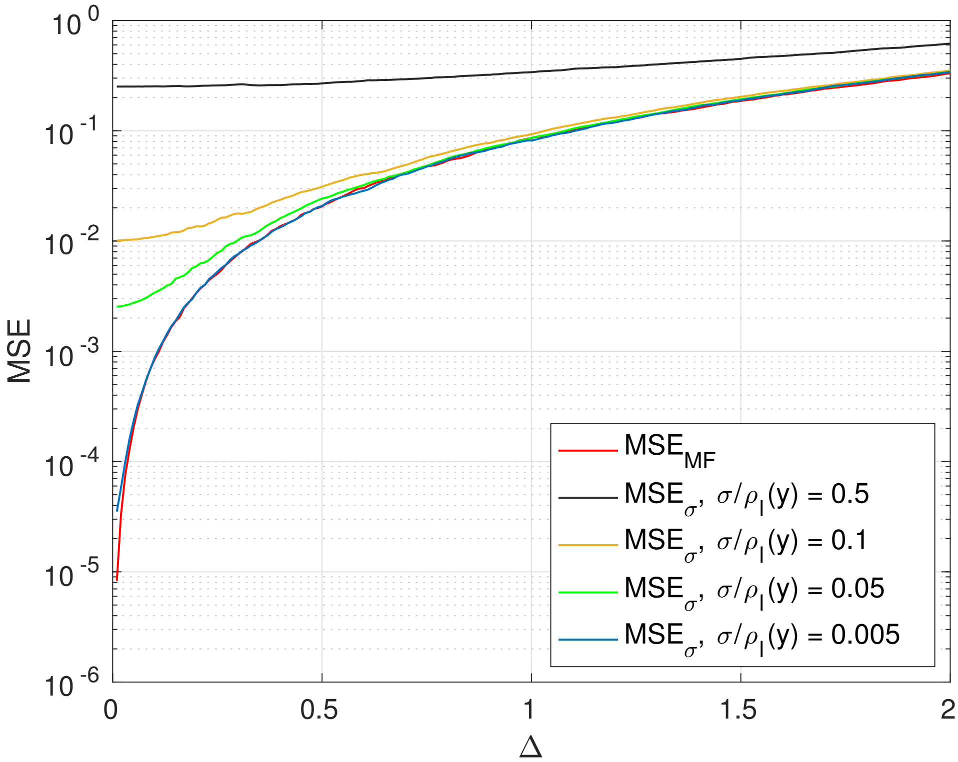

Figure 7.5: MSE_{MF} and MSE_σ for several $\sigma/\rho_l(\mathbf{y})$.

In this subchapter, an approximate overcomplete representation based on ℓ_∞-norm representations is proposed to outperform the MOF based communication systems by creating approximate overcomplete representations with lower envelopes. Introduced method can be applied in many fields which utilize frame theory such as source-channel coding, filter banks, robust transmission, classification and many others. Since interference management is an important topic in *cloud radio access networks* (C-RANs), C-RANs downlink precoding scheme can be chosen as an application to show the advantage of the proposed method over the *zero-forcing* (ZF) precoding method which is a linear precoding scheme and basically MOF of the signal to be coded.

7.2.1.5 C-RAN Fronthaul Downlink Precoding and Quantization

In the C-RANs cellular architecture, mobile devices are connected to *remote radio heads* (RRHs) which basically serve as access points to the network and RRHs are connected to the *baseband unit* (BBU) with wired fronthaul links. In order to allow interference management, signals are precoded in the BBU, then quantized and sent to the RRHs through wired fronthaul links. Let us assume that the signal vector to be linearly precoded is $\mathbf{s}_k \in \mathbb{C}^M$ with a matrix $\mathbf{P}_k \in \mathbb{C}^{N\times M}$ such

$$\mathbf{x}_k = \mathcal{Q}(\mathbf{P}_k \mathbf{s}_k), \quad k = 1, ..., M \tag{7.19}$$

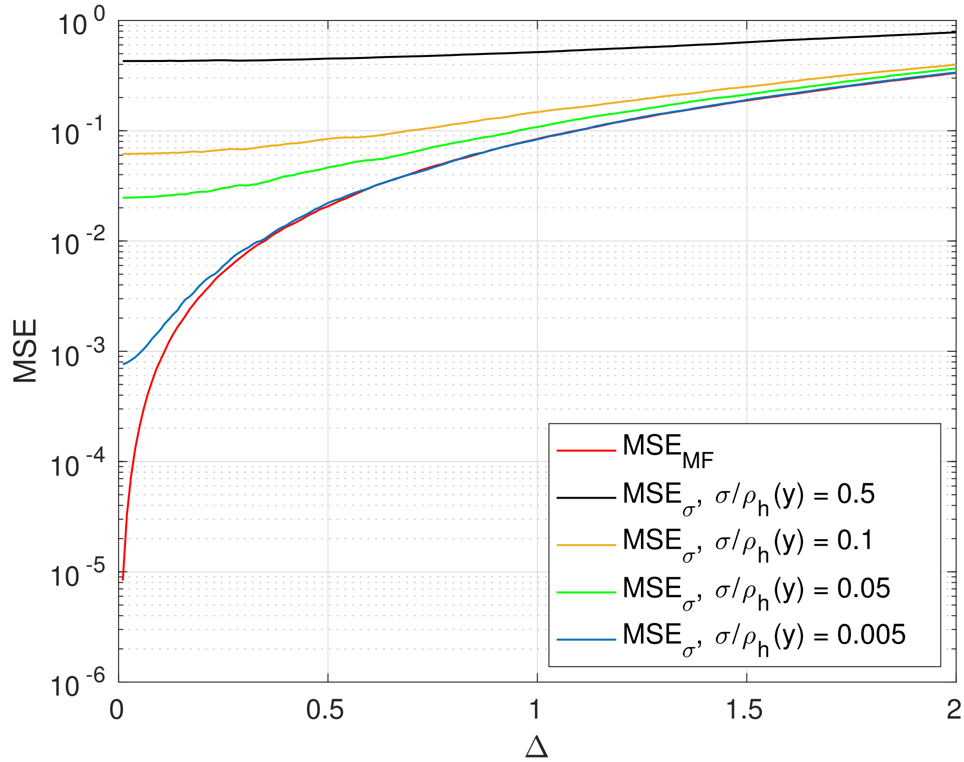

Figure 7.6: MSE_{MF} and MSE_σ for several $\sigma/\rho_h(\mathbf{y})$.

where $\mathbf{x}_k \in \mathbb{C}^N$ is the precoded vector, and $\mathcal{Q}(.) : \mathbb{C}^N \to \mathcal{X}^N$ is the quantization operation that maps input into the quantization alphabet set $\mathcal{X}$. C-RAN downlink system with M RRHs and N *user equipments* (UEs) are shown in Fig. 7.9.

There are several linear and nonlinear precoding schemes have been proposed in the literature [Fat+18]. One very common and widely utilized linear precoding technique is to use the pseudoinverse of the channel matrix (which is $\mathbf{H}^\dagger = \mathbf{H}^T(\mathbf{H}\mathbf{H}^T)^{-1}$) as precoding matrix. This method is called linear ZF precoding. In general, the input-output relation of the channel with ZF coding is defined as

$$\mathbf{y}_k = \mathbf{H}_k\mathbf{x}_k + \mathbf{n}_k = \mathbf{H}\mathcal{Q}(\mathbf{H}_k^\dagger \mathbf{s}_k) + \mathbf{n}_k \quad k = 1, ..., M \tag{7.20}$$

where $\mathbf{n}_k$ represents the channel noise and $\mathbf{H}_k \in \mathbb{C}^{M\times N}$ is the channel matrix which is known perfectly at the BBU.

ZF precoding simply creates the MOF representation of the signal vector $\mathbf{s}_k$. By replacing ZF with the proposed communication architecture, one can use a lower resolution quantizer for same quantization noise budget. In Figure 7.8, required rates to obtain same quantization noise variances are shown for the MOF and the proposed approximate overcomplete representation.

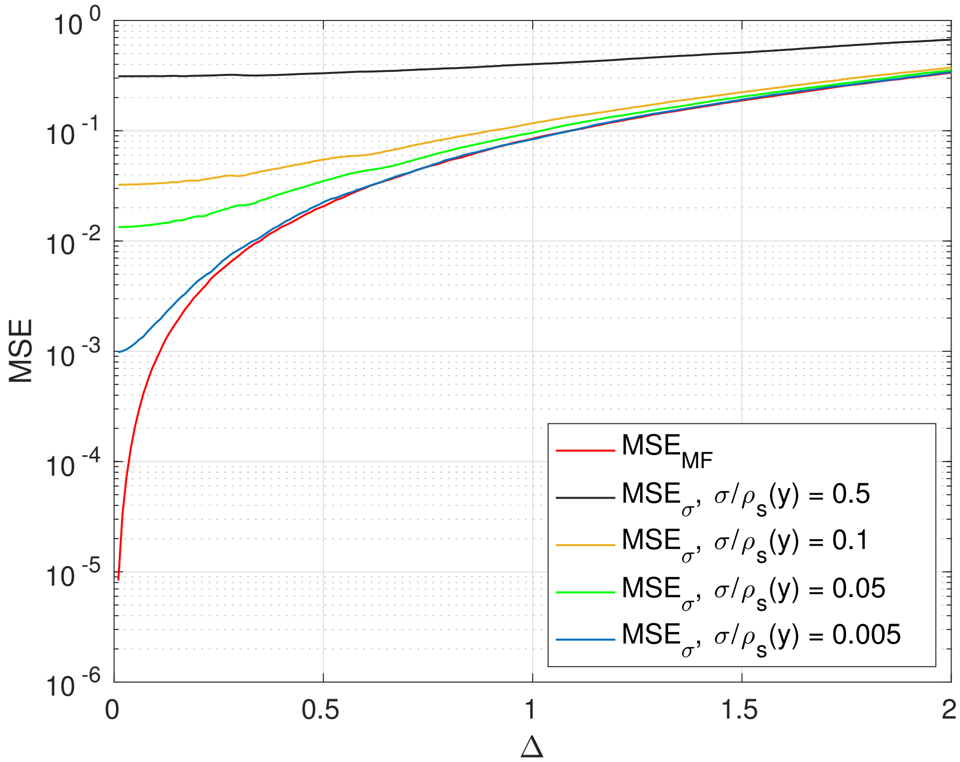

Figure 7.7: MSE_{MF} and MSE_σ for several $\sigma/\rho_s(\mathbf{y})$.

As a conclusion, in this subchapter, a new approximate overcomplete representation scheme is presented to outperform the MOF based communication systems by producing representations with lower envelopes. Proposed scheme is compared with the MOF representation. The approach shown here may be used in a variety of disciplines that make use of frame theory, including source-channel coding, filter banks, resilient transmission, classification, etc.

7.2.2 ℓ_∞-norm Representations Based Outlier Detection

Sparse representations of signals have received important attention in recent years and been widely used in signal processing. It is a powerful tool for many purposes like compressing, representing, efficiently acquiring and reconstructing of signals and etc. [Wri+10]. Although the sparse penalties, ℓ_0-norm and the ℓ_1-norm, are well studied, anti-sparse penalty (ℓ_∞-norm minimization) did not get the attention it deserved. It is very important in many applications such as PAPR reduction, vector quantization, *approximate nearest neighbour* (ANN) search and control engineering [Stu+14], [SYB12]. The most important feature of ℓ_∞-norm minimization is enforcing the signal to be spread evenly [JFF11].

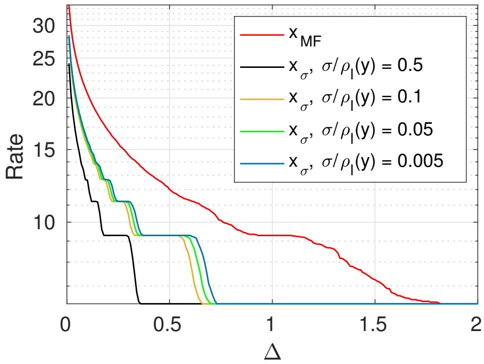

(a) Δ vs. rate $(M = 256, N = 1024)$, ρ_l.

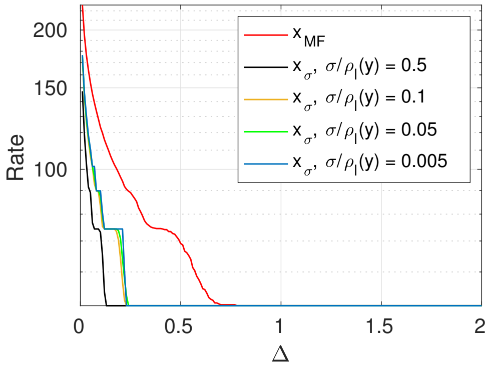

(b) Δ vs. rate $(M = 128, N = 4096)$, ρ_l.

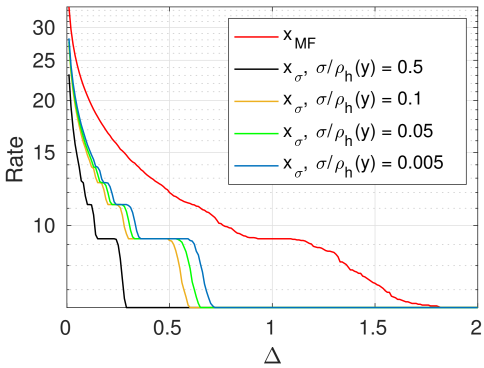

(c) Δ vs. rate $(M = 256, N = 1024)$, ρ_h.

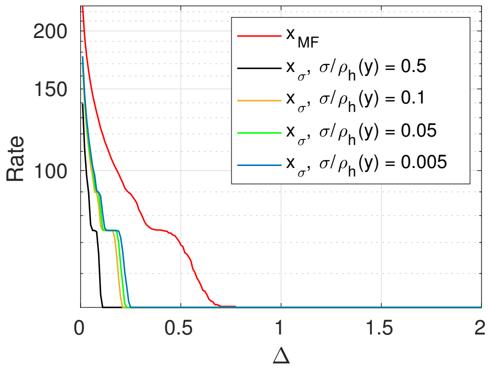

(d) Δ vs. rate $(M = 128, N = 4096)$, ρ_h.

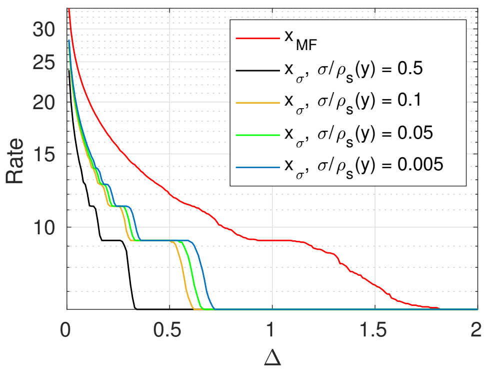

(e) Δ vs. rate $(M = 256, N = 1024)$, ρ_s.

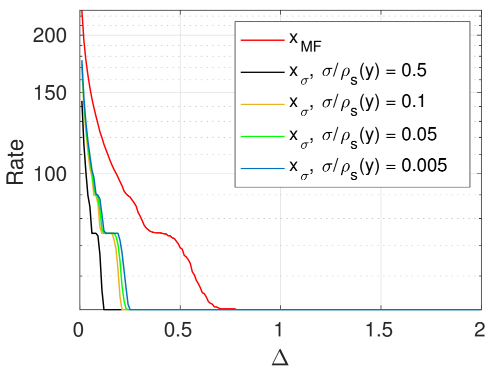

(f) Δ vs. rate $(M = 128, N = 4096)$, ρ_s.

Figure 7.8: Δ vs. rate.

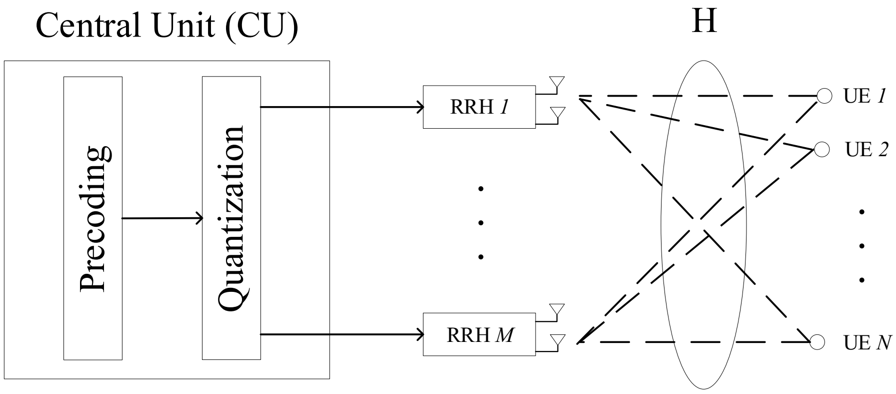

Figure 7.9: C-RAN downlink system with M RRHs and N UEs.

Recently, Lyubarskii [LV10] showed that some frames such as random subsampled discrete Fourier transform (DFT) matrices, random orthogonal matrices, random sub-Gaussian matrices which satisfy ucerainty principle yield a computable anti-sparse representation (there are some other different names in the literature such as Kashin‘s, democratic, spread) that empowers the representation with the smallest possible dynamic range.

Studer studied ℓ_∞-norm minimization and proposed efficient algorithms to obtain anti-sparse vectors and developed bounds for anti-sparsity for the representation vector [Stu+14]. Elvira proposed a prior and sample generators for anti-sparsity and by using this probabilistic behavior, Bayesian linear inverse problem for anti-sparse communication investigated [ECD17]. There are some other papers also studied ℓ_∞-norm minimization [SYB12], [JFF11], [Fuc11] for some intriguing applications. Most interesting one was about considering anti-sparsity as a binarization scheme for ANN search [JFF11]. This paper inspires us to use anti-sparsity for distance based outlier detection.

Since ℓ_∞-norm is a non-differentiable function, one important issue about the optimization problem of ℓ_∞-norm minimization is the difficulty of obtaining minimized ℓ_∞-norm of a vector. This motivates us using of smoothing concept. A smooth approximation of the optimization problem makes possible to solve optimization problems much easier. After solving optimization problem, the obtained anti-sparse vector elements must be concentrated around the boundaries (i.e., absolute maximum value) of the representation which offers a natural binarization scheme. Several binarization methods are used for various applications and main motivation of binarization is to embed input vector to a binary vector to have computational gain. One application is to use binarized vector for ANN search. By using anti-sparse binarization scheme nearest neighbor search based outlier detection can also be performed. Detection of outliers provide very important knowledge for many applications. For example, one can identify *denial-of-service* (DoS) attacks which are simple and powerful attempts to make network resource inaccessible. Since behaviours of attacks do not fit the regular attitude of the network, DoS attacks can be considered as outliers (anomalies).

In this subchapter, a new outlier detection method based on anti-sparse representation is proposed. First of all, obtaining anti-sparse vector, i.e. minimizing ℓ_∞-norm, is investigated. By inspired of the derived approximate absolute maximum value function in [Lan+], a smooth objective function is presented to cope with the non-smoothness of ℓ_∞-norm. Anti-sparse representations offers to spread the signal over representation elements evenly. As a result of this favorable property, anti-sparse representation is considered as a natural binarization scheme. Finally, anti-sparse binarization scheme is used for ANN search to detect DoS attacks.

7.2.2.1 Smooth Approximation of ℓ_∞-norm

ℓ_∞-norm representation of a signal can be obtained by finding $\hat{\mathbf{x}} = \arg\min_{\mathbf{x}} F_\infty(\mathbf{x})$, where

$$F_\infty(\mathbf{x}) = \frac{1}{2}||\mathbf{y} - \mathbf{D}\mathbf{x}||_2^2 + \lambda||\mathbf{x}||_\infty, \tag{7.21}$$

$\mathbf{y} \in \mathbb{R}^M$ is the signal to be represented, $\mathbf{D} \in \mathbb{R}^{M\times N}$ denotes the representation matrix with $M < N$. , and $\lambda > 0$ is the regularization parameter. Noting that $F_\infty(\mathbf{x})$ is $(\mathrm{P}_\lambda^\infty)$ with ρ is ℓ_2-norm. Because of ℓ_∞-norm term, $F_\infty(\mathbf{x})$, the objective function, is a non-smooth function. Solving non-smooth convex optimization problems is much more difficult than solving smooth differentiable ones. One way to deal with non-smoothness is deriving sub-differentiable of a non-smooth function. Proximal gradient methods are also widely used. There are some other methods like cutting-plane and bundle methods.

One interesting way to solve non-smooth optimization problems is transforming the problem to a differentiable smooth one. In this study, eq. (7.21) is transformed a differentiable optimization problem by smoothing ℓ_∞-norm.

Smooth approximations for the maximum function are used in many different studies for several applications [Zha+13; HCB11; RB15]. One of the most recent, simple and common utilized smoothing function for the maximum function is called soft maximum, proposed in [Coo11] and defined as follows

$$S_\alpha(\{x_i\}_{i=1}^n) = \frac{1}{\alpha}\log\left(\sum_{i=1}^n e^{\alpha x_i}\right), \tag{7.22}$$

with α smoothing parameter which is necessary to regulate the quality of the approximation.

In addition to smooth function for maximum of a function, smooth approximation of the absolute value function is also necessary to generate a smoothing function for

ℓ_∞-norm. One of the commonly used smooth approximation of the absolute value can be found in [SFR07]. According to [SFR07], a smooth approximation of the absolute value ($|x|_\alpha \approx |x|$) with an approximation parameter α, can be written as $|x|_\alpha = (x)^+_\alpha + (-x)^+_\alpha$ where

$$(x)^+_\alpha = x + \frac{1}{\alpha}\log(1 + e^{-\alpha x}), \tag{7.23}$$

and smooth approximation of the absolute value can be derived as follows:

$$|x|_\alpha = \frac{1}{\alpha}\log(2 + e^{-\alpha x} + e^{\alpha x}). \tag{7.24}$$

For mathematical convenience, approximation parameter for absolute function and smoothing parameter for maximum function considered as equal. By using (7.22) and (7.24), smoothing function of ℓ_∞-norm can be formulated as:

$$S^\infty_\alpha(\{x_i\}^n_{i=1}) = \frac{1}{\alpha}\log\left(\sum_{i=1}^n (2 + e^{-\alpha x_i} + e^{\alpha x_i})\right), \tag{7.25}$$

and the derivative of absolute maximum function can be calculated as:

$$\frac{\partial S^\infty_\alpha(x_i)}{\partial x_i} = \frac{e^{\alpha x_i} - e^{-\alpha x_i}}{2 + e^{\alpha x_i} + e^{-\alpha x_i}} = \tanh\left(\frac{\alpha x_i}{2}\right). \tag{7.26}$$

As a consequence of smoothing ℓ_∞-norm, objective function can be replaced with an approximate objective function ($F_\infty(\mathbf{x}) \approx F^S_\infty(\mathbf{x})$) which is differentiable,

$$F^S_\infty(\mathbf{x}) = \frac{1}{2}||\mathbf{y} - \mathbf{D}\mathbf{x}||^2_2 + \frac{\lambda}{\alpha}\left(\sum_{i=1}^n (2 + e^{-\alpha x_i} + e^{\alpha x_i})\right). \tag{7.27}$$

The new approximate objective function makes possible to solve eq. (7.21) with descent methods which are commonly utilized algorithms to solve optimization problems.

7.2.2.2 Gradient and Hessian of $F^S_\infty(\mathbf{x})$

In order optimize convex, twice differentiable function without constrains, one can use Newton's method which is a frequently used descent optimization algorithm. In order to use Newton's method, gradient vector and Hessian matrix of $F^S_\infty(\mathbf{x})$ ($\nabla F^S_\infty(\mathbf{x})$ and $\nabla^2 F^S_\infty(\mathbf{x})$ respectively) need to be computed. With the help of smoothing function, gradient vector of approximate objective function,

$$\begin{aligned}\nabla F^S_\infty(\mathbf{x}) &= \mathbf{D}^T(\mathbf{D}\mathbf{x} - \mathbf{y}) + \lambda\Big\{\frac{\partial S^\infty_\alpha(x)}{\partial x_i}\Big\}^n_{i=1} \\ &= \mathbf{D}^T(\mathbf{D}\mathbf{x} - \mathbf{y}) + \lambda\Big\{\tanh\left(\frac{\alpha x_i}{2}\right)\Big\}^n_{i=1},\end{aligned} \tag{7.28}$$

and Hessian matrix of approximate objective function,

$$\nabla^2 F_\infty^S(\mathbf{x}) = \mathbf{D}^T\mathbf{D} + \frac{\lambda\alpha}{2}\mathrm{Diag}\left(\mathrm{sech}^2\left(\frac{\alpha x_i}{2}\right)\right), \tag{7.29}$$

can be computed conveniently.

7.2.2.3 Newton's Method for ℓ_∞-norm Minimizaton

One of the well-known method for solving unconstrained optimization problems is the Newton's method that minimizes a cost function iteratively. When the cost function (objective function) is a twice differentiable, then Newton's method is a very efficient way to solve the minimization problem.

In this subsection, Newton's method for ℓ_∞-norm minimizaton is presented with the help of approximate objective function. One can easily find $\hat{\mathbf{x}} = \arg\min_{\mathbf{x}} F_\infty^S(\mathbf{x})$ by following the steps that are shown in Algorithm 4.

Algorithm 4 Newton's Method for ℓ_∞-Norm Minimizaton

Input: $\mathbf{y} \in \mathbb{R}^m$, $\mathbf{x}^{(0)} \in \mathbb{R}^n$, $\mathbf{D} \in \mathbb{R}^{M\times N}$, ∇F_∞^S and $\nabla^2 F_\infty^S$

1: **for** k=1,2,3,...,iter **do**
2: $\quad\mathbf{x}^{(k)} = \mathbf{x}^{(k-1)} - \gamma\delta^{(k-1)});$
3: $\quad$with $\delta^{(k-1)} = -(\nabla^2 F_\infty^S(\mathbf{x}^{(k)})^{-1}\nabla F_\infty^S(\mathbf{x}^{(k)}))$
4: **end for**

where γ is a constant ($\gamma \in (0,1)$) to satisfy Wolfe conditions.

Output: $\hat{\mathbf{x}}$, anti-sparse representation vector

Outliers are the data points that deviates too much from the other observed data points. Detection of outliers can lead to use of important knowledge and will be very crucial for some applications such as credit card fraud detection, network intrusion, anomalous traffic pattern in a network spotting, data cleansing, and other many statistics, machine learning and data-mining related tasks [HA04]. There are several approaches to detect outliers. Most utilized methods include density based methods, graph-based methods and distance-based methods. In this study anti-sparse representation is employed for distance based outlier detection.

Distance-based outlier detection method, first studied for statics datasets [KN98], is a computationally efficient approach because of monotonic non-increasing functions of outlier scores [PDN10]. Besides computational advantage, another aspect of distance-based outlier detection method is being not dependent on the distribution of data which is a good feature for many applications. The idea behind the distance based outliers detection methods, mostly based on nearest neighbor search, is that the greater distance of the object to its neighbors is most likely an outlier. One outlier example could be the DoS attacks.

DoS attacks are simple and powerful techniques to make network resource inaccessible. Attacks are mostly the behaviours that do not fit the regular attitude of the network. That is why they can be considered as outliers (anomalies). Furthermore, detection of these attacks important to create an intrusion (attack) prevention systems.

7.2.2.4 Approximate Nearest Neighbor Search with ℓ_∞ Representations

One of the promising application area of ℓ_∞-norm representations, a.k.a anti-sparse representations, is nearest neighbor search related applications [JFF11]. The motivation is to embed anti-sparse signal to Hamming space which is a set of binary strings. The purpose of embedding approach is to map query vectors to the target vector in order to perform fast and efficient comparison. In this study, anti-sparse representation is considered as an application for ANN search as done in [JFF11].

By considering anti-sparse representations offers to spread the signal over representation elements evenly, a binarization scheme with anti-sparse signal can be created as: $b(\mathbf{k}) = \text{sign}(\mathbf{x})$, where $\mathbf{x}$ is the anti-sparse representation of relevant input vector, $\mathbf{k}$.

The idea is to compute approximate nearest neighbor for a query vector ($\mathbf{q}$) and determine whether it is an outlier or not. In order to determine how far query and target vector, anti-sparse based ANN search can be considered as *maximum inner product search* (MIPS). MIPS is an effective tool to search similarity for binary coding techniques [SL14] and MIPS problem formulated as:

$$\text{NN}(b(\mathbf{q})) = \underset{\mathbf{y}\in\mathbb{R}^M}{\arg\max}\; b(\mathbf{q})^T b(\mathbf{y}). \tag{7.30}$$

The input vectors correspond to $\text{NN}(b(\mathbf{q})) < d$, considered as outliers, where d is the distance metric.

In order to analyze the performance of anti-sparse outlier detection method, well known KDDCup99 dataset [Lic13] is used. This dataset includes several types of network intrusions which are considered outliers. In this study, as an intrusion 'back', 'land', 'pod', 'teardrop' type DoS attacks and regarding to these attacks, most relevant features 'src_bytes' (number of data bytes sent from source to destination), 'dst_bytes' (number of data bytes sent from destination to source), 'land' (whether the connection is from/to the same host/port or not), 'wrong_fragment'(number of wrong fragments) are used.

Small set of the dataset is chosen randomly. 1000 outliers (DoS attacks) and 6000 inliers (normal) are used for analysis. Sample number of attributes are shown in Table 7.6.

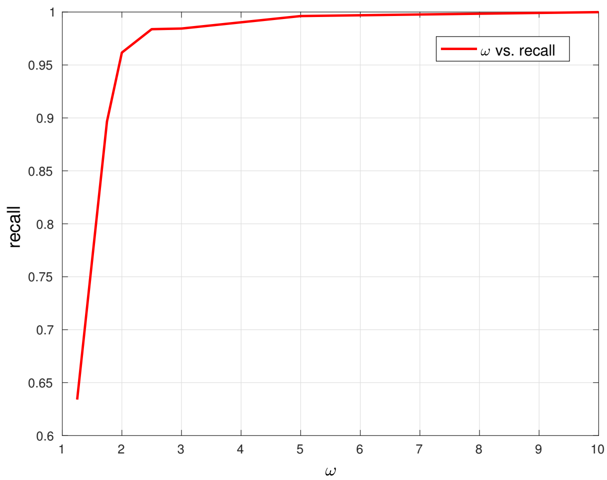

Figure 7.10: ω vs. Recall.

	normal	back	land	teardrop	pod
number of samples	6000	600	150	150	100

Table 7.6: Sample numbers of attributes for simulations.

In order to measure the performance of anti-sparse representation based outlier detection method, two well known methods are employed which are *recall* and *precision*, defined as:

$$Recall = \frac{\text{number of detected relevant outliers}}{\text{number of outliers}}, \tag{7.31}$$

$$Precision = \frac{\text{number of detected relevant outliers}}{\text{number of relevant outliers}}. \tag{7.32}$$

One important observation should be about how performance metrics varies depending on the redundancy ratio $\omega = N/M$. It should be noticed again, M and N is the dimension of the input vector (which is feature number), and binarized anti sparse signal respectively.

Figure 7.10 and 7.11 show the performance of the proposed outlier detection method on KDDCup99 data set. It can be easily seen that when ω increases, proposed approach gives impressive result in terms of *recall* and *precision*.

In this subchapter, a new outlier detection method based on anti-sparse representations is introduced. As a consequence of anti-sparse representation spreads the signal over representation elements evenly, anti-sparse signal is used for binarization and

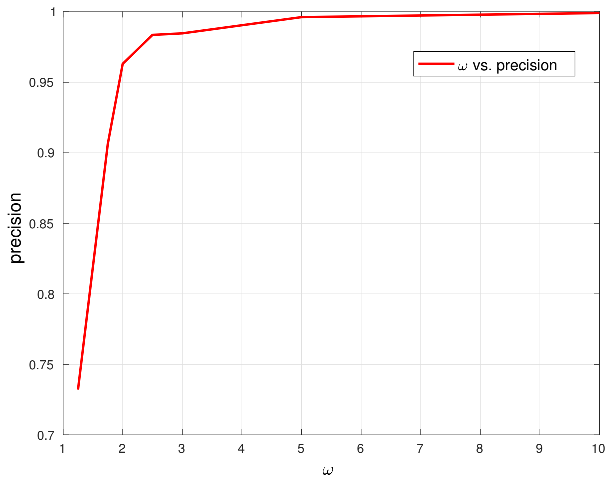

Figure 7.11: ω vs. Precision.

embedded ANN search. Distance based anti-sparse ANN search is employed for DoS attacks detection on a real data set.

7.2.3 Effect of ℓ_∞-norm Representation Prior on PAPR Preformance Analysis

Dynamic range of a signal plays a significant role in many communication applications. In most applications, high dynamic range is considered a problem for technical reasons. ℓ_∞-norm minimization, or in other words anti-sparse penalty, offers to spread the signal over representation elements evenly. One of the advantage of spreading the signal is reducing the dynamic range of a signal which is a pleasant feature for many application; e.g. PAPR reduction for OFDM systems. In this subchapter, some of main proximal splitting algorithms are deployed for ℓ_∞-norm minimization. Stochastic model of anti-sparsity is investigated with the empirical results of proximal methods and already existing ℓ_∞-norm minimization methods. A flexible prior is proposed to model anti-sparsity and it is used for more realistic PAPR performance analysis.

Sparse representations have gained significant attention in recent years and been widely used in signal processing. It is a powerful tool for many purposes like compressing, representing, efficiently acquiring and reconstructing of signals, etc. [Wri+10]. Although the sparse penalties, ℓ_0-norm and the ℓ_1-norm, are well studied, anti-sparse penalty (ℓ_∞-norm minimization) did not get the attention it deserved. It is very useful tool in many applications such as PAPR reduction, vector quantization, approximate neighbour search and control engineering [Stu+14], [SYB12]. The most important feature of ℓ_∞-norm minimization is enforcing the signal to be spread evenly [JFF11].

Lyubarskii presented that some frames such as random subsampled discrete Fourier transform (DFT) matrices, random orthogonal matrices, random sub-Gaussian matrices which satisfy uncertainty principle yield a computable anti-sparse representation (there are some other different nomenclatures in the literature like Kashin's, democratic, spread) that empowers the representation with the smallest possible dynamic range [LV10]. Studer studied ℓ_∞-norm minimization and proposed efficient algorithms to obtain anti-sparse vectors and developed bounds for anti-sparsity for the representation vector [Stu+14]. There are some other papers which have also studied ℓ_∞-norm minimization such as [SYB12], [JFF11], [Fuc11], however stochastic analysis of the anti-sparsity was out of scope in these related works. Recently, [ECD17] proposed a prior and sample generators for anti-sparsity and by using this probabilistic behavior, Bayesian linear inverse problem for anti-sparse communication is studied.

There are some existing algorithms to obtain anti-sparse vector and we show that all of them provides similar prior information about the anti-sparse signal, in this subchapter. Availability of the prior information about a signal gives the opportunity to have more computationally tractable performance measures. A realiable priori information allows us to benefit from anti-sparsity in many areas. It also offers effective solutions for Bayesian linear inverse problems, provides better quantization approaches, gives statistically enhanced of the characteristics of the PAPR distribution. Therefore stochastic behavior of anti-sparse representation is an important topic and need to be investigated.

In this subchapter, main proximal splitting algorithms are deployed for ℓ_∞-norm minimization. Stochastic model of anti-sparsity is investigated with the empirical results of proximal methods and existed other some ℓ_∞-norm minimization methods. Based on empirical observations, a flexible prior is introduced to model anti-sparsity and it is used to improve statistical characteristics of PAPR distribution.

7.2.3.1 ℓ_∞-norm Minimizaton with Proximal Gradient Methods

Anti-sparse representation of a vector can be found by solving the following optimization problem

$$\underset{\tilde{\mathbf{x}}\in\mathbb{R}^N}{\text{minimize}} \quad \frac{1}{2}||\mathbf{y}-\mathbf{D}\tilde{\mathbf{x}}||_2^2+\lambda||\tilde{\mathbf{x}}||_\infty, \tag{7.33}$$

where $\mathbf{D}\in\mathbb{R}^{M\times N}$ denotes the representation matrix with $M<N$, $\mathbf{y}\in\mathbb{R}^M$ is the signal to be represented, and $\lambda>0$ is the regularization parameter. Noting that (7.33) is ($\mathrm{P}_\lambda^\infty$) with ρ is ℓ_2-norm. Solution of (7.33) provides a vector with elements that are evenly spread.

Many constrained convex optimization problems can be interpreted as the following composite form:

$$\underset{\mathbf{x}\in\mathbb{R}^N}{\text{minimize}} \quad f(x)=g(x)+h(x), \tag{7.34}$$

where $g(x)$ represents the convex, differentiable loss function, and $h(x)$ is a convex, yet not necessarily differentiable penalty function. By using composite form representation, (7.33) can be presented with $g(x)$ and $h(x)$ where $g(x) = \frac{1}{2}||\mathbf{y} - \mathrm{D}\mathbf{x}||_2^2$ and $h(x) = \lambda||\mathbf{x}||_\infty$. Since ℓ_∞-norm term is not differentiable, solving (7.34) with simple gradient-descent methods is not possible. However, one can solve (7.34) efficiently with proximal gradient methods (also known as forward-backward splitting methods). In order to employ proximal gradient methods to solve ($\mathrm{P}_{\infty,2}$), proximal operator for h, which is equation (7.35), need to be calculated. The algorithm that is defined in [Stu+14] to have efficient solution for (7.35) can be used.

$$\mathrm{prox}_h(\mathbf{z}, \lambda) = \arg\min_{\mathbf{x}\in\mathbb{R}^N} \lambda||\mathbf{x}||_\infty + \frac{1}{2}||\mathbf{x} - \mathbf{z}||_2^2. \tag{7.35}$$

Owing to the many applications of forward-backward splitting (FB) methods for sparse coding, several variations of FB are developed to enhance performance. One improvement is about the speed of FB. Since the raw forward-backward method generally may be considered slow, in order to overcome this slowness some accelerated methods are introduced like Nesterov‘s method (NM) [Y83] and fast iterative shrinkage-thresholding algorithm (FISTA) [BT09]. In this study, we deployed the raw FB algorithm and it's variants NM and FISTA to solve ($\mathrm{P}_{\infty,2}$) as detailed in Algorithm 5.

7.2.3.2 Anti-Sparse Prior

Stochastic model of sparsity is investigated throughout many different works. There are many several prior proposals for sparsity. Most of the effective priors considered as mixture models (mostly with two mixtures) where one distribution imitates the "significant" elements of the representation vector. However, probabilistic behavior of anti-sparse representations is not well studied. In this section, a prior for anti-sparsity based on empirical results of several ℓ_∞-minimization methods is introduced.

Anti-sparse representation has some specific magnitude properties. With the help of this knowledge, vector $\mathbf{x}$ can be categorized as it is described in [Stu+14],

Definition *Extreme and Moderate Components of The Representation Vector* $\mathbf{x}$*:* Assuming $\mathbf{x}= [x_1, x_2, ..., x_N]$ is the representation vector, an element of the vector $\mathbf{x} \in \mathbb{C}^N$, x_i, is called *extreme* if $|x_i| = ||\mathbf{x}||_\infty + \epsilon$, in the meantime it is *moderate* if $|x_i| < ||\mathbf{x}||_\infty + \epsilon$ where $\epsilon \approx 0$. By using this definition, let denote $\mathbf{x}_{ext}$ for the sub-vector of $\mathbf{x}$ which consists of extreme components and $\mathbf{x}_{mod}$ is the sub-vector of $\mathbf{x}$ which consists of moderate components.

In order to model anti-sparsity, symmetric Beta distribution is considered for each sub-vector. Although the mathematical convenience of the Beta distribution is not favorable for many applications, it is very flexible and can take on many different shapes. Because of that reason, it is assummed that $\mathbf{x}$ is drawn independent and

Algorithm 5 Main Proximal Gradient Methods to Solve ($\mathrm{P}_{\infty,2}$)

Raw Forward-Backward Algorithm (FB)

Input: $\mathbf{y}^{(0)} \in \mathbb{R}^M$, $\mathbf{x}^{(0)} \in \mathbb{R}^N$, $\mathbf{D} \in \mathbb{R}^{M\times N}$, c_1

for k=1,2,3,...,iter **do**
- $\mathbf{t}^{(k)} = \mathbf{x}^{(k-1)} - \frac{c_1}{L}\nabla g(\mathbf{x}^{(k-1)}), \frac{c_1}{L})$
- $\mathbf{x}^{(k)} = \mathrm{prox}_h(\mathbf{t}^{(k)}, \frac{c}{L})$

end for

Nesterov's Method (NM)

Input: $\mathbf{y}^{(0)} \in \mathbb{R}^M$, $\mathbf{x}^{(0)} \in \mathbb{R}^N$, $\mathrm{D} \in \mathbb{R}^{M\times N}$, $\kappa^{(0)}$, $\xi^{(0)}$, c_2

for k=1,2,3,...,iter **do**
- $\zeta^{(k)} = \left(\frac{c_2}{L} + \sqrt{\left(\frac{c_2}{L}\right)^2 + 4\left(\frac{c_2}{L}\right)\kappa^{(k-1)}}\right)/2$
- $\mathbf{p}^{(k)} = \mathrm{prox}_h(\mathbf{x}^{(0)} - \xi^{(k-1)}, \kappa^{(k-1)})$
- $\mathbf{r}^{(k)} = \frac{(\kappa^{(k-1)}\mathbf{x}^{(k)} + \zeta^{(k)}\mathbf{p}^{(k)})}{\kappa^{(k-1)} + \zeta^{(k)}}$
- $\mathbf{x}^{(k)} = \mathrm{prox}_h(\mathbf{r}^{(k)} - \frac{1}{L}\nabla g(\mathbf{r}^{(k)}), \frac{1}{L})$
- $\xi^{(k)} = \xi^{(k-1)} + \zeta^{(k)}\nabla g(\mathbf{x}^{(k)})$
- $\kappa^{(k)} = \kappa^{(k-1)} + \zeta^{(k)}$

end for

FISTA

Input: $\mathbf{y}^{(0)} \in \mathbb{R}^M$, $\mathbf{x}^{(0)} \in \mathbb{R}^N$, $\mathrm{D} \in \mathbb{R}^{M\times N}$, $\gamma^{(1)} = 1$

for k=1,2,3,...,iter **do**
- $\mathbf{x}^{(k)} = \mathrm{prox}_h(\mathbf{y}^{(k-1)} - \frac{1}{L}\nabla g(\mathbf{y}^{(k-1)}), \frac{1}{L})$
- $\gamma^{(k+1)} = (1 + \frac{\sqrt{1+4(\gamma^{(k)})^2}}{2})$
- $\mathbf{y}^{(k)} = \mathbf{x}^{(k)} + \frac{\gamma^{(k)}-1}{\gamma^{(k+1)}}(\mathbf{x}^{(k)} - \mathbf{x}^{(k-1)})$

end for

where ∇g is Lipschitz-continuous with constant $L > 0$.

identically distributed (i.i.d.) from the marginal pdf

$$f(x) = \mathrm{w}_{ext}\mathrm{Be}(a_{ext}, a_{ext}) + \mathrm{w}_{mod}\mathrm{Be}(a_{mod}, a_{mod}), \tag{7.36}$$

where

$$\mathrm{Be}(a,b) = \frac{(x-m)^{(a-1)}(n-x)^{(b-1)}}{\mathrm{B}(a,b)(n-m)^{(a+b-1)}}, \tag{7.37}$$

w_{ext} and w_{mod} are the weights ($\mathrm{w}_{ext} + \mathrm{w}_{mod} = 1$), a_{ext} and a_{mod} are the shape parameters of the Beta distributions for sub-vectors $\mathbf{x}_{ext}$ and $\mathbf{x}_{mod}$ respectively. m and n represent the lower and upper bounds of $f(x)$ (which are $-||\mathbf{x}||_\infty$ and $||\mathbf{x}||_\infty$) and B(.,.) is the beta function which is a normalization constant. To ensure the symmetry for ℓ_p-norm, shape parameters of Beta distributions considered as equal.

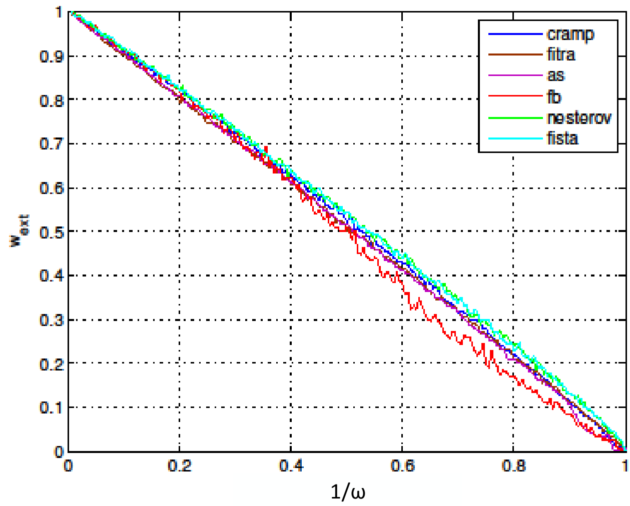

Figure 7.12: Linear relation between w_{ext} and ω

7.2.3.3 Anti-Sparse Behavior Depending Redundancy Ratio

Behavior of anti-sparse distribution is empirically investigated with different ℓ_∞-norm minimization methods. These methods includes convex reduction of amplitudes for Parseval frames (CRAMP) [Stu+14], the fast iterative truncation algorithm (FITRA) [SL13], anti-sparse solver (AS) [JFF11], and main proximal splitting algorithms (introduced in Section 7.2.3.1) like raw FB, NM, and FISTA.

One important attitude of the anti-sparse pdf that should be examined is the changes on weights of $\mathbf{x}_{ext}$ and $\mathbf{x}_{mod}$ depending redundancy ratio ($\omega = N/M$). Although, the optimum weights for $\mathbf{x}_{ext}$ and $\mathbf{x}_{mod}$ are investigated hypothetically in [Stu+14], [Fuc11], Figure 7.12 shows the empirical w_{ext} for the sub-vector $\mathbf{x}_{ext}$ depending ω and one should remember w_{mod} is equals to the $1 - \mathrm{w}_{ext}$. Linear relationship between ω and weights can be modeled as $\mathrm{w}_{ext} = -\mathrm{k}/\omega + C_1$ and $\mathrm{w}_{mod} = \mathrm{k}/\omega + C_2$ where C_1, C_2 are some constants and k values are shown in Table 7.7.

Other important observation about anti-sparse prior is the changes of Beta distribution parameters with ω. Since the proposed pdf is a mixture of two Beta distributions, finding parameters is a challenging *maximum likelihood estimation* (MLE) problem that can not be analytically solved. The *expectation maximization* (EM) algorithm is originally developed to simplify difficult MLE problems and provide a closed form expression for the mixture model. It is frequently used for finding mixture model parameters [BVK15; VKS15; VEA14; VJS16]. With the help of EM algorithm, a_{ext} and a_{mod} with varying ω are found and shown in Figure 7.13. EM algorithm steps for Beta mixture can be followed in [Ji+05].

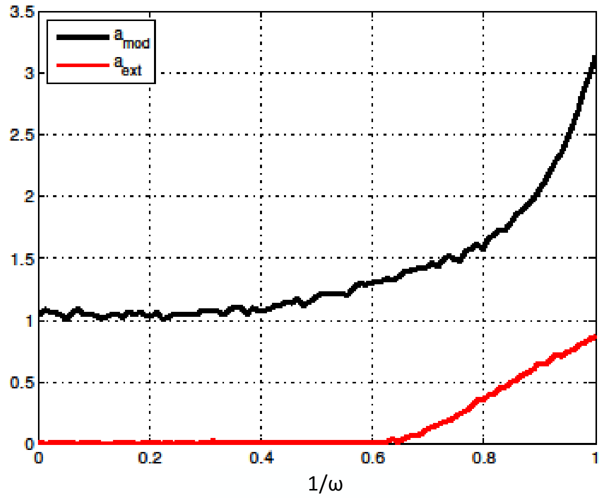

Figure 7.13: Anti-sparse prior parameters behavior.

One fact about a symmetric Beta distribution is when $\lim_{a=b\to 0} \mathrm{Be}(x|a,b)$, the minimum value of excess kurtosis for Beta distribution is ensured. That means the pdf is concentrated at the lower and upper bounds with equal 1/2 probability, or in other words Beta distribution becomes a Bernoulli distribution. It should also be remembered that when $\lim_{a=b\to 1} \mathrm{Be}(x|a,b)$, Beta distribution becomes a uniform distribution. By using these observations, it is also possible to use other more mathematical convenient priors[1]; however, we will move on with the Beta mixture.

Figure 7.14 shows an empirical pdf of an anti-sparse representation obtained using a 2240×2560 overcomplete Gaussian matrix via FISTA with a proper anti-sparse pdf fit (eq. (7.36)) with parameters $a_{ext} = 0.58$, $a_{mod} = 1.9398$). In order to determine whether the proposed anti-sparse model is suitable for the actual histogram Kolmogorov-Smirnov (KS) test is used as goodness-of-fit test.

[1]Probability distribution of the anti-sparse representation can also be represented with a Dirac delta function for the extreme sub-vector and a Gaussian distribution for moderate sub-vector:

$$f(x) = w_{ext}\delta(||\mathbf{x}||_\infty - |x|) + w_{mod}\mathcal{N}(x|0,\sigma^2_{mod}). \tag{7.38}$$

Using Dirac+Gaussian distribution prior (7.38) will provide mathematical convenience for some performance analysis. For example, when $\mathbf{D} \in \mathbb{R}^{M\times N}$ is a DFT matrix, envelope distribution of the $f(x)$ need to be defined for CCDF of PAPR distribution. By using (7.38), envelope distribution can be found as a Rayleigh mixture. One could model Dirac function as a Gaussian distribution with an arbitrary small variance ($\delta(x-\mu) = \mathcal{N}(x|\mu,\sigma^2), \sigma^2 > 0$ and μ is the mean).

Table 7.7: k values for different algorithms.

	CRAMP	FITRA	AS	FB	NM	FISTA
k	0.998	0.983	1.002	1.054	0.979	0.979

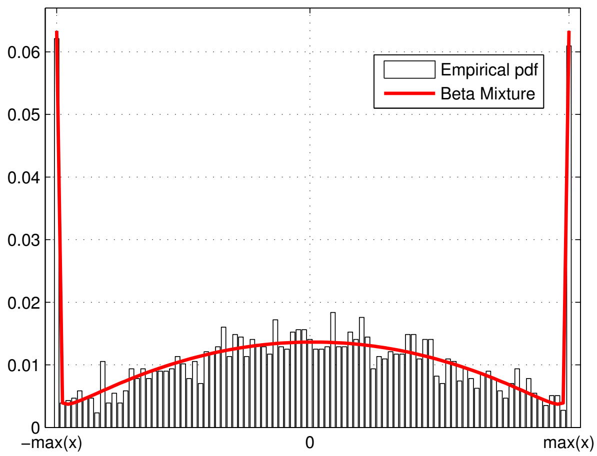

Figure 7.14: Empirical anti-sparse pdf with a proper fit.

7.2.3.4 Anti Sparse Prior on Dynamic Range Reduction

One significant advantage of the anti-sparse representation is reducing (or narrowing) the dynamic range of a signal. One important promising area of using anti-sparse signals with this purpose is PAPR reduction for OFDM signals.

OFDM is a widely used technique in many digital communication systems. Despite the fact that it has many advantages like high spectral efficiency, simple channel equalisation and more resistance communication channels, it has some problems to be addressed and the major problem of OFDM signals is having potentially high PAPR. The signals with high PAPR require power amplifiers with a large range of dynamic linearity. However, this kind of power amplifier has poor efficiency and they are expensive. Therefore PAPR reduction is an important and necessary field to investigate. Anti-sparsity offers PAPR reduction and studied for this goal in [SL13], [IS09]. In this study, by using prior for the anti-sparse representation, we offer statistically improved of the characteristics of the PAPR distribution. PAPR of a signal $\mathbf{x}$ is defined as follows

$$\mathrm{PAPR}(\mathbf{x}) = \frac{N||\mathbf{x}||_\infty^2}{||\mathbf{x}||_2^2}. \tag{7.39}$$

7.2.3.5 Performance of PAPR Reduction

One of the important characteristics of the PAPR is its distribution and it can be expressed in terms of complementary cumulative distribution function (CCDF). It is the most frequently used metric for measuring PAPR performance of a signal. It can be considered as the probability of the PAPR that below some threshold.

It is assumed that magnitudes (elements) of the vector $\mathbf{x}$ are i.i.d random variables which are drawn from the pdf (7.36). Then cumulative distribution function (CDF) of the anti-sparse pdf can be written as

$$\begin{aligned} F(x) = {} & \frac{w_{ext}}{\mathrm{B}(a_{ext}, a_{ext})} \int_0^x t^{a_{ext}-1}(1-t)^{a_{ext}-1}\, dt \\ & + \frac{w_{mod}}{\mathrm{B}(a_{mod}, a_{mod})} \int_0^x t^{a_{mod}-1}(1-t)^{a_{mod}-1}\, dt. \end{aligned} \tag{7.40}$$

Then the probability of the PAPR exceeding a threshold (CCDF) can be written as follow

$$CCDF = 1 - f(PAPR \leq x), \tag{7.41}$$

where

$$f(PAPR \leq x) = F(x)^N. \tag{7.42}$$

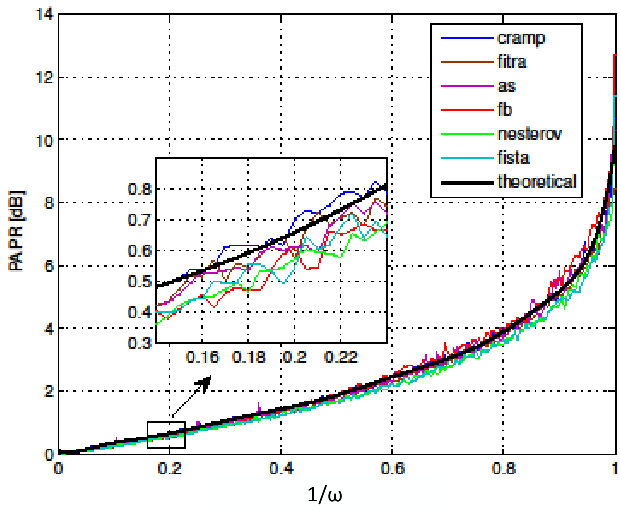

Figure 7.15: ω vs PAPR

Figure 7.15 and 7.16 shows the PAPR performance depending ω and the empirical CCDF with theoretical results according to proposed pdf (eq. (7.36)). It can be seen that well defined anti-sparse prior will let us have an more accurate PAPR performance analysis.

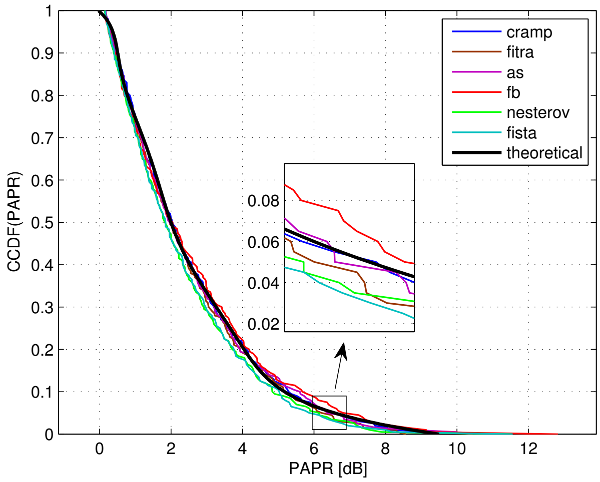

Figure 7.16: PAPR vs CCDF

In this subchapter, main proximal splitting algorithms are deployed for ℓ_∞-norm minimization. Stochastic model of anti-sparsity is investigated with the empirical results of proximal methods and already existing ℓ_∞-norm minimization methods. Based on empirical observations, a reliable and flexible prior is introduced to model anti-sparsity. Effect of the anti-sparse prior on dynamic range reduction is investigated.

7.3 Nuclear Norm Minimization

In this subchapter, Nuclear norm minimization, i.e. trace minimization, is studied and an iterative algorithm for the *Euclidean distance matrix completion* (EDMC) problem with noisy and incomplete distance measurements is introduced by using the approach presented in Chapter 5. An abstract EDMC problem is depicted in Figure 7.17. The proposed method is based on *semidefinite programming* (SDP) and combines the Pareto approach with a projection-free convex optimization over the spectrahedron that is formulated as a level-set problem. The optimality trade-off between the trace of a positive semidefinite matrix and a loss function is traced with Regula Falsi-type nonlinear equation root finding iterations since they are simple, derivative-free, costly efficient and offer convergence guarantee with the proper choices of the root searching interval: two initial points with the opposite signs assures convergence [DB03].

In EDMC applications different incidences cause noises with many variety of distributions. One of the high likely noise models to occur in EDMC problems is the heavy-tailed ones, e.g. the distance error in wireless sensor network localization is expected to be lognormal [BVK15; VKS15; Vur14], weibull [Bit09] or similar. Thus, in

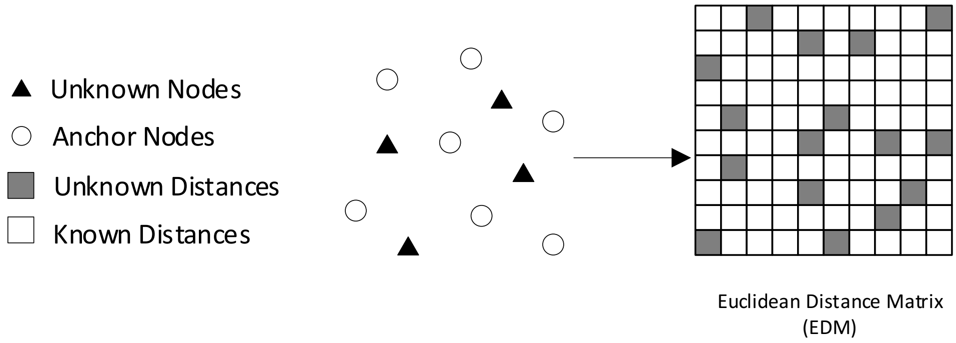

Figure 7.17: An abstract EDMC problem.

various papers it is investigated to complete an *Euclidean distance matrix* (EDM) with the loss functions like absolute value, Huber and pseudo-Huber losses which are more robust against heavy-tailed noises [EG16; CA16; EM19; SGS11]. In order to inspect the performance of the proposed algorithm, two loss functions are used to measure the data misfit that are least-squares and Huber which is less sensitive to heavy-tailed noise.

Two test setups are established to inspect the performance of the introduced algorithm. First one is created using real signal strength data obtained from sensors for *wireless sensor network* (WSN) 3D-localization problem. For the second tests, a dataset that comprises of the repesentive cartesian coordinates of 128 cities in North America is downloaded from [Bur09] and utilized. Coordinates are used to create a distance matrix. Both of the setups are suitable for EDMC problem.

7.3.1 Euclidean Distance Matrix Completion Problem

An EDM is a matrix that comprises of the squared distances between points in a set. Distance matrices like EDMs have been receiving increasing interest during the past decade in numerous fields since they intrinsically arise when describing pairwise geometric relationships. Especially after the developments in machine learning and statistics, EDMs have become an important tool in e.g. genetics, biochemistry, ecomomics, geography, pyschology and signal processing etc. Although they are not oftenly exploited in signal processing, with the production of low-cost sensors EDMs gained an increased attention for the applications such wireless sensor network localization [Din+10]. EDMs first appeared in [Sch35], [YH38], a comprehensive literature review can be found in [Dok+15] and references therein.

Most of the problems that involve EDMs seek to reconstruct a point set from noisy and/or incomplete distance information, i.e. an incomplete EDM. As an alternative approach to geometric methods, e.g. triangularization, a semidefinite programming (SDP) method is developed in [AKW99] to deal with completing the EDM, i.e. to solve the EDMC problem. Several SDP formulations are investigated to provide solutions for different application requirements. An important necessity of EDMC problems is to constrain the penalty that measures the data misfit between the estimated and correct data points since many EDMC problems involve noisy distance measurements. SDP formulation of EDMC problems with noisy and/or incomplete distance information are investigated in [Bis+06a; Bis+06b; Dru+17] with the application of wireless sensor network localization.

7.3.2 Euclidean Distance Matrices

In the EDMC problem, the spatial distances between sensor nodes are expressed as a matrix called EDM. The EDM comprises of the squares of distances between the sensor locations. Let us consider the points $\mathbf{p}_1, ..., \mathbf{p}_n \in \mathbb{R}^r$, and a vertex set $\mathcal{V} = \{1, \ldots, n\}$ where $r = 3$ for the 3D-problem formulation. The elements of the EDM $\mathbf{D} \in \mathbb{R}^{n\times n}$ can be written for all known edges $(ij) \in \Theta \subseteq \mathcal{V} \times \mathcal{V}$ as

$$\mathrm{D}_{ij} = \mathbf{p}_i^T \mathbf{p}_i + \mathbf{p}_j^T \mathbf{p}_j - 2\mathbf{p}_i^T \mathbf{p}_j = \|\mathbf{p}_i - \mathbf{p}_j\|_2^2 \tag{7.43}$$

Every EDM is a nonnegative symmetric matrix with zeros on the diagonal. The EDM can be rewritten with the Gram matrix $\mathbf{X} := (\mathbf{p}_i^T \mathbf{p}_j)_{i,j=1}^n = \mathbf{P}\mathbf{P}^T$ where the rows of $\mathbf{P} \in \mathbb{R}^{n\times r}$ are the transpose of $\mathbf{p}_1, \ldots, \mathbf{p}_n$. The EDM then takes the form

$$\mathrm{D}_{ij} = \langle \mathbf{\Phi}_{ij}, \mathbf{X} \rangle := \mathrm{tr}(\mathbf{\Phi}_{ij}^T \mathbf{X}), \tag{7.44}$$

where $\mathbf{\Phi}_{ij} := (\mathbf{e}_i - \mathbf{e}_j)(\mathbf{e}_i - \mathbf{e}_j)^T$, and $\mathbf{e}_i$ and $\mathbf{e}_j$ are n dimensional i-th and j-th unit vectors respectively [Dat10].

An EDM can also be represented with a linear transformation. One of the most practical and commonly used one is applied at [Dat10], defined as

$$\mathcal{K}(\mathbf{X})_{ij} := \mathbf{X}_{ii} + \mathbf{X}_{jj} - 2\mathbf{X}_{ij}, \tag{7.45}$$

leads $\mathrm{D} = \mathcal{K}(\mathbf{X})$ and the adjoint of the linear transformation $\mathcal{K}$ is given

$$\mathcal{K}^*(\mathbf{X}) = 2\left(\mathrm{Diag}(\mathbf{X}\mathbf{1}) - \mathbf{X}\right), \tag{7.46}$$

satisfies $\langle \mathcal{K}(\mathbf{X}), \mathbf{Y} \rangle = \langle \mathbf{Y}, \mathcal{K}^*(\mathbf{X}) \rangle$, $\forall \mathbf{X}, \mathbf{Y}$ where $\mathbf{1}$ represents the vector of ones, $\mathrm{Diag}(\mathbf{X}\mathbf{1})$ is the column vector of the diagonal entries of $\mathbf{X}\mathbf{1}$, and the pseudoinverse of $\mathcal{K}$ is written as

$$\mathcal{K}^\dagger(\mathbf{X}) = -\frac{1}{2}\mathbf{J}\mathbf{X}\mathbf{J}, \tag{7.47}$$

where $\mathbf{J} := \mathbf{I} - \frac{1}{n}\mathbf{1}\mathbf{1}^T$ and $\mathbf{I}$ is the identity matrix [Dat10; KW].

7.3.3 Low-Rank Matrix Completion Problem Formulation with Incomplete and Noisy Distance Measurements

There has been several SDP formulations introduced for low-rank matrix completion from incomplete distance measurements. In this thesis, the following problem is considered:

$$
\begin{aligned}
(\mathrm{P}_\sigma) \qquad \min_{\mathbf{X}} \; \operatorname{tr}(\mathbf{X}) \;\; \text{s.t} \sum_{(i,j)\in\Theta} \rho\left(\mathbf{W}_{ij}\cdot(\langle\Phi_{ij},\mathbf{X}\rangle - \mathrm{D}_{ij})\right) &\le \sigma,\\
\mathbf{X}\mathbf{1} &= 0,\\
\mathbf{X} &\succcurlyeq 0,
\end{aligned}
$$

where σ is the noise level on the distance measurements, $\operatorname{tr}(.)$ denotes the trace and $\mathbf{W}$ is the mask matrix with zeros for the incomplete entries. Solving (P_σ) promotes low rank solutions since minimizing $\operatorname{tr}(\mathbf{X})$ implies to minimize the sum of eigenvalues the eigenvalues of positive semidefinite $\mathbf{X}$.

(P_σ) is useful in applications where the obtained data contains noise and if a prior information about the noise level is available. However, solving (P_σ) can be challenging since its feasible area is still complicated. Therefore, the Pareto optimality concept is used where one can obtain the solution of (P_σ) efficiently, i.e., under computational limitations (on low-cost hardware) by solving a couple of times an another relatively easier problem.

7.3.3.1 Pareto Optimality

Let us look at the following problem

$$
(\mathrm{P}_\tau) \qquad \min_{\mathbf{X}\in\tau\mathbb{S}} \sum_{(i,j)\in\Theta} \rho\left(\mathbf{W}_{ij}\cdot(\langle\Phi_{ij},\mathbf{X}\rangle - \mathrm{D}_{ij})\right),
$$

where $\mathbb{S} := \{\mathbf{X} \succcurlyeq 0, \operatorname{tr}(\mathbf{X}) = 1, \mathbf{X}\mathbf{1} = 0\}$ is the set of positive semidefinite matrices with unit trace and occasionally called *spectrahedron*. Although it is difficult to find a closed form expression between the parameters of (P_τ) and (P_σ) that provide the same solutions of (P_τ) and (P_σ), it can be shown that a solution of (P_τ) is also a solution of (P_σ) with Pareto frontiers [FR13].

Let us write the following optimal objective value of the (P_τ) for a given τ and $\mathbf{D}$,

$$
\nu(\tau) := \inf_{\mathbf{X}}\{\sum_{(i,j)\in\Theta} \rho\left(\mathbf{W}_{ij}\cdot(\langle\Phi_{ij},\mathbf{X}\rangle - \mathrm{D}_{ij})\right) \mid \mathbf{X}\in\tau\mathbb{S}\}, \tag{7.48}
$$

and the corresponding Pareto frontier[2] can be defined as

$$\psi(\tau) := \nu(\tau) - \sigma. \tag{7.49}$$

Obtaining the solution of (P_σ) by solving (P_τ) proceeds as follows. We start with a τ parameter to solve (P_τ), and using the solution of (P_τ), find a new τ value. We proceed iteratively until τ_σ which leads $\psi(\tau_\sigma) \to 0$. We immediately see that the solution of (P_τ) is also a solution of the (P_σ). Finding τ_σ can be formulated as a nonlinear root finding problem.

For the purpose of solving (P_σ), our aim is to

$$\text{find} \quad \tau \quad \text{such that} \quad \psi(\tau) = 0. \tag{7.50}$$

To solve (7.50), we employ Regula Falsi-type methods given in Section 5.3.2.2. Pareto frontier approaches use root finding and inexact solutions to a sequence of (P_τ) to solve (P_σ).

7.3.3.2 Solving ($\mathbf{P}_\tau$)

In order to solve (P_τ) efficiently, a projection-free first order method, also called *Hazan's Algorithm* [Haz08], [GM12] and given in Algorithm 3, is employed. The geometry of the feasible set of (P_τ) is uncomplicated [Pla] and solving (P_τ) only requires a maximal eigenvalue calculation of the gradient matrix of the loss function which can be simply done by Lanczos' or the Power method.

Algorithm 6 Projection-free Convex Optimization over the Spectrahedron to Solve (P_τ)

Input: τ, C_f, ζ_1

```
repeat
    for k = 1, ... do
        γ_k = 2/(k+1)
        ε_k = γ_k C_f / τ
        ν_k = ApproxEV(−∇f(X_k), ε_k)
        X_{k+1} = X_k + γ_k(τ ν_k ν_k^T − X_k)
    end for
until g_τ ≤ ζ_1
```

where $f(\mathbf{X}_k) = \sum_{(i,j)\in\Theta} \rho\left(\mathbf{W}_{ij} \cdot (\langle \Phi_{ij}, \mathbf{X}\rangle - \mathrm{D}_{ij})\right)$.
Output: $\mathbf{X}_\tau = \arg\min$ (P_τ).

In Algorithm 6, ApproxEV($\mathbf{A}, \epsilon$) returns an approximate largest eigenvector to the matrix $\mathbf{A}$ with the accuracy ϵ, in order words a unit length vector $\mathbf{v}$ such that $\mathbf{v}^T\mathbf{A}\mathbf{v} \geq \lambda_{\max}(\mathbf{A}) - \epsilon$. C_f is called the *curvature constant* which is used to measure

[2] *Pareto optimal* is the the minimal achievable feasible point of a feasible set. The set that comprised of Pareto optimal points is called *Pareto frontier*.

the deviation of the function $f(\mathbf{X})$ from its linear approximation and given as

$$C_f := \sup_{\substack{\mathbf{X},\mathbf{V}\in\mathcal{S},\gamma\in[0,1],\\ \mathbf{Y}=\mathbf{X}+\gamma(\mathbf{V}-\mathbf{X})}} \frac{1}{\gamma^2}\left(f(\mathbf{Y}) - f(\mathbf{X}) + \langle \mathbf{Y}-\mathbf{X}, \nabla f(\mathbf{X})\rangle\right) \tag{7.51}$$

C_f values for several exemplary classes could be found in [Cla10].

Algorithm 6, performs a linear optimization over the constraint set and most oftenly enforces a duality gap as a stopping condition which is given in [Lau12] such

$$g_\tau := \max_{\mathbf{Y}\in\tau\mathbb{S}} \langle \mathbf{X}-\mathbf{Y}, \nabla f\,(\mathbf{X})\rangle = \tau\lambda_{\max}(-\nabla f\,(\mathbf{X})) + \langle \mathbf{X}, \nabla f\,(\mathbf{X})\rangle. \tag{7.52}$$

7.3.3.3 Solving ($\mathbf{P}_\sigma$)

The Regula falsi-type methods and Algorithm 6 can be combined to to solve (P_σ) as follows:

- Choose initial τ values.

  Choose two initial values with opposite signs to ensure convergence of Regula falsi-type methods, i.e. bracket the root.

- Apply the steps of the Regula Falsi-type methods.

  Every iteration of the Regula falsi-type methods requires solving (P_τ).

- Terminate once the stopping criteria are met.

7.3.3.4 Bracketing the Root

Most classes of the loss functions are nonnegative and vanish at the origin such as gauges as well as the one that is considered in this study. For these kind of losses linear inverse mappings can be useful since for an observed measurement that will be $\mathcal{K}^\dagger(\mathbf{D}) - \mathbf{D} = 0$, i.e. $\psi(\tau) = -\sigma$. At the point $\tau = 0$, $\psi(\tau = 0)$ is positive since unless $\mathbf{W}\circ\mathbf{D} \neq \mathbf{0}$, thus finding another point where ψ is negative guarantees convergence by bracketing the root. $\mathcal{K}^\dagger(\mathbf{D})$ provides negative ψ for the aforementioned losses.

7.3.3.5 Loss Functions and the Gradient

Huber and least-squares losses are employed to solve (P_σ). While *least-squares* is the most commonly used loss function in numerous optimziation problems, *Huber* loss is less sensitive to outliers in the data than *least-squares.* Especially if the error distribution is expected to be heavy-tailed, *Huber* loss could be a more proper choice to calculate the error. *Huber* and *least-squares* losses are

$$\rho_H(x) = \begin{cases} \frac{x^2}{2\delta}, & \text{if } \ |x| \leq \delta \\ |x| - \frac{\delta}{2}, & \text{otherwise} \end{cases}, \tag{7.53}$$

and $\rho_L(x) = |x|^2$ respectively. δ is the tuning parameter of the *Huber* loss and depends on the distribution of the error [EG+18]. The derivative of ρ_H is

$$\rho'_H(x) = \begin{cases} \frac{x}{\delta}, & \text{if } |x| \leq \delta \\ \text{sign}(x), & \text{otherwise} \end{cases} \tag{7.54}$$

Let us rewrite the loss function f entry-wise such that $f(\mathbf{X}) = \sum_{(i,j)\in\omega} \rho\left(\langle \Phi_{ij}, \mathbf{X}\rangle - \mathrm{D}_{ij}\right)$. Then the gradient of f with respect to $\mathbf{X}$ will be

$$\nabla f(\mathbf{X}) = \sum_{(i,j)\in\Theta} \Phi_{ij}^T \rho'\left(\langle \Phi_{ij}, \mathbf{X}\rangle - \mathrm{D}_{ij}\right) \tag{7.55}$$

Let f be least squares, i.e. $f(\mathbf{X}) = \sum_{(i,j)\in\Theta} |\mathbf{W}_{ij} \cdot (\langle \Phi_{ij}, \mathbf{X}\rangle - \mathrm{D}_{ij})|^2 = \|\mathbf{W} \circ (\mathcal{K}(\mathbf{X}) - \mathbf{D})\|_2$, then the gradient of f with respect to $\mathbf{X}$ can simply be written in terms of the linear transformation $\mathcal{K}$ as

$$\nabla f(\mathbf{X}) = \mathbf{W}^* \circ \mathcal{K}^*(\mathbf{W} \circ (\mathcal{K}(\mathbf{X}) - \mathbf{D})). \tag{7.56}$$

7.3.3.6 Reconstruction Points From the Gram Matrix

Solving (P_σ) provides a Gram matrix $\mathbf{X}$ that yields an EDM fulfilling the optimization problem constraints. Numerous approaches have been introduced to reconstruct the points from a Gram matrix. If all distances are measured, there is a simple and efficient algorithm called *multidimensional scaling* (MDS) [Tor65] that finds the configuration of nodes exactly. The following two steps have to be carried out to find the configuration of points with MDS:

- Calculate the Gram matrix $\mathbf{X}$ for a given EDM $\mathbf{D} \in \mathbb{R}^{n\times n}$.

  That step can be performed such that $\mathbf{X} = \mathcal{K}^\dagger(\mathbf{D})$.

- Execute eigendecomposition for the matrix $\mathbf{X}$.

  The rows of $\mathbf{Y} = \mathbf{V}_r \Lambda_r^{1/2}$ are the relative coordinates of nodes where $\Lambda_r = \mathrm{Diag}(\lambda_1 \ldots, \lambda_r) \in \mathbb{R}^{r\times r}$ is the matrix that comprises the λ_is on the diagonal which are ith largest eigenvalues and $\mathbf{V}_r = (v_1, \ldots, v_r) \in \mathbb{R}^{n\times r}$ is the matrix contains the corresponding eigenvectors. In other words, every point $p_i \in \mathbb{R}^r$ is mapped to the ith row of $\mathbf{Y}$.

EDMs are invariant under rigid transformation (including translations, rotations, reflections) [FO12] and MDS gives us a point configuration that we therefore call relative points which is equal to absolute points up to a rigid transformation. Estimating the absolute points is not possible without additional information.

In many applications there are therefore some known points that can provide the link between the absolute and relative point set. This points are called terminal points

Table 7.8: Iteration complexity.

CVX	$\mathcal{O}\left(n^6\right)$
Proposed Algorithm (with Lanczos Method)	$\mathcal{O}\left(\text{nnz}(\nabla\rho) \times \sqrt{\|\nabla\rho\|_2} \times \min\{\epsilon^{-1/2}, \log(1/\epsilon)/\chi^{1/2}\}\right)$
Proposed Algorithm (with Power Method)	$\mathcal{O}\left(\text{nnz}(\nabla\rho) \times \sqrt{\|\nabla\rho\|_2} \times \min\{\epsilon^{-1}, \log(1/\epsilon)/\chi^{1/2}\}\right)$

or anchor points in the nomenclature of sensor network localization problems. It is possible to align the relative point set with the set of anchors since their coordinates are known and fixed. This alignment can be done with the *orthogonal procrustes analysis*.

7.3.3.7 Orthogonal Procrustes Problem

Orthogonal procrustes analysis is an approximation problem that looks for an orthogonal matrix $\mathbf{O}$ which closely maps given two matrices. Consider $\mathbf{A}$, $\mathbf{B}$ are centered at the origin, orthogonal procrustes problem seeks best maps $\mathbf{A}$ onto $\mathbf{B}$ by

$$\underset{\mathbf{O}:\mathbf{O}\mathbf{O}^T=\mathbf{I}}{\arg\min} \;\; \|\mathbf{O}\mathbf{A}-\mathbf{B}\|_F^2 \,. \tag{7.57}$$

Eq. (7.57) evaluates the squared distances of the points in $\mathbf{B}$ and corresponding points in $\mathbf{OA}$. The optimal $\mathbf{O}$ can be computed by the singular value decomposition of $\mathbf{A}\mathbf{B}^T$, for details one can check [Sch64b; BG07; Dok+15].

In the applications where anchors exist, their points can be aligned with the relative points that are obtained from MDS. After finding the optimal $\mathbf{O}$, the alignment can be applied to the whole relative point set.

Iteration complexity of the introduced algorithm is given in Table 7.8 and reached from [Gar16; All+17] where nnz denotes the number of nonzeo entries, ϵ is the target accuracy, χ is the difference between the two smallest eigenvalues of the gradient. Comparing to the CVX [Van+05] which is an off-the-shelf solver and uses interior point method to solve the SDP, introduced approach quite beneficial, especially in large dimensions.

7.3.3.8 Test Setup 1: Wireless Sensor Network Localization

In this subchapter, so far, an approach for the matrix completion problem is proposed with the instructions of how one can find the coordinates of a given distance matrix.

In order to test the introduced algorithm, we created a test setup and conducted several experiments for WSN localization. We utilized 25 sensors of [Gro]. Most of them placed in a building which has cellar + 6 floors and is approximately 150 years old with solid brick walls, while couple of them are distributed in the surrounding buildings. Positions of the sensors are shown in Figure 7.18. Sensors operated at an

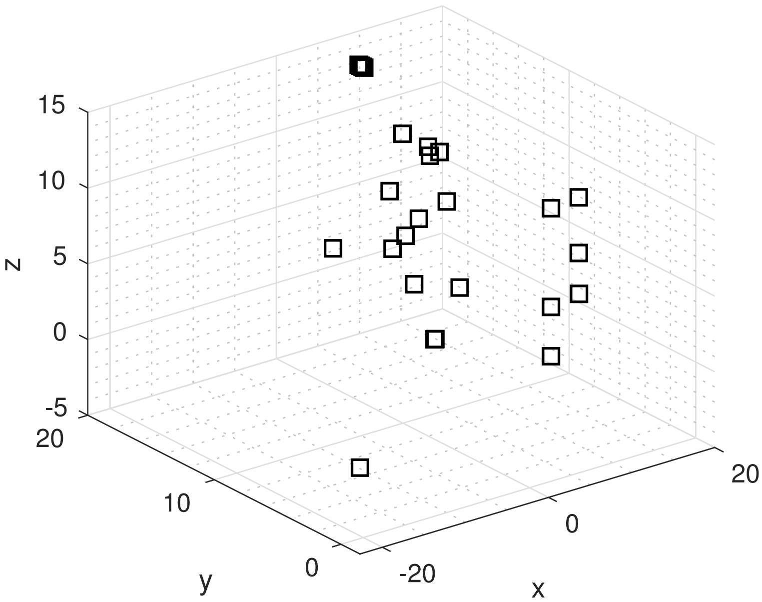

Figure 7.18: Sensor locations

ISM band, 896 MHz at 0.5 watt. We measured the *received signal strengths* (RSS) values.

7.3.3.9 RSS and Propogation Model

There are several approaches to localize wireless devices [MFA07]. One of the most common one is based on the RSS values. Conventionally, RSS of a communication system is modeled with the log-distance path loss radio propagation model which is defined in decibel (dB) scale for a given distance according to following

$$\mathbf{r} = P_T - 10n\log_{10}(d) + \mathcal{X}_g \quad [\text{dB}] \tag{7.58}$$

where n is the path loss exponent, P_T is the transmit power, d is the distance between transmit and receiver and $\mathcal{X}_g$ is the shadow fading term which is an empirically justified normal distributed random variable with zero mean [Rap01], i.e. it is a lognormal random variable in linear scale.

Scatter plot of the 267340 measurements and the histogram of the shawoding is depicted in Figure 7.19a and in Figure 7.19b respectively. The histogram of the distance error corresponding to the path loss model given in (7.58) is also plotted in Figure 7.19c which follows a lognormal distribution as expected.

In our experiments, the matrix that comprises of the mean RSS values between sensor pairs is incomplete. Because some radio links are either noisy, erroneous or weak etc., therefore some sensors could not get the signal. So, by using any path loss

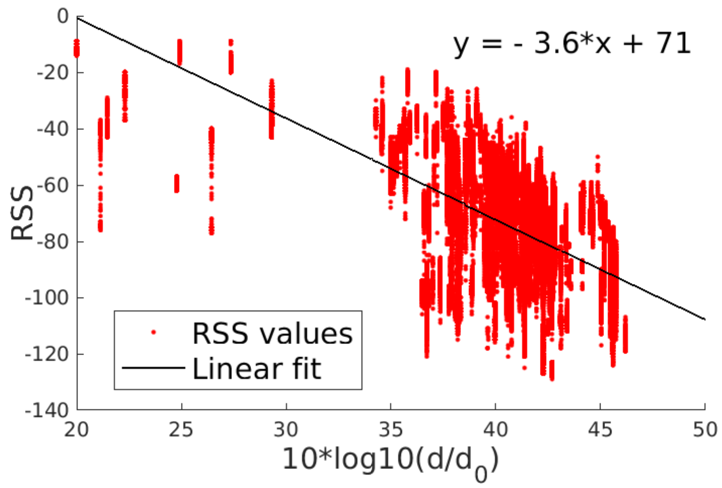

(a) Scatter plot of the 267340 measurements.

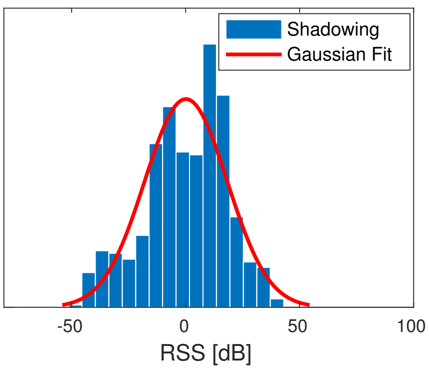

(b) Histogram of the shadowing.

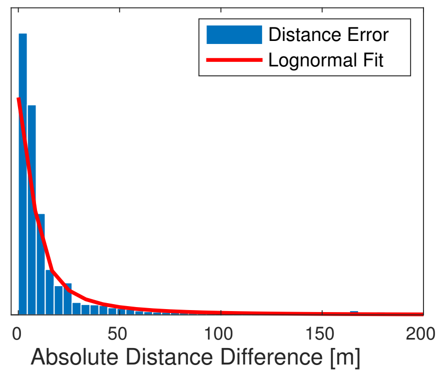

(c) Histogram of the distance error.

Figure 7.19: Measurement characteristics.

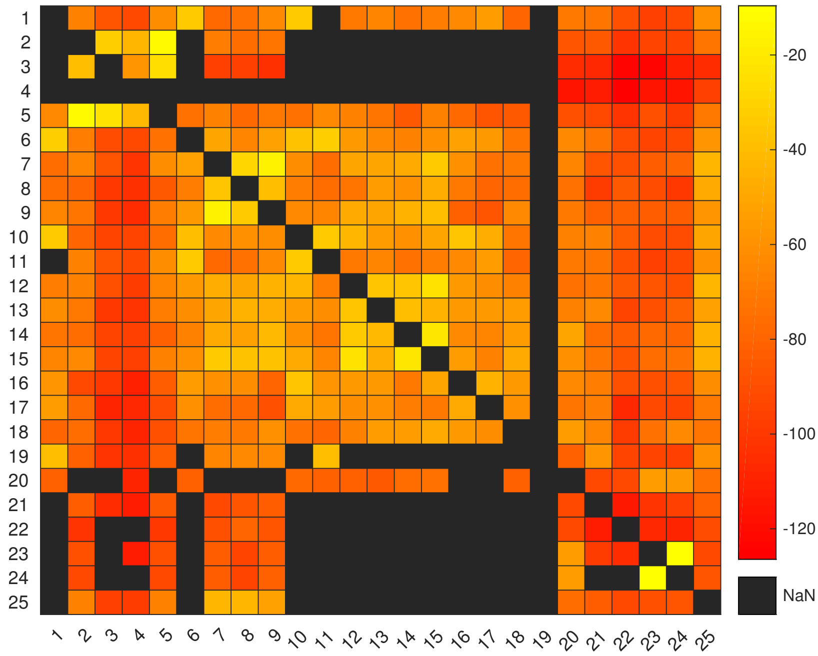

Figure 7.20: Partial mean RSS distance matrix.

model or any other method that helps to find distances are obsolete because it is not possible to construct an EDM using only RSS values since they are incomplete. The motivation is to fill the gaps in the EDM.

The partial mean RSS distance matrix is depicted in Figure 7.20. It is a dense matrix, to make it more sparse, we randomly blocked some distance information and created two more test scenarios as well. In the Scenario 1, we used the distance map which we have from the experiments. Scenarios are shown in Figure 7.21. Density of the scenarios are 0.7296, 0.3648 and 0.2144 for the Scenario 1, 2 and 3 respectively which is calculated by following formula

$$Density = \frac{number\ of\ non-missing\ entries}{number\ of\ all\ entries}. \tag{7.59}$$

7.3.3.10 Simulations

For every scenario (Scenario 1, 2 and 3), there is an incomplete EDM with different densities. (P_σ) is solved to find the missing entries and complete them. Here, only raw Regula falsi method is employed to solve (7.50), i.e. $\mu = 1$ is taken from the Table 5.2. Huber loss with $\delta = 0.001$ is utilized as a penalty function ρ with the parameter delta to better address the heavy-tailed character of distance estimations can be obtained by RSS values. σ is chosen as $\sigma = n \times n \times \alpha$ (reminding that n is the sensor number).

Solving (P_σ) gives a Gram matrix $\mathbf{X}$ that yields an EDM that satisfies the optimization problem requirements. Relative coordinates of the sensors are reconstructed

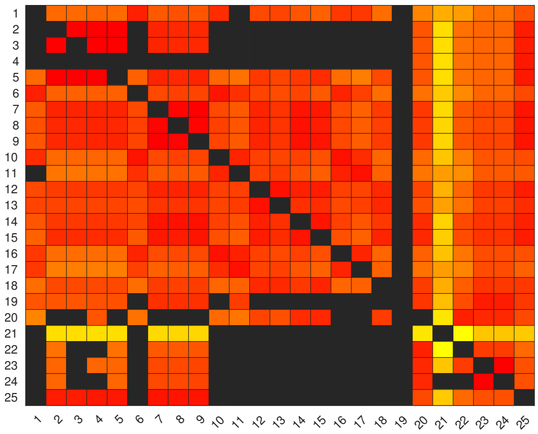

(a) Scenario 1.

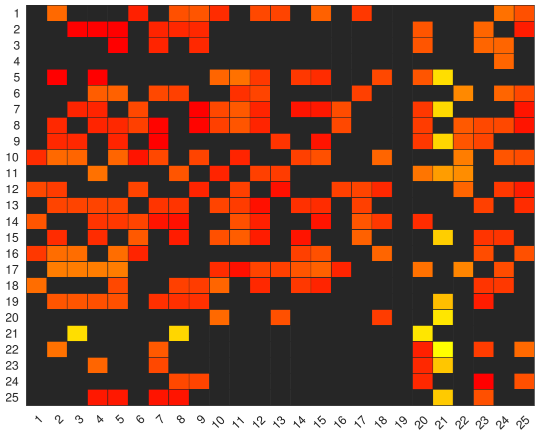

(b) Scenario 2.

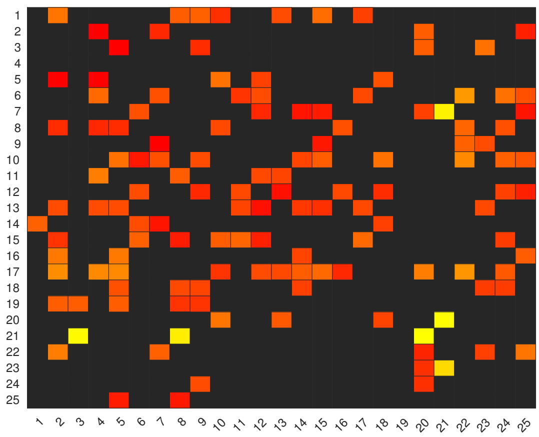

(c) Scenario 3.

Figure 7.21: Test scenarios.

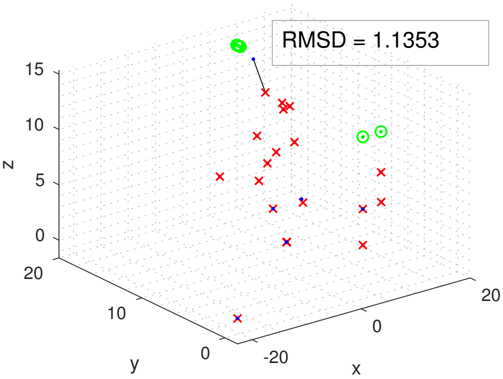

(a) $\alpha = 0.1$, $\sigma = 62.5$

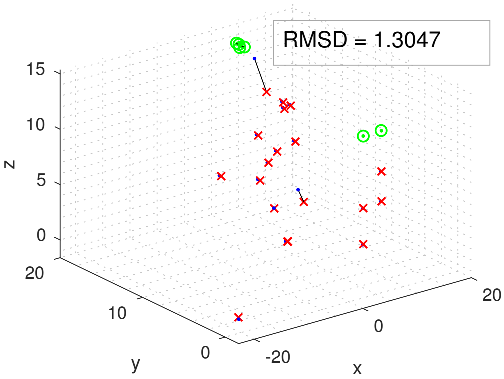

(b) $\alpha = 1$, $\sigma = 625$

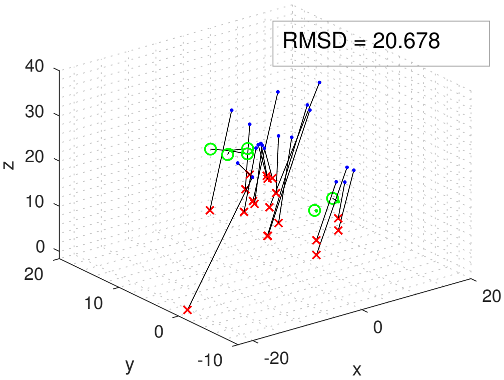

(c) $\alpha = 10$, $\sigma = 6250$

Figure 7.22: Localization results for the Scenario 1. Green dots represent the anchor points, green circle shows the anchor point alignment, red x shows the real points while black dots are used for the corresponding estimated points.

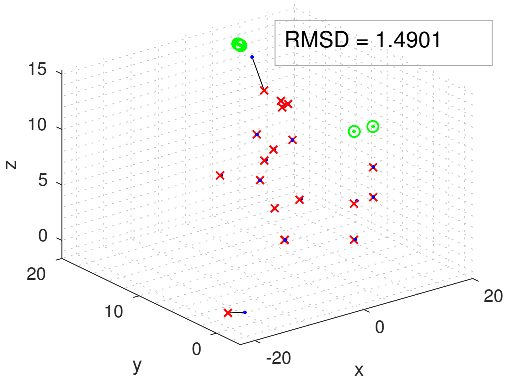

(a) $\alpha = 0.1$, $\sigma = 62.5$

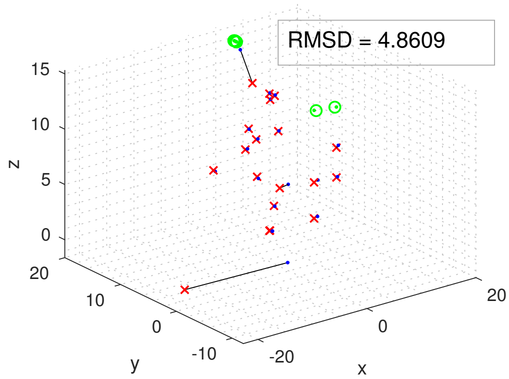

(b) $\alpha = 1$, $\sigma = 625$

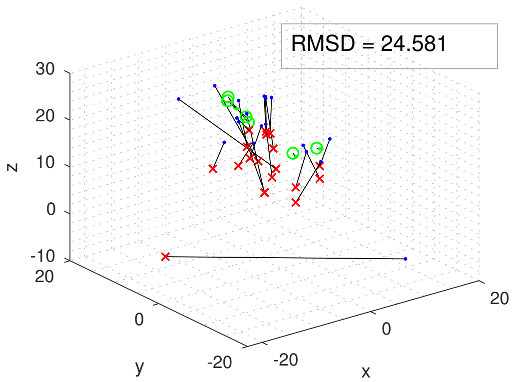

(c) $\alpha = 10$, $\sigma = 6250$

Figure 7.23: Localization results for the Scenario 2. Green dots represent the anchor points, green circle shows the anchor point alignment, red x shows the real points while black dots are used for the corresponding estimated points.

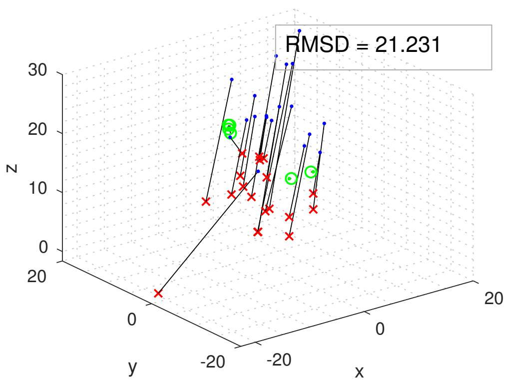

(a) $\alpha = 0.1$, $\sigma = 62.5$

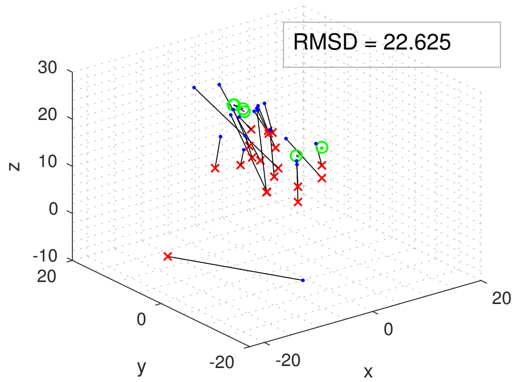

(b) $\alpha = 1$, $\sigma = 625$

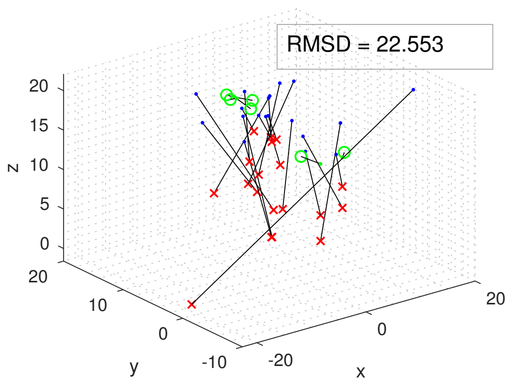

(c) $\alpha = 10$, $\sigma = 6250$

Figure 7.24: Localization results for the Scenario 1. Green dots represent the anchor points, green circle shows the anchor point alignment, red x shows the real points while black dots are used for the corresponding estimated points.

with using the MDS. 6 anchor points are assigned and the alignment between the real and relative coordinates are performed with the Orthogonal procrustes analysis given in Section 7.3.3.7. *root mean square deviation* (RMSD) between the estimated point coordinates and their real coordinates is calculated.

$$\text{RMSD} = \sqrt{\frac{\sum_{i=1}^{n} (p_i - \hat{p}_i)^2}{n}} \quad [m] \tag{7.60}$$

We used 3 alfa values such as $0.1, 1$ and 10 to indicate low, medium and high noise tolerances. Localization results for the Scenario 1, 2 and 3 are shown in Figure 7.22, 7.23 and 7.24 respectively.

Results are consistent to CVX [GB14].

7.3.3.11 Test Setup 2: Graph Realization Perspective

Approximating the missing edges of a given graph is often equivalent of completing an EDM. Algorithm 7 is presented to generate random graph instances for the EDMC problems with noisy and incomplete distance measurements. A multiplicative noise model comprising a Gaussian random variable with the zero mean and variance of 1, $\mathcal{N}(0,1)$, is employed to perturb the distance matrix as it is done in [Bis+06a; Bis+06b; Dru+17].

Algorithm 7 Graph construction, the noise model and the mask matrix

Input: kn and $(1-k)n$ as the number of terminal points (anchors) and other points respectively with $0 \leq k \leq 1$, noise factor α, radio range R

Generate nodes

- Generate n uniformly distributed nodes $p_i \in \mathbb{R}^r$,

Perturb the distance matrix

$$\hat{\mathbf{D}}_{ij} = \begin{cases} (1 + \alpha\mathcal{N}(0,1))^2 \left\|p_i - p_j\right\|_2^2, \text{if } \max\{i,j\} \leq kn \\ \left\|p_i - p_j\right\|_2^2, \quad \text{otherwise} \end{cases},$$

Build a graph

- Form the graph $\mathcal{G} = (\{1, \ldots, n\}, \mathcal{E})$ where

$$\mathcal{E} = \{ij : \left\|p_i - p_j\right\|_2 < R \ \text{ or } \ \max\{i,j\} \leq kn\},$$

Generate the mask matrix W

$$\mathbf{W}_{ij} := \begin{cases} 1, & \text{if } ij \in \mathcal{E} \\ 0, & \text{otherwise} \end{cases}$$

In order to create a suitable test setup, we utilized a dataset which comprises of the representative cartesian coordinates of 128 cities in North America that is created in [Knu09] and can be downloaded from [Bur09]. The positions of the cities are shown in

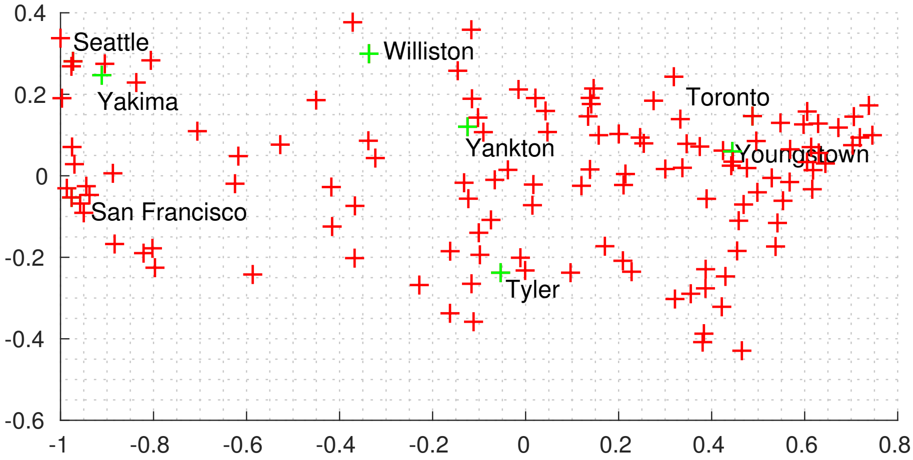

Figure 7.25: Position of the cities.

Figure 7.25. The distance matrix of the points is perturbed with the Algorithm 7 with $k = 1/16$, i.e. 8 of the 128 points are considered to be terminal points. (P_σ) is solved with several R, α and σ values where σ chosen as $\sigma = ||\mathbf{W} \circ (\hat{\mathbf{D}} - \mathbf{D})||_2$. R and α values create graphs with various densities and the density of a graph is formulated as density $:= \frac{\text{number of edges}}{0.5n(n-1)}$ where n is the number of points. After solving (P_σ), relative points are reconstructed with MDS. Then the relative point set is aligned with the the terminal points via *orthogonal procrustes analysis*. The average density, σ and RMSD between the estimated point coordinates and their real coordinates, over 100 instances are given in Table 7.9. *iter* is the total solves of (P_τ) to reach the solution of (P_σ).

An instance of a constructed graph for $\alpha = 0.001$ and $R = 0.05$ with $k = 1/16, n = 128$ is depicted in Fig. 7.26a. Blue and red lines represent the noisy and noiseless edges respectively and green dots stand for the terminals. In Fig. 7.26b, estimated points are shown for the corresponding graph. Green dots represent the terminal points, green circles show the anchor point alignment, red x shows the real points while black dots are used for the corresponding estimated points.

In this subchapter, an algorithm for the EDMC problem with noisy and incomplete distance measurements is introduced. The algorithm efficiently solves the optimization problem and the results are consistent to generic but less efficient semidefinite solvers like CVX. Although not being in the focus of this thesis, our approach does not require differentiable loss functions, which opens new possibilities for future research questions and guarantees finding a solution since we use bracketing-type root finding approaches.

Table 7.9: Simulation results for solving (P_σ).

α	R	density	σ	method	RMSD	iter
0.005	0.05	0.1409	0.0027	Regula Falsi	0.8632	3
				Illinois	0.8632	3
				Pegasus	0.8632	3
				Anderson-Björk	0.8632	3
	0.1	0.2323	0.0066	Regula Falsi	0.8669	3
				Illinois	0.8669	3
				Pegasus	0.8669	3
				Anderson-Björk	0.8669	3
	0.5	0.6158	0.0429	Regula Falsi	0.7977	3
				Illinois	0.7977	3
				Pegasus	0.7977	3
				Anderson-Björk	0.7977	3
0.05	0.05	0.1411	0.0296	Regula Falsi	0.8629	3
				Illinois	0.8629	3
				Pegasus	0.8629	3
				Anderson-Björk	0.8629	3
	0.1	0.2327	0.0702	Regula Falsi	0.8674	3
				Illinois	0.8674	3
				Pegasus	0.8674	3
				Anderson-Björk	0.8674	3
	0.5	0.6154	0.4443	Regula Falsi	2.8561	4
				Illinois	2.8561	3.53
				Pegasus	2.8561	3.43
				Anderson-Björk	2.8561	3.53
0.5	0.05	0.2282	6.32	Regula Falsi	13.37	9.1667
				Illinois	13.32	6.5833
				Pegasus	13.32	5.9167
				Anderson-Björk	13.33	6.75
	0.1	0.3232	8.2173	Regula Falsi	5.98	8.6667
				Illinois	6.03	6.11
				Pegasus	6.03	6
				Anderson-Björk	6.03	6.08
	0.5	0.6375	15.501	Regula Falsi	2.163	16.25
				Illinois	2.162	7.875
				Pegasus	2.16	7
				Anderson-Björk	2.16	8.125

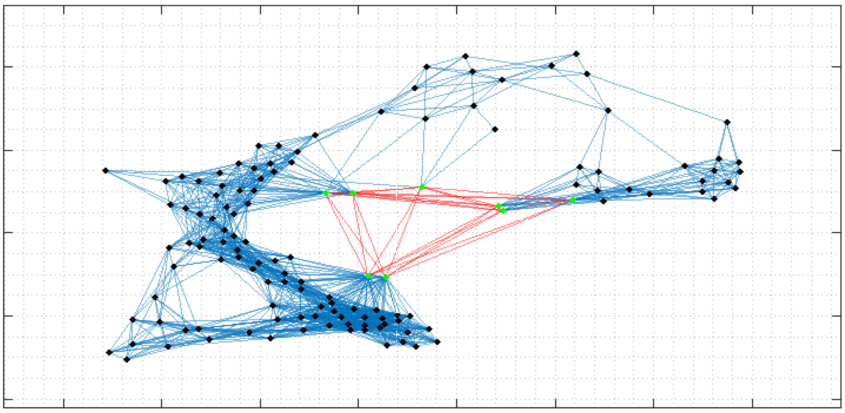

(a) A graph for $\alpha = 0.001, R = 0.05$ with the density 0.141.

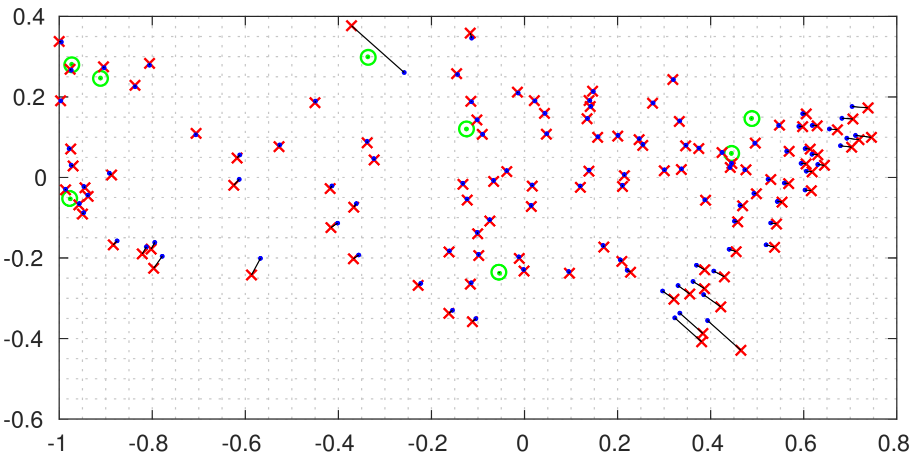

(b) Estimated points.

Figure 7.26: A graph instance and corresponding estimated points.

Chapter 8

Summary and Conclusions

ℓ_p-norm minimization is a noteworthy subject in various disciplines not only for signal recovery but also for finding meaningful signal representations. In this thesis, we introduce noise-constrained ℓ_p-norm minimization structure for $1 \leq p \leq \infty$. Formulating ℓ_p-norm minimization problems by constraining the noise tolerance level is required in many applications since it is easier to constrain the noise level and to establish the optimization problem. However, solving noise-constrained ℓ_p-norm minimization can be challenging and therefore there is a lack of computationally efficient algorithms in the literature. Different formulations of optimization problems can provide equivalent results. Thus, it may be appealing to solve one computationally efficient problem in order to obtain the solution to another. By using this fact, we solved constrained ℓ_p-norm regularization to reach the solution of noise-constrained ℓ_p-norm problem by tracing the optimality between the objective ℓ_p-norm and a loss function. This optimality trade-off between both objectives is formulated as a nonlinear equation root finding problem. To trace this optimality over a Pareto frontier, we present and utilize several simple, derivative-free, and cost-effective open-type and bracketing-type nonlinear equation root finding methods. Each of the existing nonlinear equation root finding methods has their own advantages and disadvantages. The applicability and efficiency of these methods depend on the function. Thus, choosing one of them is function dependent, e.g. bracketing-type methods converge slowly if the function has significant curvature and most open-type methods can be inapplicable if the function is non-differentiable.

Using a warm-start strategy while designing an algorithm might result in costly efficient iterations. Choosing a starting point close to the solution point is desired. In this thesis, we also introduce a warm-start strategy for the ℓ_p-norm minimization problems by using the relation between n-widths and ℓ_p-norms. Effect of the given warm-start strategy and root finding methods for solving noise-constrained ℓ_p-norm minimization, i.e. (P_σ^p), is shown by minimizing ℓ_1 and ℓ_∞-norm in Chapter 6.

Convergence analysis of (P_{σ}^{p}) solvers are given in Chapter 4 by using the matrix properties UUP and UP which are formerly introduced to investigate the performance of random matrices in ℓ_1 and ℓ_∞-norm related applications. Convergence bounds using UUP and UP allow us to understand the performance of the measurement matrix and inspect the quality of them for related recovery or representation methods. In order to derive the convergence bounds, the slope of the Pareto curve is utilized which is bounded by matrix property inequality in Chapter 5.

Some of the root finders presented in this thesis can handle solving ℓ_p-norm minimization problem with nonconvex losses. Nonconvex losses are significantly more difficult to cope with, yet they can outperform their convex counterparts [MBM18]. Considering the loss functions can be more likely to be nonconvex in real world applications [GBC16], moving outside of the convex class is an appealing property. The applicability of nonconvex losses is examined in Chapter 5.4. In this thesis, we show how some root finding methods, e.g. OPR and Regula Falsi type methods like Illinois, Pegasus, Anderson-Björck, can be used with the nonconvex Student's t loss, as well the convex least-squares and Huber losses.

Steps of (P_{σ}^{p}) solvers given in Chapter 6 and results of ℓ_p-norm minimization are applied in Chapter 7. ℓ_1-norm minimization is an important topic for CS. We solved (P_{σ}^{1}) with a typical CS example. Ability to use of nonconvex losses inspired us to develop an outlier-robust approach and for that we illustrated the performance of ℓ_1-norm regularized Student's t inversion. We also examine the ℓ_∞-norm minimization which is relatively less investigated than ℓ_1-norm. We introduce a new communication scheme based on ℓ_∞-norm representations. MOF has already been employed in many applications to obtain an overcomplete representation and robust communication channels with additive noises like quantization noise. Since the warm-start strategy that we introduce is based on MOF, we tried to get some extra gains that MOF already offers. Compared to MOF, ℓ_∞-norm representations are spread evenly, meaning that the representation elements are forced to be equal. We showed that one can use fewer bits with the same MSE budget by using ℓ_∞-norm representation based communication architecture instead of MOF based one. Introduced architecture can be used where MOF is already used as precoding like C-RANs fronthaul downlink precoding. We also introduced a new outlier detection method based on ℓ_∞-norm representations. Since the representation elements spread evenly for ℓ_∞-norm representations, they are considered as a natural binarization scheme which we use this favorable property for ANN search to detect DoS attacks. A smooth approximation of an optimization problem makes it considerably easier to solve. In addition to these ℓ_∞-norm related applications, we also introduce a smooth approximation of ℓ_∞-norm minimization problem. Lastly, we offer a prior for ℓ_∞-norm representations and investigate the performance of this prior on PAPR reduction. Beside ℓ_1 and ℓ_∞-norms, noise constrained nuclear norm is also minimized with the introduced Pareto approach. Minimizing nuclear norm promotes low rank solutions since it implies to minimize the sum of the eigenvalues of a positive semidefinite matrix. Several SDP formulations for low-rank matrix completion problems from incomplete distance measurements have been proposed. We formulated a noise constrained nuclear norm minimization problem as an SDP, and solve it for the EDMC problem with noisy and incomplete distance measurements. We minimize the noise-constrained nuclear norm with the presented Pareto approach for the EDMC problem with the application of noisy Euclidean distance realization and WSN localization.

List of Publications

[1] **[Journal]** M. Vural, P. Jung and S. Stańczak, "ℓ_p-norm Minimization with Simple Iterations," to be submitted to *IEEE Transactions on Signal Processing*

[2] **[Journal]** M. Vural, C. Yuan, N. Kleppmann, P. Jung, S. Stańczak, "An SDP Approach for Noisy Euclidean Distance Realization with Illinois-type Methods," to be submitted to *IEEE Signal Processing Letters*

[3] **[Journal]** M. Vural, A. Y. Aravkin and S. Stańczak, "ℓ_1-Norm Minimization With Regula Falsi Type Root Finding Methods," in IEEE Signal Processing Letters, vol. 28, pp. 2132-2136, 2021, doi: 10.1109/LSP.2021.3120327.

[4] **[Conference]** M. Vural, C. Yuan, N. Kleppmann, P. Jung, "Robust Distance Matrix Completion for Localization using Frank-Wolfe Iterations," Asilomar Conference on Signals, Systems, and Computers (Asilomar), 2021

[5] **[Conference]** M. Vural, C. Yuan, N. Kleppmann, P. Jung, "A Semidefinite Programming Approach for Obstacle Prediction and Localization," 25th International ITG Workshop on Smart Antennas (WSA), 2021 (invited paper)

[6] **[Patent]** Nicola Kleppmann, Metin Vural, Peter Jung and Chun Yuan "Radio network for position detection of field devices by means of signal strength based distance detection," [Provisional Patent, with the number EP21166074 on the date 30.03.2021]

[7] **[Conference]** M. Vural, P. Jung and S. Stańczak, "Effect of anti-sparse prior on PAPR performance analysis," 2017 25th Signal Processing and Communications Applications Conference (SIU), 2017, pp. 1-4, doi: 10.1109/SIU.2017.7960517.

[8] **[Conference]** M. Vural, P. Jung and S. Stańczak, "A new outlier detection method based on anti-sparse representations," 2017 25th Signal Processing and Communications Applications Conference (SIU), 2017, pp. 1-4, doi: 10.1109/SIU.2017.7960516.

[9] **[Conference]** M. Vural, P. Jung and S. Stanczak, "On Some Physical Layer Design Aspects for Machine Type Communication," WSA 2016; 20th International ITG Workshop on Smart Antennas, 2016, pp. 1-8.

[10] **[Conference]** M. Vural, G. K. Kurt and C. Schneider, "The Effect of Shadow Fading Distributions on Outage Probability and Coverage Area," 2015 IEEE 81st Vehicular Technology Conference (VTC Spring), 2015, pp. 1-6, doi: 10.1109/VTC-Spring.2015.7146127.

[11] **[Journal]** S. Büyükçorak, M. Vural and G. K. Kurt, "Lognormal Mixture Shadowing," in IEEE Transactions on Vehicular Technology, vol. 64, no. 10, pp. 4386-4398, Oct. 2015, doi: 10.1109/TVT.2014.2369577.

[12] **[Conference]** M. Vural, P. Erdem and O. Agin, "Regression clustering with lower error VIA EM algorithm," 2014 22nd Signal Processing and Communications Applications Conference (SIU), 2014, pp. 979-982, doi: 10.1109/SIU.2014.6830395.

[13] **[Conference]** M. Vural and G. K. Kurt, "Effect of cooperative communications on power consumption in smart grid," 2013 21st Signal Processing and Communications Applications Conference (SIU), 2013, pp. 1-4, doi: 10.1109/SIU.2013.6531330.

References

[Can+06] Emmanuel J Candès et al. “Compressive sampling”. In: *Proceedings of the international congress of mathematicians*. Vol. 3. Madrid, Spain. 2006, pp. 1433–1452.

[CRT06] Emmanuel J. Candès, Justin K. Romberg, and Terence Tao. “Stable signal recovery from incomplete and inaccurate measurements”. In: *Communications on Pure and Applied Mathematics* 59.8 (2006), pp. 1207–1223. DOI: 10.1002/cpa.20124. eprint: https://onlinelibrary.wiley.com/doi/pdf/10.1002/cpa.20124. URL: https://onlinelibrary.wiley.com/doi/abs/10.1002/cpa.20124.

[CT06a] E. J. Candes and T. Tao. “Near-Optimal Signal Recovery From Random Projections: Universal Encoding Strategies?” In: *IEEE Transactions on Information Theory* 52.12 (Dec. 2006), pp. 5406–5425. ISSN: 0018-9448. DOI: 10.1109/TIT.2006.885507.

[Don06] D. L. Donoho. “Compressed sensing”. In: *IEEE Transactions on Information Theory* 52.4 (Apr. 2006), pp. 1289–1306. ISSN: 1557-9654. DOI: 10.1109/TIT.2006.871582.

[Yar15] Leonid Yaroslavsky. “Is" Compressed Sensing" compressive? Can it beat the Nyquist Sampling Approach?” In: *arXiv preprint arXiv:1501.01811* (2015).

[SCE01] Athanassios Skodras, Charilaos Christopoulos, and Touradj Ebrahimi. “The jpeg 2000 still image compression standard”. In: *IEEE Signal processing magazine* 18.5 (2001), pp. 36–58.

[PM92] William B Pennebaker and Joan L Mitchell. *JPEG: Still image data compression standard*. Springer Science & Business Media, 1992.

[DD95] L David and J Donoho. “Denoising by soft-thresholding”. In: *IEEE Transactions on information theory* 41.3 (1995), pp. 613–627.

[FR13] S. Foucart and H. Rauhut. *A Mathematical Introduction to Compressive Sensing*. Applied and Numerical Harmonic Analysis. Springer New York, 2013. ISBN: 9780817649487.

[Mut05] Shanmugavelayutham Muthukrishnan. *Data streams: Algorithms and applications*. Now Publishers Inc, 2005.

[Nat95] Balas Kausik Natarajan. "Sparse approximate solutions to linear systems". In: *SIAM journal on computing* 24.2 (1995), pp. 227–234.

[HP02] R. W. Heath and A. J. Paulraj. "Linear dispersion codes for MIMO systems based on frame theory". In: *IEEE Transactions on Signal Processing* (2002).

[BH01] H. Bolcskei and F. Hlawatsch. "Noise reduction in oversampled filter banks using predictive quantization". In: *IEEE Transactions on Information Theory* 47.1 (Jan. 2001). ISSN: 0018-9448. DOI: 10.1109/18.904519.

[BPY06] J. J. Benedetto, A. M. Powell, and O. Yilmaz. "Sigma-delta (/spl Sigma//spl Delta/) quantization and finite frames". In: *IEEE Transactions on Information Theory* 52.5 (May 2006), pp. 1990–2005. ISSN: 0018-9448. DOI: 10.1109/TIT.2006.872849.

[CT06b] E. J. Candes and T. Tao. "Near-Optimal Signal Recovery From Random Projections: Universal Encoding Strategies?" In: *IEEE Transactions on Information Theory* 52.12 (Dec. 2006), pp. 5406–5425. ISSN: 0018-9448. DOI: 10.1109/TIT.2006.885507.

[VA99] P. Viswanath and V. Anantharam. "Optimal sequences and sum capacity of synchronous CDMA systems". In: *IEEE Transactions on Information Theory* 45.6 (Sept. 1999), pp. 1984–1991. ISSN: 0018-9448. DOI: 10.1109/18.782121.

[CA07] G. Chen and R. Ansari. "Frame Expansion Based Peak to Average Power Ratio Reduction in MIMO OFDM Systems". In: *2007 IEEE Workshop on Signal Processing Systems*. Oct. 2007, pp. 61–66. DOI: 10.1109/SIPS.2007.4387518.

[Dra+03] Pier Luigi Dragotti et al. *Discrete directional wavelet bases for image compression*. 2003. DOI: 10.1117/12.509905. URL: https://doi.org/10.1117/12.509905.

[Uns95] M. Unser. "Texture classification and segmentation using wavelet frames". In: *IEEE Transactions on Image Processing* 4.11 (Nov. 1995), pp. 1549–1560. ISSN: 1057-7149. DOI: 10.1109/83.469936.

[Sho+01] A. Shokrollahi et al. "Representation theory for high-rate multiple-antenna code design". In: *IEEE Transactions on Information Theory* 47.6 (Sept. 2001), pp. 2335–2367. ISSN: 0018-9448.

[GKV99] V. K. Goyal, J. Kovacevic, and M. Vetterli. "Quantized frame expansions as source-channel codes for erasure channels". In: *Data Compression Conference, 1999. Proceedings. DCC '99*. Mar. 1999, pp. 326–335. DOI: 10.1109/DCC.1999.755682.

[GKK01] Vivek K. Goyal, Jelena Kovačević, and Jonathan A. Kelner. "Quantized Frame Expansions with Erasures". In: *Applied and Computational Harmonic Analysis* 10.3 (2001), pp. 203–233. ISSN: 1063-5203. DOI: https://doi.org/10.1006/acha.2000.0340. URL: http://www.sciencedirect.com/science/article/pii/S1063520300903403.

[BF09] E. van den Berg and M. Friedlander. "Probing the Pareto Frontier for Basis Pursuit Solutions". In: *SIAM Journal on Scientific Computing* 31.2 (2009), pp. 890–912. DOI: 10.1137/080714488. eprint: https://doi.org/10.1137/080714488. URL: https://doi.org/10.1137/080714488.

[BF11] E. van den Berg and M. Friedlander. "Sparse Optimization with Least-Squares Constraints". In: *SIAM Journal on Optimization* 21.4 (2011), pp. 1201–1229. DOI: 10.1137/100785028. eprint: https://doi.org/10.1137/100785028. URL: https://doi.org/10.1137/100785028.

[GLW12] Ming Gu, Lek-Heng Lim, and Cinna Julie Wu. "ParNes: a rapidly convergent algorithm for accurate recovery of sparse and approximately sparse signals". In: *Numerical Algorithms* 64 (2012), pp. 321–347.

[Ara+19] Aleksandr Y Aravkin et al. "Level-set methods for convex optimization". In: *Mathematical Programming* 174.1 (2019), pp. 359–390.

[ABF13] A. Aravkin, J. Burke, and M. Friedlander. "Variational Properties of Value Functions". In: *SIAM Journal on Optimization* 23.3 (2013), pp. 1689–1717. DOI: 10.1137/120899157. eprint: https://doi.org/10.1137/120899157. URL: https://doi.org/10.1137/120899157.

[Van09] Ewout Van den Berg. "Convex optimization for generalized sparse recovery". PhD thesis. University of British Columbia, 2009.

[GBC16] I Goodfellow, Y Bengio, and A Courville. *Deep Learning MIT Press (2016)*. 2016.

[SBV10] Nicolas Städler, Peter Buehlmann, and Sara Van De Geer. "l1-penalization for mixture regression models". In: *Test* 19.2 (2010), pp. 209–256.

[BG11] Peter Buehlmann and Sara Geer. "Non-convex loss functions and l1-regularization". In: *Statistics for High-Dimensional Data* (2011), pp. 293–338.

[MBM18] Song Mei, Yu Bai, and Andrea Montanari. "The landscape of empirical risk for nonconvex losses". In: *The Annals of Statistics* 46.6A (2018), pp. 2747–2774.

[VAS21] Metin Vural, Aleksandr Y. Aravkin, and Sławomir Stańczak. "ℓ_1-Norm Minimization With Regula Falsi Type Root Finding Methods". In: *IEEE Signal Processing Letters* 28 (2021), pp. 2132–2136. DOI: 10.1109/LSP.2021.3120327.

[ABP12] Aleksandr Aravkin, James V Burke, and Gianluigi Pillonetto. "Robust and Trend-following Kalman Smoothers using Student's t". In: *IFAC Proceedings Volumes* 45.16 (2012), pp. 1215–1220.

[ABP13] Aleksandr Y Aravkin, James V Burke, and Gianluigi Pillonetto. "Sparse/Robust Estimation and Kalman Smoothing with Nonsmooth Log-Concave Densities: Modeling, Computation, and Theory." In: *Journal of Machine Learning Research* 14 (2013).

[Ara+12] Aleksandr Aravkin et al. "Robust inversion, dimensionality reduction, and randomized sampling". In: *Mathematical Programming* 134.1 (2012), pp. 101–125.

[ROC70] R. TYRRELL ROCKAFELLAR. *Convex Analysis*. Princeton University Press, 1970. ISBN: 9780691015866.

[DS52] R. J. Duffin and A. C. Schaeffer. "A Class of Nonharmonic Fourier Series". In: *Transactions of the American Mathematical Society* 72.2 (1952), pp. 341–366. ISSN: 00029947. URL: http://www.jstor.org/stable/1990760.

[Dau88] I. Daubechies. "Time-frequency localization operators: a geometric phase space approach". In: *IEEE Transactions on Information Theory* 34.4 (July 1988), pp. 605–612. ISSN: 0018-9448. DOI: 10.1109/18.9761.

[Dau90] I. Daubechies. "The wavelet transform, time-frequency localization and signal analysis". In: *IEEE Transactions on Information Theory* 36.5 (1990), pp. 961–1005. DOI: 10.1109/18.57199.

[Dau92] Ingrid Daubechies. *Ten lectures on wavelets*. SIAM, 1992.

[DGM09] Ingrid Daubechies, Alex Grossmann, and Yves Meyer. "Painless nonorthogonal expansions". In: *Fundamental Papers in Wavelet Theory*. Princeton University Press, 2009, pp. 372–384.

[HW89] Christopher E Heil and David F Walnut. "Continuous and discrete wavelet transforms". In: *SIAM review* 31.4 (1989), pp. 628–666.

[Sid98] Burrus C Sidney. *Introduction to wavelets and wavelet transforms: a primer*. 1998.

[BES06] Radu V. Balan, Yonina C. Eldar, and Thomas Strohmer. “Frames and Overcomplete Representations in Signal Processing, Communications, and Information Theory”. In: *EURASIP Journal on Advances in Signal Processing* 2006.1 (Dec. 2006), p. 091786. ISSN: 1687-6180. DOI: 10.1155/ASP/2006/91786.

[KC08] Jelena Kovacevic and Amina Chebira. *An Introduction to Frames.* Hanover, MA, USA: Now Publishers Inc., 2008. ISBN: 160198068X, 9781601980687.

[CDS01] Scott Shaobing Chen, David L. Donoho, and Michael A. Saunders. “Atomic Decomposition by Basis Pursuit”. In: *SIAM Rev.* 43.1 (Jan. 2001), pp. 129–159. ISSN: 0036-1445. DOI: 10.1137/S003614450037906X. URL: http://dx.doi.org/10.1137/S003614450037906X.

[MZ93] Stéphane G Mallat and Zhifeng Zhang. “Matching pursuits with time-frequency dictionaries”. In: *IEEE Transactions on signal processing* 41.12 (1993), pp. 3397–3415.

[CD94] Shaobing Chen and David Donoho. “Basis pursuit”. In: *Proceedings of 1994 28th Asilomar Conference on Signals, Systems and Computers.* Vol. 1. IEEE. 1994, pp. 41–44.

[CW92] Ronald R Coifman and M Victor Wickerhauser. “Entropy-based algorithms for best basis selection”. In: *IEEE Transactions on information theory* 38.2 (1992), pp. 713–718.

[Wri+10] J. Wright et al. “Sparse Representation for Computer Vision and Pattern Recognition”. In: *Proceedings of the IEEE* 98.6 (June 2010), pp. 1031–1044. ISSN: 0018-9219. DOI: 10.1109/JPROC.2010.2044470.

[DE03] David L Donoho and Michael Elad. “Optimally sparse representation in general (nonorthogonal) dictionaries via L1 minimization”. In: *Proceedings of the National Academy of Sciences* 100.5 (2003), pp. 2197–2202.

[Ela10] Michael Elad. “Sparse and redundant representations: from theory to applications in signal and image processing”. In: (2010).

[EFM10] Michael Elad, Mario AT Figueiredo, and Yi Ma. “On the role of sparse and redundant representations in image processing”. In: *Proceedings of the IEEE* 98.6 (2010), pp. 972–982.

[Fuc04] J-J Fuchs. “On sparse representations in arbitrary redundant bases”. In: *IEEE transactions on Information theory* 50.6 (2004), pp. 1341–1344.

[ZEP10] Roman Zeyde, Michael Elad, and Matan Protter. “On single image scale-up using sparse-representations”. In: *International conference on curves and surfaces.* Springer. 2010, pp. 711–730.

[GN03] Rémi Gribonval and Morten Nielsen. "Sparse representations in unions of bases". In: *IEEE transactions on Information theory* 49.12 (2003), pp. 3320–3325.

[Yan+11] Meng Yang et al. "Robust sparse coding for face recognition". In: *CVPR 2011*. 2011, pp. 625–632. DOI: `10.1109/CVPR.2011.5995393`.

[Mo+13] Xuan Mo et al. "Adaptive sparse representations for video anomaly detection". In: *IEEE Transactions on Circuits and Systems for Video Technology* 24.4 (2013), pp. 631–645.

[Nik+15] Milad Niknejad et al. "A dictionary learning method for sparse representation using a homotopy approach". In: *International Conference on Latent Variable Analysis and Signal Separation*. Springer. 2015, pp. 271–278.

[Zha+15] Zheng Zhang et al. "A survey of sparse representation: algorithms and applications". In: *IEEE access* 3 (2015), pp. 490–530.

[SL13] C. Studer and E. G. Larsson. "PAR-Aware Large-Scale Multi-User MIMO-OFDM Downlink". In: *IEEE Journal on Selected Areas in Communications* 31.2 (Feb. 2013), pp. 303–313. ISSN: 0733-8716. DOI: `10.1109/JSAC.2013.130217`.

[WES08] Ami Wiesel, Yonina C Eldar, and Shlomo Shamai. "Zero-forcing precoding and generalized inverses". In: *IEEE Transactions on Signal Processing* 56.9 (2008), pp. 4409–4418.

[Stu+14] Christoph Studer et al. "Democratic Representations". In: *CoRR* abs/1401.3420 (2014). URL: `http://arxiv.org/abs/1401.3420`.

[SYB12] C. Studer, W. Yin, and R. G. Baraniuk. "Signal representations with minimum l-infinity norm". In: *Communication, Control, and Computing (Allerton), 2012 50th Annual Allerton Conference on*. Oct. 2012, pp. 1270–1277.

[JFF11] H. Jégou, T. Furon, and J. Fuchs. *Anti-sparse coding for approximate nearest neighbor search*. 2011.

[Fuc11] J. J. Fuchs. "Spread representations". In: *Signals, Systems and Computers (ASILOMAR), 2011 Conference Record of the Forty Fifth Asilomar Conference on*. Nov. 2011, pp. 814–817.

[LV10] Y. Lyubarskii and R. Vershynin. "Uncertainty Principles and Vector Quantization". In: *IEEE Transactions on Information Theory* 56.7 (July 2010), pp. 3491–3501. ISSN: 0018-9448. DOI: `10.1109/TIT.2010.2048458`.

[VJS17a] M. Vural, P. Jung, and S. Stańczak. "A new outlier detection method based on anti-sparse representations". In: *2017 25th Signal Processing and Communications Applications Conference (SIU)*. May 2017, pp. 1–4. DOI: `10.1109/SIU.2017.7960516`.

[ECD17] C. Elvira, P. Chainais, and N. Dobigeon. "Bayesian Antisparse Coding". In: *IEEE Transactions on Signal Processing* 65.7 (2017), pp. 1660–1672.

[VJS17b] M. Vural, P. Jung, and S. Stańczak. "Effect of anti-sparse prior on PAPR performance analysis". In: *2017 25th Signal Processing and Communications Applications Conference (SIU)*. May 2017, pp. 1–4. DOI: `10.1109/SIU.2017.7960517`.

[Jia+18] Xue Jiang et al. "Large-Scale Robust Beamforming via ℓ_∞-Minimization". In: *IEEE Transactions on Signal Processing* 66.14 (2018), pp. 3824–3837.

[Neu62] Lucien W Neustadt. "Minimum effort control systems". In: *Journal of the Society for Industrial and Applied Mathematics, Series A: Control* 1.1 (1962), pp. 16–31.

[Cad71] J Cadzow. "Algorithm for the minimum-effort problem". In: *IEEE Transactions on Automatic Control* 16.1 (1971), pp. 60–63.

[FJ09] Brendan Farrell and Peter Jung. "A Kashin approach to the capacity of the discrete amplitude constrained Gaussian channel". In: *SAMPTA'09*. 2009, Special–Session.

[EH20] Clément Elvira and Cédric Herzet. "Safe Squeezing for Antisparse Coding". In: *IEEE Transactions on Signal Processing* 68 (2020), pp. 3252–3265. DOI: `10.1109/TSP.2020.2995192`.

[Pin85] A. Pinkus. *N-widths in Approximation Theory*. Ergebnisse der Mathematik und ihrer Grenzgebiete : a series of modern surveys in mathematics. Folge 3. U.S. Government Printing Office, 1985. ISBN: 9780387136387.

[FR11] Massimo Fornasier and Holger Rauhut. "Compressive Sensing". In: *Handbook of Mathematical Methods in Imaging*. Ed. by Otmar Scherzer. New York, NY: Springer New York, 2011, pp. 187–228. ISBN: 978-0-387-92920-0. DOI: `10.1007/978-0-387-92920-0_6`. URL: `https://doi.org/10.1007/978-0-387-92920-0_6`.

[Glu84] E. D. Gluskin. "Norms of random matrices and widths of finite-dimensional sets." English. In: *Math. USSR, Sb.* 48 (1984), pp. 173–182. ISSN: 0025-5734.

[GG84] A.Y. Garnaev and E.D. Gluskin. "On Widths of the Euclidean Ball." In: *Doklady - Akademiya Nauk SSSR, Earth Science Sections* 277.5 (1984), pp. 1048–1052. ISSN: 0002-3264.

[Vyb08] Jan Vybíral. “Widths of embeddings in function spaces”. In: *Journal of Complexity* 24.4 (2008), pp. 545–570. ISSN: 0885-064X. DOI: https://doi.org/10.1016/j.jco.2008.01.002.

[Kas77] Boris Sergeevich Kashin. “Diameters of some finite-dimensional sets and classes of smooth functions”. In: *Izvestiya Rossiiskoi Akademii Nauk. Seriya Matematicheskaya* 41.2 (1977), pp. 334–351.

[DT05] David L. Donoho and Jared Tanner. “Sparse nonnegative solution of underdetermined linear equations by linear programming”. In: *Proceedings of the National Academy of Sciences* 102.27 (2005), pp. 9446–9451. ISSN: 0027-8424. DOI: 10.1073/pnas.0502269102. eprint: https://www.pnas.org/content/102/27/9446.full.pdf. URL: https://www.pnas.org/content/102/27/9446.

[Ber+08] Radu Berinde et al. “Combining geometry and combinatorics: A unified approach to sparse signal recovery”. In: *CoRR* abs/0804.4666 (2008). arXiv: 0804.4666. URL: http://arxiv.org/abs/0804.4666.

[IR08] P. Indyk and M. Ruzic. “Near-Optimal Sparse Recovery in the L1 Norm”. In: *2008 49th Annual IEEE Symposium on Foundations of Computer Science*. Oct. 2008, pp. 199–207. DOI: 10.1109/FOCS.2008.82.

[CT05] Emmanuel J. Candès and Terence Tao. “Decoding by linear programming”. In: *IEEE Transactions on Information Theory* 51 (2005), pp. 4203–4215.

[Lit+05] A.E. Litvak et al. “Smallest singular value of random matrices and geometry of random polytopes”. In: *Advances in Mathematics* 195.2 (2005), pp. 491–523. ISSN: 0001-8708. DOI: https://doi.org/10.1016/j.aim.2004.08.004. URL: http://www.sciencedirect.com/science/article/pii/S0001870804002750.

[PMP08] Panos M Pardalos, Athanasios Migdalas, and Leonidas Pitsoulis. *Pareto optimality, game theory and equilibria.* Vol. 17. Springer Science & Business Media, 2008.

[SM12] Roman B Statnikov and Joseph B Matusov. *Multicriteria optimization and engineering.* Springer Science & Business Media, 2012.

[PŽŽ17] Panos M Pardalos, Antanas Žilinskas, and Julius Žilinskas. *Non-convex multi-objective optimization.* Springer, 2017.

[Mie01] Kaisa Miettinen. “Some methods for nonlinear multi-objective optimization”. In: *International conference on evolutionary multi-criterion optimization.* Springer. 2001, pp. 1–20.

[DB03] G. Dahlquist and Å. Björck. *Numerical Methods.* Dover Books on Mathematics. Dover Publications, 2003. ISBN: 9780486428079.

[Ara+18] A. Y. Aravkin et al. “Foundations of Gauge and Perspective Duality”. In: *SIAM Journal on Optimization* 28.3 (2018), pp. 2406–2434. DOI: 10.1137/17M1119020. eprint: https://doi.org/10.1137/17M1119020. URL: https://doi.org/10.1137/17M1119020.

[TCS19] J.R. Torregrosa, A. Cordero, and F. Soleymani. *Iterative Methods for Solving Nonlinear Equations and Systems*. Online access: OAPEN DOAB Directory of Open Access Books. MDPI AG, 2019. ISBN: 9783039219407. URL: https://books.google.de/books?id=BvzBDwAAQBAJ.

[New11] Isaac Newton. *De analysi per aequationes numero terminorum infinitas*. 1711.

[Hal07] Edmond Halley. “Methodus nova accurata & facilis inveniendi radices æqnationum quarumcumque generaliter, sine praviæ reductione”. In: *Philosophical Transactions of the Royal Society of London* 18.210 (1707), pp. 136–148.

[Ste33] J. F. Steffensen. “Remarks on iteration.” In: *Scandinavian Actuarial Journal* 1933.1 (1933), pp. 64–72. DOI: 10.1080/03461238.1933.10419209.

[Mul56] David E Muller. “A method for solving algebraic equations using an automatic computer”. In: *Mathematical tables and other aids to computation* 10.56 (1956), pp. 208–215.

[Kou07] Jisheng Kou. “The improvements of modified Newton’s method”. In: *Applied Mathematics and Computation* 189.1 (2007), pp. 602–609.

[Hom03] HHH Homeier. “A modified Newton method for rootfinding with cubic convergence”. In: *Journal of Computational and Applied Mathematics* 157.1 (2003), pp. 227–230.

[RAS+21] Mohammed RASHEED et al. “Experimental Results for a Nonlinear Equation Using Improved Newton-Raphson Estimation Method”. In: *Journal of Al-Qadisiyah for Computer Science and Mathematics* 13.1 (2021), Page–193.

[Xin99] Wu Xinyuan. “A significant improvement on Newton’s interative method”. In: *Applied Mathematics and Mechanics* 20.8 (1999), pp. 924–927.

[Sah+16] B Saheya et al. “A new Newton-like method for solving nonlinear equations”. In: *SpringerPlus* 5.1 (2016), pp. 1–13.

[Tir19] Ababu Teklemariam Tiruneh. “A modified three-point Secant method with improved rate and characteristics of convergence”. In: *arXiv preprint arXiv:1902.09058* (2019).

[MT13] James Matthew Moten Jr and Chris Thron. “Improvements on secant method for estimating internal rate of return (IRR)”. In: *Int. J. Appl. Math. Stat* 42.12 (2013), pp. 84–93.

[Bar65] John GP Barnes. “An algorithm for solving non-linear equations based on the secant method”. In: *The Computer Journal* 8.1 (1965), pp. 66–72.

[Tek19] Ababu Teklemariam Tiruneh. “A modified three-point Secant method with improved rate and characteristics of convergence”. In: *arXiv e-prints* (2019), arXiv–1902.

[Chh14] Chetan Chhabra. “Improvements in the bisection method of finding roots of an equation”. In: *2014 IEEE International Advance Computing Conference (IACC)*. IEEE. 2014, pp. 11–16.

[OT20] Ivo FD Oliveira and Ricardo HC Takahashi. “An Enhancement of the Bisection Method Average Performance Preserving Minmax Optimality”. In: *ACM Transactions on Mathematical Software (TOMS)* 47.1 (2020), pp. 1–24.

[MR16] C Martin and V Rayskin. “An improved bisection method in two dimensions”. In: *Preprint submitted to Elsevier* (2016), pp. 1–21.

[Gal] Sergio Galdino. “A family of regula falsi root-finding methods”. In.

[For] J. A. Ford. “Improved Algorithms of Illinois-type for the Numerical Solution of Nonlinear Equations”. In.

[SM15] Soumen Shaw and Basudeb Mukhopadhyay. “An improved Regula falsi method for finding simple roots of nonlinear equations”. In: *Applied Mathematics and Computation* 254 (2015), pp. 370–374.

[Che07] Jinhai Chen. “New modified regula falsi method for nonlinear equations”. In: *Applied mathematics and computation* 184.2 (2007), pp. 965–971.

[Kin73] Richard F King. “An improved Pegasus method for root finding”. In: *BIT Numerical Mathematics* 13.4 (1973), pp. 423–427.

[Bol17] B Bolzano. “Rein analytischer Beweis des Lehrsatzes dass zwischen je zwey [sic] Werthen, die ein entgegengesetztes Resultat gewaehren, wenigstens eine reele Wurzel der Gleichung liege”. In: *Prague: Gottlieb Haase. English translation in Russ, SB (1980). A translation of Bolzano's paper on the intermediate value theorem. Historia Mathematica* 7 (1817), pp. 251–278.

[YW02] E Alper Yildirim and Stephen J Wright. “Warm-start strategies in interior-point methods for linear programming”. In: *SIAM Journal on Optimization* 12.3 (2002), pp. 782–810.

[JY08] Elizabeth John and E Alper Yıldırım. “Implementation of warm-start strategies in interior-point methods for linear programming in fixed dimension”. In: *Computational Optimization and Applications* 41.2 (2008), pp. 151–183.

[SKC10] Amir Shahzad, Eric C Kerrigan, and George A Constantinides. “A warm-start interior-point method for predictive control”. In: *UKACC International Conference on Control 2010*. IET. 2010, pp. 1–6.

[CGG11] Marco Colombo, Jacek Gondzio, and Andreas Grothey. “A warm-start approach for large-scale stochastic linear programs”. In: *Mathematical Programming* 127.2 (2011), pp. 371–397.

[CPT17] Sertalp B Cay, Imre Pólik, and Tamás Terlaky. “Warm-start of interior point methods for second order cone optimization via rounding over optimal Jordan frames”. In: *ISE TechnicalReport 17T-006, Lehigh University* (2017).

[Dan+20] Marina Danilova et al. “Recent theoretical advances in non-convex optimization”. In: *arXiv preprint arXiv:2012.06188* (2020).

[Duc+08] John Duchi et al. “Efficient projections onto the l1-ball for learning in high dimensions”. In: *ICML ’08: Proceedings of the 25th international conference on Machine learning*. New York, NY, USA, 2008, pp. 272–279. URL: `http://doi.acm.org/10.1145/1390156.1390191`.

[HWC74] Michael Held, Philip Wolfe, and Harlan P. Crowder. “Validation of Subgradient Optimization”. In: *Math. Program.* 6.1 (Dec. 1974), pp. 62–88. ISSN: 0025-5610. DOI: `10.1007/BF01580223`. URL: `https://doi.org/10.1007/BF01580223`.

[Con16] Laurent Condat. “Fast Projection onto the Simplex and the l1 Ball”. In: *Mathematical Programming, Series A* 158.1 (July 2016), pp. 575–585. DOI: `10.1007/s10107-015-0946-6`. URL: `https://hal.archives-ouvertes.fr/hal-01056171`.

[HK12] Elad Hazan and Satyen Kale. “Projection-free online learning”. In: *arXiv preprint arXiv:1206.4657* (2012).

[FW+56] Marguerite Frank, Philip Wolfe, et al. “An algorithm for quadratic programming”. In: *Naval research logistics quarterly* 3.1-2 (1956), pp. 95–110.

[DU18] Lijun Ding and Madeleine Udell. “Frank-wolfe style algorithms for large scale optimization”. In: *Large-Scale and Distributed Optimization*. Springer, 2018, pp. 215–245.

[Jag13] Martin Jaggi. “Revisiting Frank-Wolfe: Projection-free sparse convex optimization”. In: *International Conference on Machine Learning*. PMLR. 2013, pp. 427–435.

[Glu81] E. D. Gluskin. "On lower estimates for the diameters of some finite-dimensional sets." English. In: *Russ. Math. Surv.* 36.2 (1981), pp. 173–174. ISSN: 0036-0279; 1468-4829/e.

[Ber+09] Ewout van den Berg et al. "Algorithm 890: Sparco: A Testing Framework for Sparse Reconstruction". In: *ACM Trans. Math. Softw.* 35.4 (Feb. 2009). ISSN: 0098-3500. DOI: 10.1145/1462173.1462178. URL: https://doi.org/10.1145/1462173.1462178.

[Sch64a] L. Schuchman. "Dither Signals and Their Effect on Quantization Noise". In: *IEEE Transactions on Communication Technology* 12.4 (Dec. 1964), pp. 162–165. ISSN: 0018-9332. DOI: 10.1109/TCOM.1964.1088973.

[Fat+18] N. Fatema et al. "Massive MIMO Linear Precoding: A Survey". In: *IEEE Systems Journal* 12.4 (Dec. 2018), pp. 3920–3931. ISSN: 1932-8184. DOI: 10.1109/JSYST.2017.2776401.

[Lan+] Mandy Lange et al. "Applications of lp-Norms and their Smooth Approximations for Gradient Based Learning Vector Quantization". In: *22th European Symposium on Artificial Neural Networks, ESANN 2014, Bruges, Belgium, April 23-25*.

[Zha+13] S. Zhang et al. "Max-consensus using the soft maximum". In: *2013 Asilomar Conference on Signals, Systems and Computers*. Nov. 2013, pp. 433–437. DOI: 10.1109/ACSSC.2013.6810313.

[HCB11] M. K. Hsu, Y. W. Chang, and V. Balabanov. "TSV-aware analytical placement for 3D IC designs". In: *2011 48th ACM/EDAC/IEEE Design Automation Conference (DAC)*. June 2011, pp. 664–669.

[RB15] B. N. B. Ray and S. Balachandran. "A Recursive Model for Smooth Approximation to Wirelength and Its Impact on Analytical Placement". In: *2015 28th International Conference on VLSI Design*. Jan. 2015, pp. 417–422. DOI: 10.1109/VLSID.2015.76.

[Coo11] John D. Cook. "Basic Properties of the Soft Maximum". In: 2011.

[SFR07] Mark Schmidt, Glenn Fung, and Rómer Rosales. "Fast Optimization Methods for L1 Regularization: A Comparative Study and Two New Approaches". In: *Machine Learning: ECML 2007: 18th European Conference on Machine Learning, Warsaw, Poland, September 17-21, 2007. Proceedings*. Ed. by Joost N. Kok et al. Berlin, Heidelberg: Springer Berlin Heidelberg, 2007, pp. 286–297.

[HA04] Victoria Hodge and Jim Austin. "A Survey of Outlier Detection Methodologies". In: *Artif. Intell. Rev.* 22.2 (Oct. 2004), pp. 85–126. ISSN: 0269-2821. DOI: 10.1023/B:AIRE.0000045502.10941.a9. URL: http://dx.doi.org/10.1023/B:AIRE.0000045502.10941.a9.

[KN98] Edwin M. Knorr and Raymond T. Ng. “Algorithms for Mining Distance-Based Outliers in Large Datasets”. In: *Proceedings of the 24rd International Conference on Very Large Data Bases*. VLDB ’98. San Francisco, CA, USA: Morgan Kaufmann Publishers Inc., 1998, pp. 392–403. ISBN: 1-55860-566-5.

[PDN10] R. Pamula, J. K. Deka, and S. Nandi. “Distance based fast outlier detection method”. In: *2010 Annual IEEE India Conference (INDICON)*. Dec. 2010, pp. 1–4. DOI: `10.1109/INDCON.2010.5712706`.

[SL14] Anshumali Shrivastava and Ping Li. “Asymmetric LSH (ALSH) for Sublinear Time Maximum Inner Product Search (MIPS)”. In: *Proceedings of the 27th International Conference on Neural Information Processing Systems*. NIPS’14. Montreal, Canada: MIT Press, 2014, pp. 2321–2329. URL: `http://dl.acm.org/citation.cfm?id=2969033.2969086`.

[Lic13] M. Lichman. *UCI Machine Learning Repository*. 2013. URL: `http://archive.ics.uci.edu/ml`.

[Y83] Nesterov Y. “A method of solving a convex programming problem with convergence rate $O(1/k^2)$”. In: *Soviet Mathematics Doklady* (1983).

[BT09] A. Beck and M. Teboulle. “A Fast Iterative Shrinkage-Thresholding Algorithm for Linear Inverse Problems”. In: *SIAM Journal on Imaging Sciences* 2.1 (2009), pp. 183–202. DOI: `10.1137/080716542`.

[BVK15] S. Buyukcorak, M. Vural, and G.K. Kurt. “Lognormal Mixture Shadowing”. In: *Vehicular Technology, IEEE Transactions on* 64.10 (Oct. 2015), pp. 4386–4398. ISSN: 0018-9545. DOI: `10.1109/TVT.2014.2369577`.

[VKS15] M. Vural, G. K. Kurt, and C. Schneider. “The Effect of Shadow Fading Distributions on Outage Probability and Coverage Area”. In: *2015 IEEE 81st Vehicular Technology Conference (VTC Spring)*. May 2015. DOI: `10.1109/VTCSpring.2015.7146127`.

[VEA14] M. Vural, P. Erdem, and O. Agin. “Regression clustering with lower error VIA EM algorithm”. In: *2014 22nd Signal Processing and Communications Applications Conference (SIU)*. Apr. 2014, pp. 979–982. DOI: `10.1109/SIU.2014.6830395`.

[VJS16] M. Vural, P. Jung, and S. Stanczak. “On Some Physical Layer Design Aspects for Machine Type Communication”. In: *WSA 2016; 20th International ITG Workshop on Smart Antennas*. Mar. 2016, pp. 1–8.

[Ji+05] Yuan Ji et al. “Applications of beta-mixture models in bioinformatics”. In: *Bioinformatics* 21.9 (2005), pp. 2118–2122. DOI: `10.1093/bioinformatics/bti318`. eprint: `http://bioinformatics.oxfordjournals.org/content/21/9/2118.full.pdf+html`. URL:

http://bioinformatics.oxfordjournals.org/content/21/9/2118.abstract.

[IS09] J. Ilic and T. Strohmer. “PAPR reductioni in OFDM using kashin’s representation”. In: *2009 IEEE 10th Workshop on Signal Processing Advances in Wireless Communications*. June 2009, pp. 444–448. DOI: 10.1109/SPAWC.2009.5161824.

[Vur14] Metin Vural. *Lognormal Karışımı Gölgeleme Modeli Ve Uygulamaları*. 2014.

[Bit09] Petros S Bithas. “Weibull-gamma composite distribution: alternative multipath/shadowing fading model”. In: *Electronics Letters* 45.14 (2009), pp. 749–751.

[EG16] Andreas Elsener and Sara Geer. “Robust Low-Rank Matrix Estimation”. In: *Annals of Statistics* 46 (Mar. 2016). DOI: 10.1214/17-AOS1666.

[CA16] Léopold Cambier and P.-A. Absil. “Robust Low-Rank Matrix Completion by Riemannian Optimization”. In: *SIAM Journal on Scientific Computing* 38.5 (2016), S440–S460. DOI: 10.1137/15M1025153.

[EM19] Ashkan Esmaeili and Farokh Marvasti. “A Novel Approach to Quantized Matrix Completion Using Huber Loss Measure”. In: *IEEE Signal Processing Letters* 26.2 (2019), pp. 337–341. DOI: 10.1109/LSP.2019.2891134.

[SGS11] Shai Shalev-Shwartz, Alon Gonen, and Ohad Shamir. “Large-Scale Convex Minimization with a Low-Rank Constraint”. In: *Proceedings of the 28th International Conference on Machine Learning, ICML 2011* (June 2011).

[Bur09] John Burkardt. *SGB128*. 2009. URL: https://people.sc.fsu.edu/~jburkardt/datasets/cities/cities.html.

[Din+10] Yichuan Ding et al. “Sensor network localization, Euclidean distance matrix completions, and graph realization”. In: *Optimization and Engineering* 11.1 (2010), pp. 45–66.

[Sch35] IJ Schoenberg. “Sur la définition axiomatique d’une classe d’espace distanciés vectoriellement applicable sur l’espace de Hilbert”. In: *Ann. Math* 36 (1935), pp. 724–732.

[YH38] Gale Young and Alston S Householder. “Discussion of a set of points in terms of their mutual distances”. In: *Psychometrika* 3.1 (1938), pp. 19–22.

[Dok+15] Ivan Dokmanic et al. “Euclidean distance matrices: essential theory, algorithms, and applications”. In: *IEEE Signal Processing Magazine* 32.6 (2015), pp. 12–30.

[AKW99] Abdo Y Alfakih, Amir Khandani, and Henry Wolkowicz. “Solving Euclidean distance matrix completion problems via semidefinite programming”. In: *Computational optimization and applications* 12.1 (1999), pp. 13–30.

[Bis+06a] Pratik Biswas et al. “Semidefinite Programming Based Algorithms for Sensor Network Localization”. In: *ACM Trans. Sen. Netw.* 2.2 (May 2006), pp. 188–220. ISSN: 1550-4859. DOI: `10.1145/1149283.1149286`. URL: `https://doi.org/10.1145/1149283.1149286`.

[Bis+06b] P. Biswas et al. “Semidefinite Programming Approaches for Sensor Network Localization With Noisy Distance Measurements”. In: *IEEE Transactions on Automation Science and Engineering* 3.4 (2006), pp. 360–371. DOI: `10.1109/TASE.2006.877401`.

[Dru+17] D. Drusvyatskiy et al. “Noisy Euclidean Distance Realization: Robust Facial Reduction and the Pareto Frontier”. In: *SIAM Journal on Optimization* 27.4 (2017), pp. 2301–2331. DOI: `10.1137/15M103710X`. eprint: `https://doi.org/10.1137/15M103710X`. URL: `https://doi.org/10.1137/15M103710X`.

[Dat10] Jon Dattorro. *Convex optimization & Euclidean distance geometry*. Lulu.com, 2010.

[KW] Nathan Krislock and Henry Wolkowicz. *Euclidean Distance Matrices and Applications.*

[Haz08] Elad Hazan. “Sparse approximate solutions to semidefinite programs”. In: *Latin American symposium on theoretical informatics*. Springer. 2008, pp. 306–316.

[GM12] Bernd Gärtner and Jiri Matousek. *Approximation algorithms and semidefinite programming*. Springer Science & Business Media, 2012.

[Pla] Daniel Plaumann. *Geometry of linear matrix inequalities. Lecture notes, University of Konstanz (2013).*

[Cla10] Kenneth L. Clarkson. “Coresets, Sparse Greedy Approximation, and the Frank-Wolfe Algorithm”. In: *ACM Trans. Algorithms* 6.4 (Sept. 2010). ISSN: 1549-6325. DOI: `10.1145/1824777.1824783`. URL: `https://doi.org/10.1145/1824777.1824783`.

[Lau12] Sören Laue. “A hybrid algorithm for convex semidefinite optimization”. In: *arXiv preprint arXiv:1206.4608* (2012).

[EG+18] Andreas Elsener, Sara van de Geer, et al. “Robust low-rank matrix estimation”. In: *The Annals of Statistics* 46.6B (2018), pp. 3481–3509.

[Tor65] Warren S Torgerson. "Multidimensional scaling of similarity". In: *Psychometrika* 30.4 (1965), pp. 379–393.

[FO12] Haw-ren Fang and Dianne P O'Leary. "Euclidean distance matrix completion problems". In: *Optimization Methods and Software* 27.4-5 (2012), pp. 695–717.

[Sch64b] P. H. Schönemann. "A Solution of the Orthogonal Procrustes Problem With Applications to Orthogonal and Oblique Rotation". In: 1964.

[BG07] I. Borg and P.J.F. Groenen. *Modern Multidimensional Scaling: Theory and Applications*. Springer Series in Statistics. Springer New York, 2007. ISBN: 9780387289816.

[Gar16] Dan Garber. "Faster projection-free convex optimization over the spectrahedron". In: *arXiv preprint arXiv:1605.06203* (2016).

[All+17] Zeyuan Allen-Zhu et al. "Linear convergence of a frank-wolfe type algorithm over trace-norm balls". In: *arXiv preprint arXiv:1708.02105* (2017).

[Van+05] Lieven Vandenberghe et al. "Interior-point algorithms for semidefinite programming problems derived from the KYP lemma". In: *Positive polynomials in control*. Springer, 2005, pp. 195–238.

[Gro] Samson Group. *Wireless Sensors*. Accessed: 01-09-2021. URL: `https://www.samsongroup.com/en/news/in-focus/details/news/know-how/sam-lan%20/`.

[MFA07] Guoqiang Mao, Barış Fidan, and Brian D.O. Anderson. "Wireless sensor network localization techniques". In: *Computer Networks* 51.10 (2007), pp. 2529–2553. ISSN: 1389-1286. DOI: `https://doi.org/10.1016/j.comnet.2006.11.018`.

[Rap01] Theodore Rappaport. *Wireless Communications: Principles and Practice*. 2nd. USA: Prentice Hall PTR, 2001. ISBN: 0130422320.

[GB14] Michael Grant and Stephen Boyd. *CVX: Matlab Software for Disciplined Convex Programming, version 2.1*. `http://cvxr.com/cvx`. Mar. 2014.

[Knu09] D.E. Knuth. *The Stanford GraphBase: A Platform for Combinatorial Computing*. Addison-Wesley, 2009. ISBN: 9780321606327.